Short Course Given at the Health
Physics Society Ninth Midyear
Topical Symposium, Denver, CO,
February 8 - 12, 1976

LBL-4655
c. 1

HEALTH PHYSICS PRACTICES AT RESEARCH ACCELERATORS

Ralph H. Thomas

February 1976

Prepared for the U. S. Energy Research and
Development Administration under Contract W-7405-ENG-48

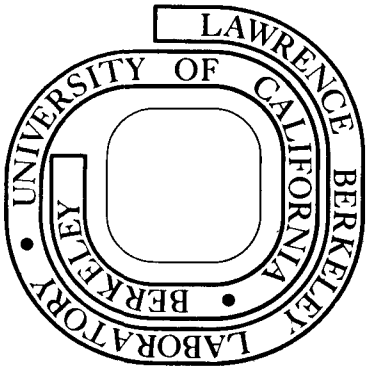

LBL-4655
c. 1

DISCLAIMER

Short Course Given at the
Health Physics Society
Ninth Midyear Topical Symposium
Denver, Colorado
February 1976

LBL-4655

HEALTH PHYSICS PRACTICES AT RESEARCH ACCELERATORS

Ralph H. Thomas

Health Physics Department
Lawrence Berkeley Laboratory
University of California
Berkeley, California 94720

"For such kind of borrowing as this,

if it be not bettered by the borrower,

among good authors is accounted plagiary."

John Milton, 1608-1674
Iconoclastes, Ch. 23

CONTENTS

1. Introduction

At first sight the health physics practices at research accelerators might appear to be of limited interest. It is certainly true that one aspect of the research accelerator health physicist's work is to identify and provide solutions to new and novel problems. The radiation fields of such accelerators are themselves to some extent subjects of research. This aspect is common to other research institutions but is accentuated at particle accelerator laboratories where the radiation fields produced may initially be completely unknown.

Experience shows us, however, that the research instruments of today are rapidly modified and adapted to become the work-a-day tools of tomorrow. This has already happened with particle accelerators. There has been a steady increase in the application of accelerators to medicine and industry.[1-8] Only a few years ago, exposure to accelerator-like radiation environments was limited to a relatively small number of institutions. However, exposure to accelerator-like radiation is no longer only of academic interest. The applied uses of ionizing radiation have increased dramatically over the past decade. This has been made possible by impressive developments in accelerator design.

Since the first development of particle accelerators in the early 1930's, the available particle kinetic energies and beam intensities have steadily increased.

Figure 1.1 demonstrates the increase in maximum energy achieved by different types of particle accelerators since that time. During the 30 years from 1935 to 1965, the maximum particle energy available increased by an order of magnitude roughly every 5.5 years. In a finite world, however, exponential growth cannot continue indefinitely and there is some indication that the rate of increase in laboratory energies has declined somewhat in the past ten years. The highest kinetic energy achieved at the present time is 500 GeV at the proton synchrotron of the Fermi National Accelerator Laboratory (1976).

Available beam intensities from the highest energy accelerators tend to be significantly lower than those from lower energy accelerators, as may be seen by inspecting Fig. 1.2. In this figure the two parameters, maximum beam energy and maximum average current, are plotted for various accelerators around the world. For the highest energy

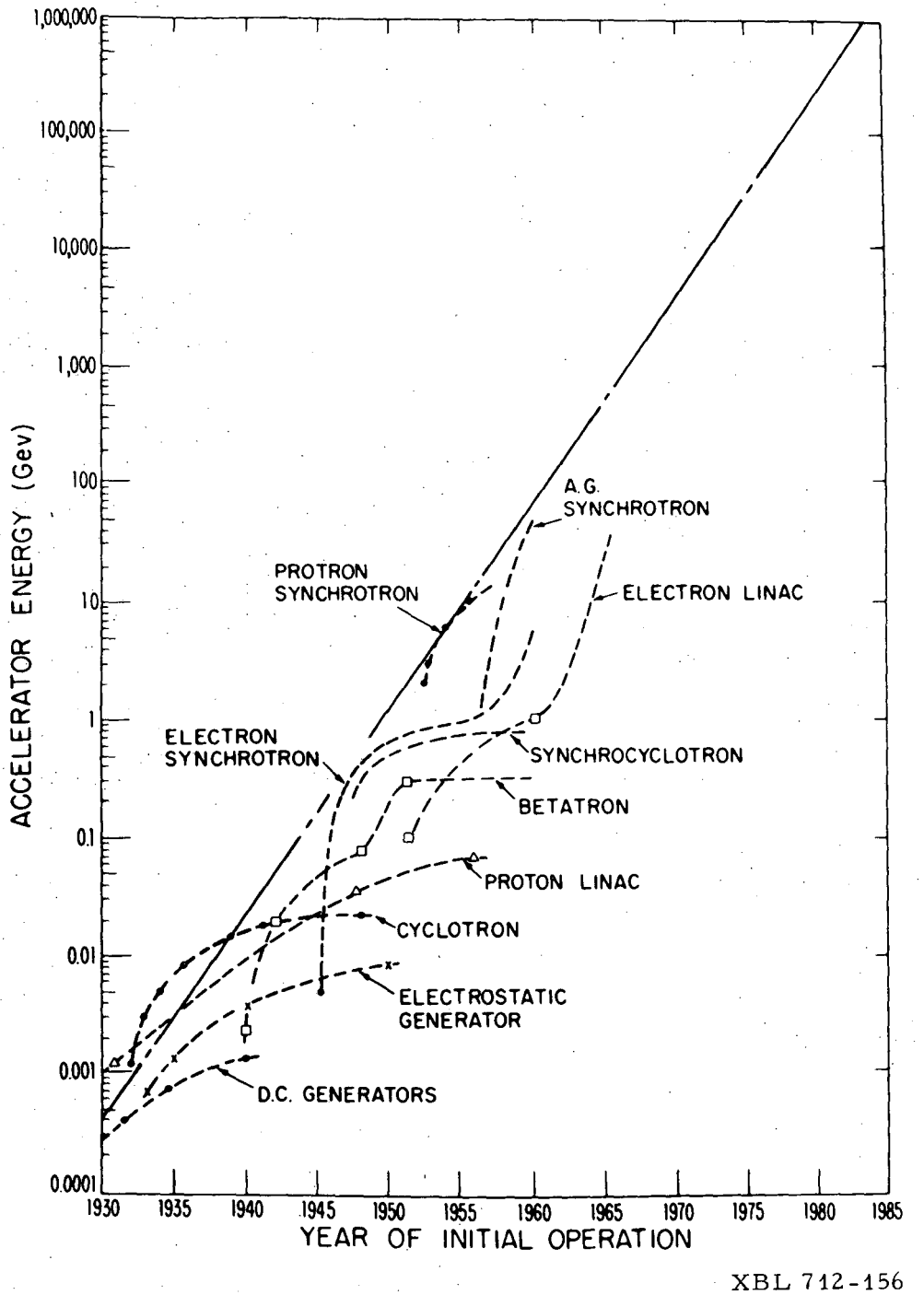

XBL 712-156

Fig. 1.1

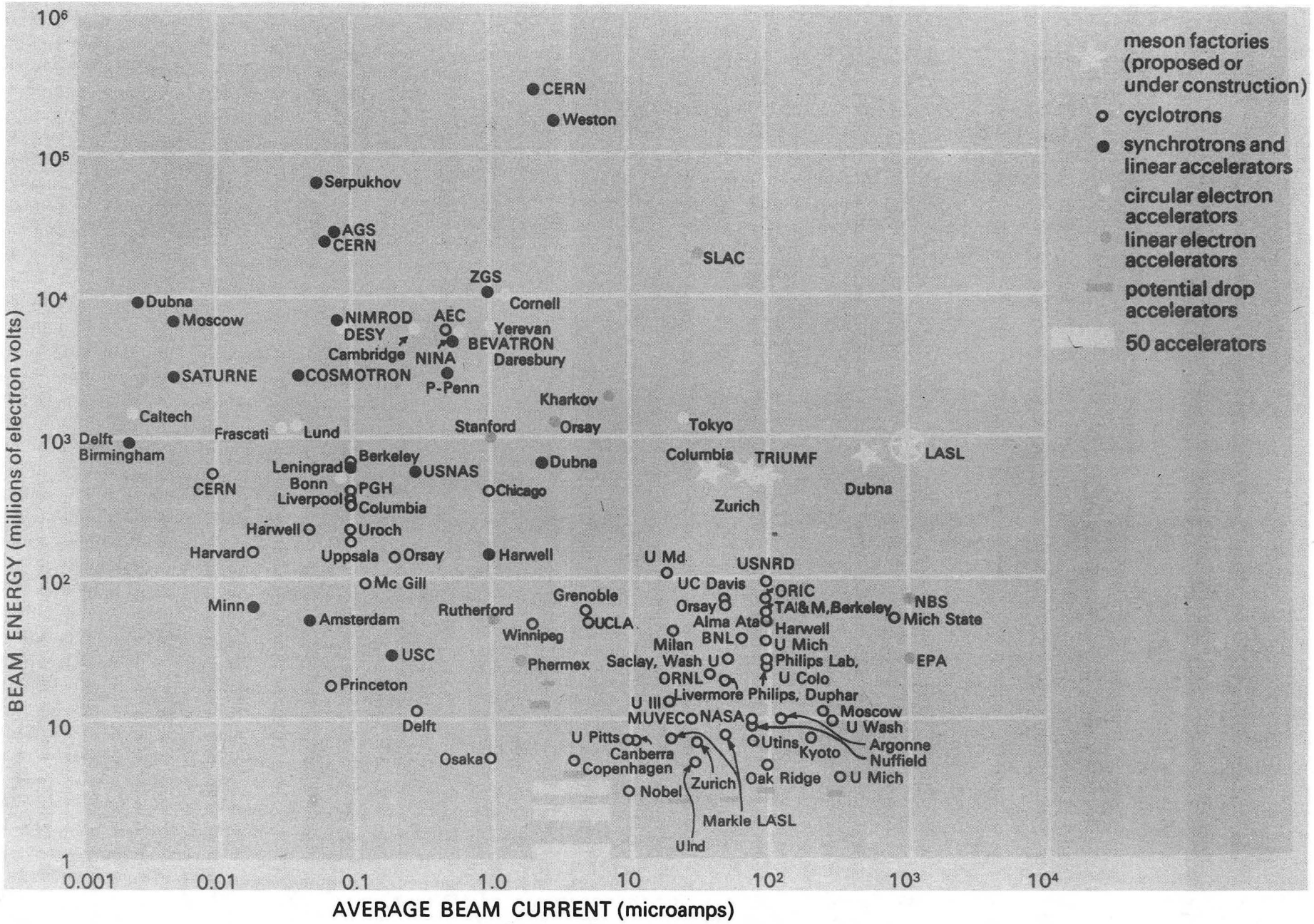

Fig. 1.2

proton accelerators, average currents of a few microamperes are now feasible (CERN II, NAL), while at the Stanford Linear Accelerator Center (which accelerates electrons) the beam current is an order of magnitude higher.

At these energies the available beam power is almost 1 MW (670 KW at SLAC) and dissipation of the heat generated by the interaction of such beams presents a difficult engineering problem. Experiments at the Stanford Linear Accelerator Center, with the electron beam focussed to a spot $\sim$ 1 mm diam, have demonstrated that 30 cm thick metal beam stops are melted through in times ranging from 1 to 10 secs, depending upon the thermal properties of the metal![9] The thermal energy density produced in targets, collimators and backstops by such accelerator beams exceeds that in the cores of fast reactors used for the generation of electricity!

These technological achievements have made possible the development of a large variety of commercially available particle accelerators which can accelerate a wide range of particles to high energies at high beam intensities. This has made possible the industrial application of accelerators to a host of diverse tasks.[1-8]

Burrill[10] documented the increasing uses of accelerators in industry and medicine during the period ending December 1968 and showed the number of accelerators in use to be increasing at the rate of roughly 10% per year, Fig. 1.3. More recently Morgan[11] showed this rate of increase had more than doubled in the interval 1968-1972.

During recent years, a variety of high LET radiation from accelerators have been applied to radiotherapeutic investigations or radiobiological studies necessary prior to their use in radiotherapy.[6,7,8] If widely adopted, considerable numbers of hospital personnel may be exposed to mixed radiation fields.

The International Commission on Radiological Protection (ICRP) has pointed out that at the present time high-LET* radiations contribute only a small fraction of the total general exposure.[12] But, it may well be that the increasing application of accelerators to industry and medicine will lead to a change in the nature of exposures to radiation workers.

---

*LET is an abbreviation for Linear Energy Transfer.

ANNUAL INCREASE IN PARTICLE ACCELERATORS THROUGHOUT THE WORLD (1930 - 1968)

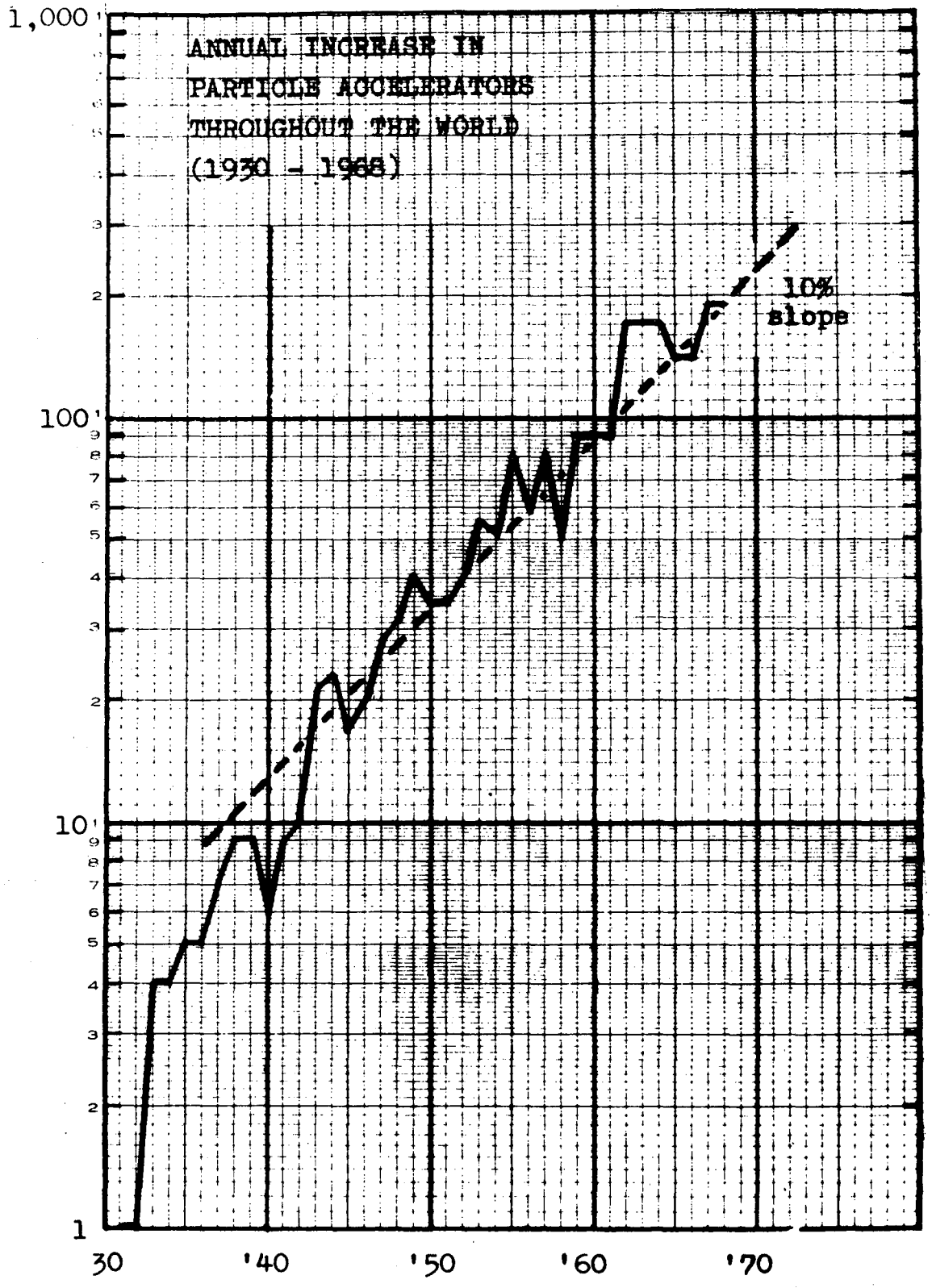

Fig. 1.3

There is still considerable speculation and even controversy as to the possible biological effects on man of the increasing uses of radiation.[13] The effects of low levels on man are not yet fully understood, but it seems probable that the radiation effects due to densely ionizing radiation (high LET) will be greater than those due to lightly ionizing radiation (low LET).[14] As we shall show later (section 2), the radiation environments of many accelerators are particularly rich in high LET radiations; so, as the uses of accelerators increase, more people may be exposed to high LET radiation.

From our present understanding of radiation effects, it is extremely possible that high-LET radiations may have a greater biological impact than their relatively small contribution to general radiation exposure. In view of recent suggestions that the induction of leukemia in man by neutron exposure is greater than has hitherto been thought,[15] the possible biological consequences of widespread exposure to high-LET radiation merits continuing study.

In addition to accelerator-produced radiation, there are other applications of technology that result in exposures to accelerator-like radiation environments. For example, the use of supersonic aircraft for mass transportation will expose large numbers of the general population to an accelerator-like radiation environment.[16]

It is perhaps because the radiation phenomena of high energy accelerators need investigation that much of our basic knowledge of accelerator health physics practices has been obtained at high-energy laboratories. It is at large research institutions that the resources for such fundamental investigations are available. Experience has shown that the radiation environments of high-energy accelerators are in many respects similar to those produced by lower-energy accelerators: neutrons and photons are the dominant components. Consequently, the techniques of measurement developed for their radiation fields may be applied equally to both high- and low-energy accelerators.

For the purposes of this paper, we define "high energy" nuclear facilities to be those that accelerate particles to a kinetic energy greater than 1 GeV. As Table 1.1 shows, there are over forty such high energy facilities in the world presently in operation. These facilities are fairly evenly distributed between the Soviet Union,

Table 1.1

High Energy Particle Accelerators
and Storage Rings

Accelerator Type	Particles Accelerated	Energy	Number
Linear Accelerator	e	$\geq$ 1 GeV	5
	p	$\geq$ 0.5 GeV	1
Synchrotron	e	$\geq$ 1 GeV	9
	p	$\geq$ 1 GeV	17 (including boosters)

Storage Ring Facilities - 10.

United States and Western Europe, with Japan operating three high energy accelerators (Table 1.2).[17]

It is largely the experience obtained at these high energy facilities that will be discussed in this paper.

Table 1.2

World-Wide Distribution of High-Energy Facilities	
Japan	3
U.S.A.	13
U.S.S.R.	10
W. Europe	16

References

Section 1

1. Rosen, L., Relevance of Particle Accelerators to National Goals, IEEE Trans. Nucl. Sci. NS-18, 3, 29 (1971).
2. Evans, A.E., The Expanding Role of the Small Van de Graaff in Nuclear Nondestructive Analysis, IEEE Trans. Nucl. Sci. NS-20, 3, 989 (1973).
3. Avery, R.T. and Keefe, D., Shattering Rock with Intense Bursts of Energetic Electrons, IEEE Trans. Nucl. Sci. NS-20, 3, 1010 (1973).
4. Reinhold, G., Gleyvod, R., and Freiburg, E., 60 KW Accelerator for a Paint Curing Facility, op cit., Ref. (3), p. 1015.
5. Servian, J.G., Production of Radionuclides and Labelled Compounds from Accelerators, Int. J. Applied Radiation and Isotopes, 26, 763 (1975).
6. Boone, M.L. and Wiley, A.L., Fast Neutrons and π^- Mesons in Cancer Therapy, IEEE Trans. Nucl. Sci. NS-18, 3, 36 (1971).
7. Fowler, P.H. and Perkins, D.H., The Possibility of Therpeutic Applications of Beams of Negative Mesons, Nature 189, 524 (1961).
8. Tobias, C.A., Lyman, J.T., and Lawrence, J.H., "Some Considerations of Physical and Biological Factors in Radiotherapy with High-LET Radiations Including Heavy Particles, pi-Mesons and Fast Neutrons:" Chapt. 6 in Progress in Atomic Medicine, 3, 167 (1971), Grune and Stratton, Inc.
9. Busick, D. et al., Beam Safety Considerations of the Stanford Linear Accelerator, Proc. Second Int. Conf. on Accelerator Dosimetry, Stanford, CA, Nov. 5-7, 1969, USAEC Report CONF-691101, p. 782.
10. Burrill, E.A., The Expanding Use of Particle Accelerators in Research Medicine and Industry: A Statistical Review, op. cit. ref. 9, p. 1.
11. Morgan, I.L., Impact of Accelerators on Technology, IEEE Trans. Nucl. Sci. NS-20, 3, 36 (1973).
12. ICRP Publication No. 18, The RBE for High-LET Radiations with Respect to Mutagenesis, Pergamon Press, Oxford, 1972.

13. See for example: Holcomb, R.W., Science 167, 853 (1970).
14. Rossi, H.H. and Kellerer, A.M., Science 175, 200 (1972).
15. Rossi, H.H., The Effects of Small Doses of Ionizing Radiation: Fundamental Biophysical Characteristics, paper read at 24th Annual Meeting of the Radiation Research Society, San Francisco, 27 June - 2 July 1976.
16. See for example: Shaefer, H.J., Science 173, 780 (1971).
17. Fischer, G.E. and Nelson, R.T., Catalogue of High-Energy Accelerators, Stanford Linear Accelerator Center Report, May 1974.

2. The Radiation Environment of High-Energy Accelerators

2.1. Introduction

Despite the large variety of high-energy particle accelerators, both with respect to beam characteristics and utilization, their external radiation environments are often quite similar, and are dominated by photons and neutrons.

In many branches of health physics it has been customary to quantify radiation fields solely in terms of gross properties such as exposure, absorbed dose, and dose equivalent (see section 3). This procedure is inadequate at accelerators. In order properly to perform the tasks required of a health physicist at an accelerator (such as personal dosimetry, the design and construction of radiation-measuring instruments, general radiation and particle beam dosimetry, shielding design or determination of induced activity), it is vital that the detailed composition of the radiation environment be understood in terms of the constituent particles. The study of these environments in terms of the energy spectra of their separate components is still being developed, and more extensive measurements are required. Consequently, the limited information that has been published only describes neutron spectra. But, when supplemented by information from cosmic-ray experiments and neutron transport theory, some general conclusions can be made concerning radiation fields produced by proton accelerators.

Shielding studies have shown that the radiation field reaches an equilibrium condition within a few mean-free paths inside an accelerator shield (see section 4 on shielding). The shape of the neutron spectrum observed at a shield air interface is very close to that which exists within the shield, but may be perturbed at the low-energy end, due to the scattering and leakage through holes in the shielding.

2.2. Historical Background

In the early fifties, following the successful operation of several accelerators in the GeV energy region, interest in accelerator radiation problems had become widespread. A conference held in New York in 1957 indicated the concern of several laboratories in the United States [1], and by 1962 an international meeting was organized in Paris. [2]

Experience at the 184 inch synchrocyclotron at Berkeley and the early proton synchrotrons — the Cosmotron and Bevatron—rapidly established the qualitative nature of their radiation environments outside thick shielding. [3-5] A general rule emerged showing that neutrons between 0.1 and 10 MeV contributed more than 50% to the dose-equivalent contribution of the radiation field; γ-rays and low energy neutrons contributed about 10-20%, and the balance made up by neutrons greater than 10 MeV in energy.

In order to quantify the high energy neutron contribution to dose-equivalent more precisely, Patterson et al. [6] suggested that the equilibrium neutron spectrum low down in the atmosphere produced by the interaction of the primary galactic cosmic radiation (mainly protons) must be very similar to that generated in the shield of a high energy proton accelerator. The cosmic ray neutron spectrum had previously been measured at several altitudes by Hess et al. [7] and was shown to reach equilibrium rapidly (at depths greater than 200 g/cm^2). Using the Hess spectrum and fluence to dose-equivalent conversions given in NBS Handbook 63 [8], Patterson et al. concluded that "by far the largest contribution to total neutron dose comes from neutrons in the energy interval from 0.10 to 30 MeV." [6] Somewhat later Tardy-Joubert [9] pointed out that, at energies above 50 MeV, the Hess spectrum was consistent with that deduced from an analysis of the prong-number distribution of stars produced in nuclear emulsion exposed at different altitudes. [10]

These similarities to the cosmic ray spectrum also explain the relative unimportance of protons in contributing to the dose-equivalent. [11] At energies greater than a few hundred MeV, protons are present in numbers comparable with neutrons. At lower energies, however, protons are depleted by ionization losses. Puppi and Dallaporta [12] have suggested that the neutron/proton ratio in an equilibrium spectrum is of the form:

$$\frac{N}{P} = \frac{W^2}{W^2 - (m_0 C^2)^2} \qquad 2.1$$

where

W is the nucleon total energy,

$m_0 C^2$ is the nucleon rest mass.

Given Eq. (2.1) it is trivial to show that protons contribute little to the dose-equivalent in an equilibrium cascade spectrum.

By early 1965 there was sufficient experience at high energy accelerators at Berkeley [3-6], CERN [13], the Rutherford Laboratory [11-14], Saclay [9], and elsewhere [15] to confirm that the cosmic ray and accelerator produced neutron spectra were indeed quite similar. Thus, for example, at the 1966 Vienna meeting Perry [11] summarized experience at the British 7 GeV proton synchrotron thus:

"...the energy spectrum varies from place to place but always falls off rapidly with increasing energy. Most of the neutron flux and dose equivalent is due to neutrons with energies between 0.1 and 10 MeV. The dose contributions from thermal and very high energy neutrons are both very small."

Table 2.1 shows a summary of data given by Perry showing the composition of the radiation field outside the shielding of a 7 GeV proton beam.

The increased confidence this experience with accelerators in the GeV energy region gave strength to the earlier arguments of Patterson et al. [6] concerning the probable shape of the neutron equilibrium spectrum and led to

Table 2.1. Radiation spectrum above Nimrod extracted proton beam shielding. (From Perry, 1967.)

Type of radiation	Energy range	Estimated % of neutron flux density	Estimated % of total dose-equivalent
Neutrons	< 1 eV	< 7	< 1
Neutrons	1 eV - 0.7 MeV	70	20
Neutrons	0.7 - 3 MeV	15	35
Neutrons	3 - 7 MeV	7	25
Neutrons	7 - 20 MeV	1.5	5
Neutrons + protons	20 - 100 MeV	1	5
Neutrons + charged particles	> 100 MeV	0.5	4
Other particles + gammas	–	–	< 2

the use of the Hess spectrum in the design of the shields of several high energy accelerators in the early sixties. [16-20] For this assumption to be valid it was necessary that the equilibrium spectrum be determined by the character of the interaction mechanisms of the nuclear cascade and essentially independent of the energy of the incident proton. Some theoretical cascade calculations by Riddell [21] lent support to this assumption but the extrapolation from experience in the GeV energy region to hundreds of GeV could not be made without reservation. Patterson [5] indicated the need for more detailed information of the neutron spectrum between 1 and 10 MeV where "there may or may not be a flattening due to the production and scattering of evaporation neutrons." Nevertheless by early 1965 there was a good quantitative understanding of the radiation environments outside particle accelerator shielding.

2.3. Operational Experience at High-Energy Accelerators

2.3.1. High-Energy Proton Accelerators

As we have seen, in the latter part of the fifties, experience at the 184-inch Synchrocyclotron and Bevatron (Lawrence Berkeley Laboratory) and the Cosmotron (Brookhaven) allowed estimation of the qualitative nature of their radiation environments outside thick shielding[3,5]. Although detailed spectra were not obtained, a general rule emerged for proton accelerators showing that neutrons between 0.1 and 10 MeV contributed more than 50% to the total dose equivalent in the radiation field (see section 2.2). This fact was explained by analogy with the cosmic ray produced neutron spectrum.

By 1965 there was sufficient experience at many high-energy proton accelerators around the world to confirm that the neutron spectra outside accelerator shields and the cosmic-ray spectrum were, in general, quite similar[3-5,9,13,14,22]; any attempts to measure proton spectra have not been reported.*

There were, however, apparent discrepancies in some data. Table 2.2[23-25] gives a typical example. The relative composition of dose equivalent measured through thick shielding above an accelerator target is given for a concrete shield and for an earth shield at the CERN proton synchrotron (CPS). The data measured above the concrete shield are very similar to those reported at other accelerators, such as the British 7-GeV proton synchrotron[11,14] and suggested a neutron spectrum similar to that produced by cosmic rays[6], while the data measured above an earth shield indicated

---

*Recently, Aleinikov et al. have reported proton spectrum measurements at the Dubna synchrocylotron, using counter telescope techniques. (Aleinkov, V.E., Gerdt, V.P. and Timoshenko, G.N., Measurement of Spectra of High-Energy Protons Generated in the Shielding of a 680 MeV Synchrocyclotron - Joint Institute of Nuclear Research, Dubna, Report P16-9400 (1975).)

a relatively large contribution to the dose equivalent by high-energy neutrons. Relative data, as in Table 2.2, are not adequate to determine whether the high fraction of dose equivalent contributed by high-energy particles was due to a deficit of low-energy neutrons or to a surfeit of high-energy neutrons. For this, more specific information on the neutron spectrum would be necessary. In the past ten years more specific information on the neutron spectra found around accelerators has been obtained by the use of nuclear emulsions and activation detectors.[26]

Table 2.2. Composition of radiation fields above thick shields at the CPS

Radiation Component	Percentage of dose equivalent	
	Above concrete shield bridge[a]	Above target through earth shield[b]
Thermal neutrons	11-12	<1-3
Fast neutrons (0.1 MeV < E < 20 MeV)	50-70	10-37
High-energy particles (E > 20 MeV)	2-25	52-89
γ rays and ionization from charged particles	2-19	1-13

[a]Reference 23

[b]References 24,25

Typical Neutron Spectra Measured at Proton Accelerators. The application of threshold detectors to accelerator radiation environments at several laboratories simultaneously, rapidly expanded our understanding.

Figure 2.1 shows several typical unnormalized neutron spectra obtained outside thick shields at proton synchrotrons, where $E\phi(E)$ is plotted as a function of neutron energy [$\phi(E)$ is the differential energy spectrum].

In such a plot 1/E spectrum becomes a horizontal line (Fig. 2.1a). This representation of the Hess cosmic-ray spectrum (Fig. 2.1b) clearly shows the large excess of neutrons in the MeV region (due to evaporation processes) in comparison with a 1/E spectrum. At lower energies the spectrum is 1/E in character, but there is a noticeable dearth of thermal neutrons.

The neutron spectrum obtained above the concrete shielding around targets at the CPS is shown in Fig. 2.1c. (Compare with Table 2.2.) The spectrum is seen to be 1/E in character from about 1 MeV down to thermal energies. This would be expected from neutron slowing-down theory in a hydrogenous medium, such as concrete. At about 1 MeV the evaporation peak, also evident in the Hess spectrum, is clearly seen, and the spectrum shows a rapid decline at energies above 50 MeV.

Figure 2.1d shows the neutron spectrum measured above the earth shield of the CPS. (Compare with Table 2.2.) This spectrum is depleted of neutrons below about 1 MeV, but in other respects is similar to the spectrum shown in Figure 2.1e. The water content of the earth shield through which the neutrons penetrated was very high (approximately 15% by weight) compared to concrete (few percent by weight), and so this paucity of low-energy neutrons is to be expected.

The neutron spectrum outside the Bevatron shielding (Fig. 2.1e) is intermediate in character between the two spectra measured at the CPS and suggests that the hydrogen content of the concrete at Berkeley is higher than that at CERN. (To the author's knowledge this speculation has never been tested.)

Finally, Fig. 2.1f shows the spectrum around a steel-shielded proton beam of the British 7-GeV synchrotron. Compared with the other spectra shown, a large buildup of neutrons below 1 keV is seen, and is attributed

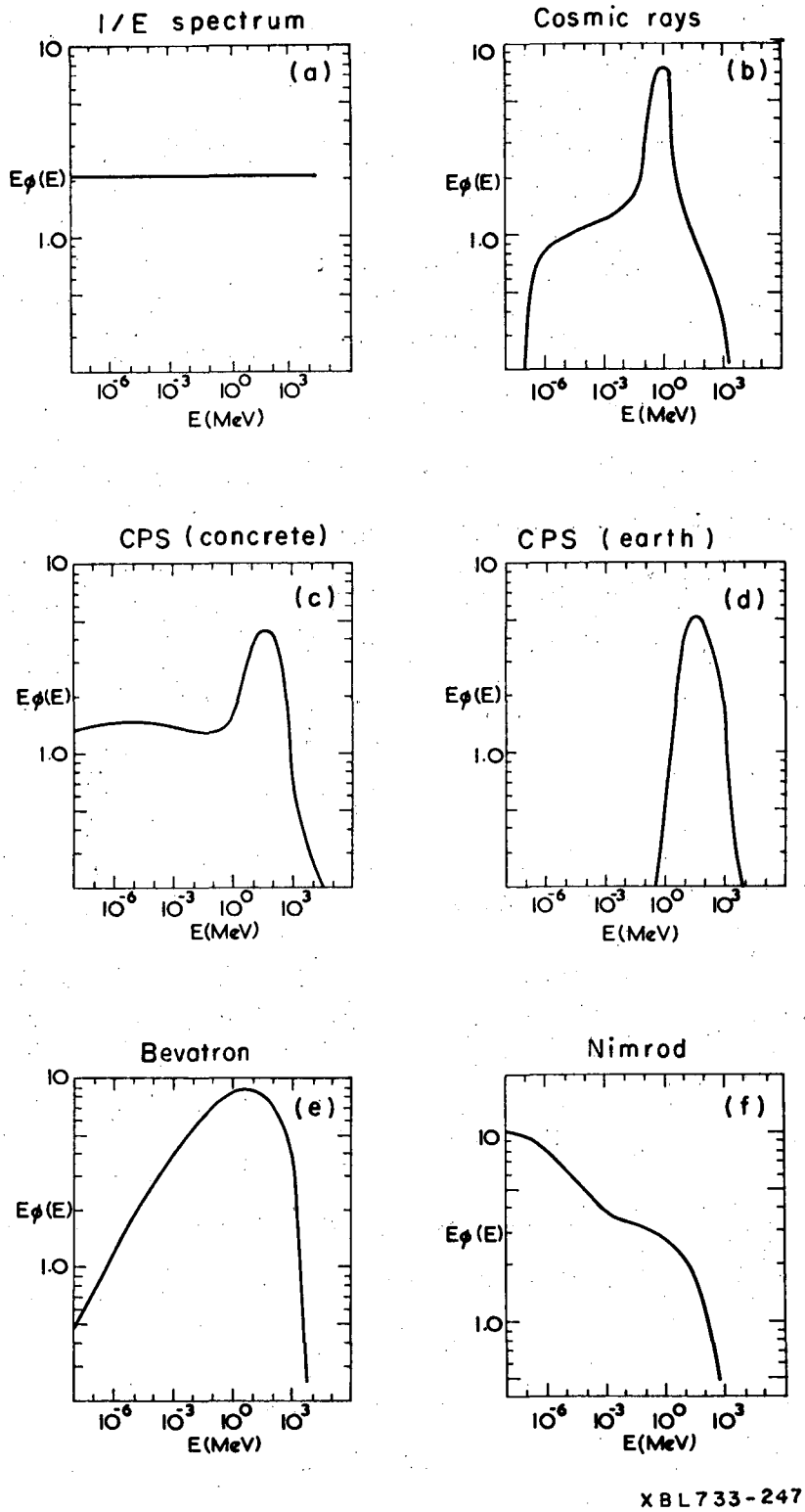

Fig. 2.1. Some typical high-energy neutron spectra. (a) 1/E spectrum (for comparison). (b) Cosmic-ray spectrum. (c) Spectrum at concrete shielding bridge at CPS. (d) Spectrum on earth shield of CPS. (e) Spectrum outside Bevatron shielding. (f) Spectrum outside steel shielding of Nimrod external proton beam.

to leakage of low-energy neutrons through holes in the shielding.[27] It is unlikely, however, that this is the entire explanation because such a buildup is frequently observed outside steel shields. For example, measurements of the neutron spectrum emerging from the main Bevatron magnet identified a very large component near 100 keV[5], while Perry and Shaw[14] observed large increases in radiation levels when steel replaced concrete in shield construction. However, recent theoretical calculations of the neutron spectrum produced in steel by the interaction of 200-GeV protons do not indicate a buildup[28]. Such a discrepancy shows that although we now have a fair understanding of high-energy environments, more needs to be done.

It will be shown later how such neutron spectral data may be used to calculate dose equivalent. Gilbert et al.[29] have given the distribution of dose equivalent as a function of energy for several of the neutron spectra shown in Fig. 2.1.

2.3.2. Electron Accelerators

Early measurements at high-energy electron accelerators were principally concerned with the development and transmission of the electromagnetic cascade through the shield.[30-34] These studies confirmed that there was good theoretical understanding of these processes.[35] Photon spectra at accelerators up to now have not been measured, but a β-γ spectrometer and a NaI(Tl) anticoincidence γ-ray spectrometer have been used to measure dose rate for space missions.[36,37] The application of such instruments to accelerator radiation fields may prove illuminating.

Bathow et al.[31,38] measured significant neutron production at the DESY 4-GeV electron synchrotron. De Staebler has shown that at high energies and intensities the radiation environments of electron and proton accelerators will be quite similar outside their shields.[16] Increasing attention

has been given to the measurement of neutrons in recent years. Thus, for example, measurements outside thick shielding at the Stanford Mark III 1-GeV electron linac showed that neutrons were the dominant component of the radiation field; in addition, a significant flux density of neutrons above 20 MeV was identified.[39-41] Neutrons are a major component of the radiation field[42] in the earth shield at the 4-GeV electron synchrotron NINA, and are the only significant radiation component surviving at large distances from the SLAC 20-GeV electron linac.* Recently Pszona et al.[43] have demonstrated the dominating presence of neutrons around the 1-GeV Frascati synchrotron by measurements with ionization chambers.

In comparing the radiation environments of electron and proton accelerators it is interesting to note that close to the primary proton beam, very high photon fluxes have been observed at the 7-GeV synchrotron Nimrod[44] and the CPS.[29] The source of these photons has not been established, but has been tentatively attributed to the decay of π^0 mesons produced by proton interactions.

2.2.3. Accelerators with Energies > 10 GeV

At high energies (greater than about 10 GeV) the production of energetic muons can be sufficiently great to pose a serious shielding problem at both electron and proton accelerators. Cowan[45] has reported that substantial muon intensities were observed downstream from targets when the BNL 33-GeV AGS first came into operation. Several authors, including Keefe[46,47], Bertel et al.[48], Theriot, Awschalom and Lee[49], and Kang et al.[50] have shown that for the new generation of accelerators above 100 GeV muons will dominate shielding requirements in regions downstream of beam targets.

*D. Busick, SLAC, Private communication.

At these high energies we need more measurements of neutron spectra outside of various shielding material in order to study the influence of shield construction. In particular we need to extend our knowledge of these spectra above 100 MeV. At these higher energies it may prove to be technically more feasible to detect the equilibrium proton spectrum. Penfold and Stevenson[51] have reported the use of a proton telescope to detect intense sources of radiation inside thick shields along an external proton beam. The application of spark chambers to this problem should prove extremely helpful; Hajnal et al.[52] have reported the use of an optical spark chamber to study the secondary-neutron energy spectra emerging from a 40-cm-thick iron shield bombarded by 2.9-GeV protons. Rindi[53] and his co-workers[54-56] described the construction of an instrument that utilizes multiwire spark chambers with magnetostrictive readout and that may be used for measuring neutron and proton spectra up to energies of about 300 MeV in low-intensity fields.

Very little data currently exist on the radiation environments of heavy-ion accelerators but it seems probable that there will be little qualitative difference from the features exhibited by proton accelerators.

References

Section 2

1. Proc. Conf. on Shielding of High-Energy Accelerators, New York, New York, April 11-13, 1957, USAEC Report TID-7545.

2. Proc. Premier Colloque International sur la Protection auprès des Grands Accelerateurs, Paris, France, January 18-20. 1962, Presses Universitaire de France, 108 Bd. Saint-Germain, Paris (1962).

3. SMITH, A. R., The Stray Radiation Field of the Bevatron, University of California Radiation Laboratory Report UCRL-8377, July 1958.

4. SMITH, A.R., Measurement of Radiation Field Around High Energy Accelerators, op cit. ref. 2, p. 137.

5. PATTERSON, H. W., Accelerator radiation monitoring and shielding at the Lawrence Radiation Laboratory, Berkeley, in Proc. First Symposium on Accelerator Radiation Dosimetry and Experience Brookhaven National Laboratory, November 1965, CONF-651109, p. 3.

6. PATTERSON, H. W., HESS, W. N., MOYER, B. J., and WALLACE, R. W., The flux and spectrum of cosmic ray produced neutrons as a function of altitude, Health Phys. 2 (1959) 2.

7. HESS, W. N., PATTERSON, H. W., WALLACE, R W., and CHUPP, E. L., The cosmic ray neutron energy spectrum, Phys. Rev. 116 (1959) 445.

8. NCRP, Protection Against Neutron Radiation Up to 30 MeV, National Bureau of Standards (NBS Handbook #63), Washington, D. C. (1957).

9. Tardy-Joubert, P., Method and Experience of Dosimetry Around Saturne, op cit ref. 5, p. 117.

10. Rossi, B., High-Energy Particles, Prentice-Hall, New York (1954), p. 488.

11. PERRY, D. R., Neutron dosimetry methods and experience on the 7 GeV proton synchrotron, Nimrod, in neutron monitoring," in Proc. Symp. on Neutron Monitoring for Radiological Protection, IAEA, Vienna (1966), p. 355.

12. PUPPI, G., and DALLAPORTA, N., "The equilibrium of the cosmic ray beam in the atmosphere," in Progress in Cosmic Ray Physics, Vol. 1, p. 317 (WILSON, J. G., ed.)

13. BAARLI, J., and SULLIVAN, A. H., Radiation dosimetry for radiation protection purposes near high-energy particle accelerators, Health Phys. 11 (1965) 353.

14. PERRY, D. R. and SHAW, K. B., Radiation levels in and around Nimrod, op. cit. Ref. 5, p. 20.

15. See for example: Proc. First Symp. on Accelerator Radiation Dosimetry and Experience Brookhaven National Laboratory, November 3-5, 1965, CONF-651109.

16. DESTAEBLER, H., Transverse Shielding for the Stanford Two-Mile Accelerator, Stanford Linear Accelerator Center Report SLAC-9, Nov. 1962. See also: Similarity of shielding problems at electron and proton accelerators, op. cit. Ref. 15, p.429.

17. Lawrence Radiation Laboratory, 200 BeV Design Study (2 Vols.), Lawrence Radiation Laboratory Report UCRL-16000, June 1965.

18. THOMAS, R. H., "Radiation field observed around high energy accelerators," in Progress in Radiology, Vol. 2, Excerpta Medica Foundation, Amsterdam (1967), p. 1829.

19. CERN Report on the Design Study of a 300 GeV Proton Synchrotron by the CERN Study Group on New Accelerators (2 vols.), CERN Internal Report, CERN 563 (1964).

20. Cochran, D.R.F., Israel, H.I., The Radiation and Shielding Design Factors for the Los Alamos Meson Physics Facility, op cit ref. (15), p. 459.

21. RIDDELL, R. J., High Energy Nuclear Cascades in Matter, Lawrence Radiation Laboratory Report UCRL-1189, April 1965.

22. Komochkov, M.M., Engineering Compendium on Radiation Shielding Vol. 3, p. 171, Springer-Verlag, New York (1970).

23. Baarli, J. 1964. Private communication to Middlekoop, W. C., reported in CERN Intern. Rep. AR/INT/SG 64-6

24. Capone, T. et al 1965. CERN Intern. Rep. DI/HP/71

25. Baarli, J., Sullivan, A. H. 1965. See Ref. 15, p 103.

26. Thomas, R.H., Neutron Dosimetry at High-Energy Accelerator Particle Accelerators, in Neutron Monitoring for Radiation Protection Purposes, Vol. 1, p. 327, IAEA, Vienna 1973.

27. Stevenson, G. R. 1972. See Ref. 26.

28. Gabriel, T. A., Santoro, R. T. 1972. ORNL-TM-3945

29. Gilbert, W. S. et al 1968. UCRL Rep. 17941

30. Bathow, G., Freytag, E., Tesch, K. 1965. Nucl. Instrum. Methods 33: 261

31. Bathow, G., Freytag, E., Tesch, K. 1967. Nucl. Phys. 82: 669

32. Tesch, K. 1969. See Ref. 23, p 595

33. Busick, D. et al. 1969. Proc. Second Int. Conference on Accelerator Dosimetry, Stanford, California, USAEC Rep. CONF-691101, p. 782 (1969).

34. Ladu, M. 1969. Progr. in Nucl. Energ. Series XII, Part 1, p 365. New York: Pergamon

35. Bathow, G., Freytag, E., Kajikawa, R., Köbberling, M. 1969. See Ref. 24, p 222

36. Farmer, B. J., Rainwater, W. J. 1968. Report 0-71100/8R-S. NASA Contract NAS 9-7565

37. Farmer, B.J., Johnson, J.H., and Boswell, R.G., Proc. Nat. Symp. Natural and Man-Made Radiation in Space, NASA-TM-X-2440, p. 142 (1972).

38. Bathow, G., Freytag, E., Tesch, K. 1967. Nucl. Instrum Methods 51: 56

39. Carter, T.G., Thomas, R.H., Stanford University Internal Report RHT/TN/69-11 (1969)

40. Chakalian, V. M., Thomas, R. H. 1969. Stanford Univ. Intern. Rep. RHT/TN/69-11

41. Thomas, R. H. 1969. Stanford Univ. Intern. Rep. RHT/TN/69-18

42. Coleman, F.J., Thomas, D.C., and Saxon, G., An Experiment to Determine Shielding Requirements for a Multi-GeV Electron Synchrotron Ring, Daresbury Nuclear Physics Laboratory Report, 1972.

43. Pszona, S. et al., INR Report 1415, Warsaw (1972).

44. Shaw, K.B. and Thomas, R.H. Health Physics 13, 1127 (1967).

45. Cowan, F.P., op cit. ref. 2., p. 143.

46. Keefe, D., LBL Internal Report UCID-1008 (1964).

47. Keefe, D. and Noble, C.M., Nucl. Instrum. Methods 69, 245 (1968).

48. Bertel, E., de Sereville, B., Freytag, E., Wachsmuth, E., in Radiation Problems Encountered in the Design of Multi-GeV Facilities (Ed. K. Goebel) CERN Internal Report 71-12, p. 79 (1971).

49. Theriot, D., Awschalom, M., Lee, K., in Proc. Int. Cong. Radiat. Prot. Accel. and Space Radiat., Geneva, CERN 71-16, p. 641.

50. Kang, Y. et al., Particle Accel. 4, 31 (1972).

51. Penfold, J. and Stevenson, G.R., Rutherford Laboratory Internal Report, RP/PN/28 (1968).

52. Hajnal, F. et al., Nucl. Instrum. Methods 69, 245 (1969).

53. Rindi, A., op cit ref. 33, p. 600.

54. Rindi, A., A Spectrometer for Measuring Charged Particles and Neutrons, Nucl. Instr. Methods 116, 471 (1974).

55. K. Mamont-Ciesla and Rindi, A., Spark Chamber Neutron and Proton Spectrometer: First Report on Performance (1974).

56. Lim, C.B., Ph.D. Thesis, University of California, Lawrence Berkeley Laboratory Report LBL-1719(1973).

3. Dosimetry at Research Accelerators

3.1. Introduction

In order to decide what techniques of dosimetry are of most value to high-energy accelerators, it is useful to delineate the purposes to which the results of these measurements will be put in carrying out radiation protection at accelerators.

Radiation protection means more than the mere measurement of radiation environments. It also means the control of the interaction of people (and sometimes instruments) with radiation. "Control of radiation hazards involves (a) their anticipation and prior estimation; (b) their measurement or field evaluation, and (c) the devising of shielding and procedures which ensure adequate safeguards, yet allow experimental freedom." (1)

Dosimetric measurements will be needed in five quite distinct areas:

1. For radiation protection purposes, normally outside extensive shielding, at radiation intensities of a few millirem per hour.
2. Beam intensity measurements, and measurements very close to particle beams to determine the intensity of source strengths for shielding calculations, regions of high beam loss to improve accelerating operating conditions and reduce the induction of radioactivity in accelerator components.
3. Accident dosimetry in the case of personnel exposure in,or close to, intense particle beams.
4. Environmental monitoring, at very low radiation intensties (~10 millirem per year) to understand and document the radiobiological impact of an accelerator facility on the environment. (These measurements are described in section 6.)
5. Interpretation of routine personnel exposures.

High Energy particle accelerators are primarily research instruments whose radiation environments are initially unknown and often complex. The dosimetry of their radiation fields therefore presents a great challenge to the health physicist. It is extremely dangerous, under these conditions, to assume that techniques of radiation measurement familiar in other applications will give reliable data. Before one begins to measure he must know what he is measuring! Some fundamental understanding of accelerator radiation environments is necessary for this purpose. A good dosimetric program for research accelerator radiation protection encompasses:

(a) Knowledge of the primary radiation produced by the accelerator, under all possible modes of operation, and understanding of the interactions of this primary radiation with targets, collimators, and other accelerator components.

(b) Understanding of the transmission of this primary radiation (and its interaction products) through shielding materials.

(c) Development of techniques to measure the great variety of radiation environments produced.

It is this fundamental approach to accelerator radiation protection that will be stressed here.

Such a program permits:

1) The prediction of the response of personal dosimeters in accelerator radiation environments.

2) The design of accelerator-radiation survey instruments.

3) The modification of accelerator radiation fields by shielding.

The lessons learned in the development of techniques of measurement in mixed radiation fields for accelerators and the interpretation of these measurements are of general interest to the health physicist because they bear directly on the problem of developing a general, self-consistent, and practical scheme of dosimetry in radiation protection. [2-5]

The techniques widely used over the past twenty years to understand accelerator radiation environments includes:

(1) For the determination of the flux density and spectrum of unidirectional fast neutrons: proportional counters, scintillation counters, photographic emulsions. [7]

(2) For the determination of thermal neutron flux densities, regardless of direction: counting techniques based on neutron capture in boron, activation foils. [7]

(3) For the approximately absolute determination of energy flux density delivered by fast neutrons, independent of energy spectrum or angular direction: polyethylene-lined proportional counter. [7]

(4) For the contribution to energy absorption in tissue due to neutrons, where the effects due to γ-rays are known and may be corrected for: cavity chambers or tissue equivalent chambers. [7]

(5) For the determination of quality factors of mixed radiation fields, recombination chambers have been used at some laboratories. [8, 9]

(6) For the determination of neutron spectra over a wide energy range threshold detectors, particularly activation threshold detectors, are extremely useful. [10]

3.2. The Dose Equivalent

Any discussion of dosimetry for radiation protection purposes -- unless it is to become "a tale told by an idiot, full of sound and fury, signifying nothing" -- cannot avoid a discussion of that much abused term --"dose equivalent."

A. The Dose Equivalent

The numerical scale used in radiation protection is expressed in terms of the parameter dose equivalent whose unit is the rem. Conceptually, dose equivalent is a measure of radiation used in radiation protection, based upon its ability to induce disease (somatic and genetic injury) in humans, who are chronically exposed to low intensities of ionizing radiations (11). (A complete definition of dose equivalent would more adequately define the terms "disease," "chronically exposed," and "low intensities." However, with our present limited understanding of the biological effects of ionizing radiations in humans, such a definition can only be approximated.) Recent discussions in the literature on the methods of evaluating the dose equivalent in high-energy radiation fields, have clarified the concept of dose equivalent. So, we believe it is useful to review this development.

Early observations in radiology and radiobiology suggested that the dominant parameter which largely determined subsequent injury to irradiated tissue was the quantity of energy absorbed per unit mass of tissue. (Absorbed dose is usually measured in units of rads where 1 rad = 100 ergs g^{-1}.) More sophisticated experiments showed that absorbed dose was not an entirely adequate parameter, and that to better express biological damage, absorbed dose had to be weighted by other parameters, which depended upon the characteristics of the radiation. This problem was empirically solved in radiobiology by expressing exposures to different radiations in terms of absorbed dose of some standard radiation (usually x or γ rays of specified energy). Thus the bio-

logical effects of irradiation by all different types of radiation would be identical to that from χ rads of standard radiation where

$$\chi = \sum_{i=1}^{n} R_i D_i \qquad (3.1)$$

and R_i is the Relative Biological Effectiveness (RBE) of the ith radiation defined by $R_i = D_x / D_i$, and D_x, D_i are, respectively, the absorbed doses of the standard radiation and the ith radiation required to produce the same biological effect.

The quantity defined in Equation 3.1 that is referred to in the literature as the RBE dose, is clearly an equivalent dose of standard radiation and has the same physical dimensions as those of absorbed dose [as does dose equivalent (12)]. Radiobiologists have measured many RBE's, even for a specific type of radiation, depending upon the biological system, the biological effect considered, the dose rate and distribution, and many other biological and physical factors. One parameter found to have an important influence on the RBE is the average LET, or collision stopping power of the ionizing radiation. [LET still continues to play an important role in the thinking of radiobiologists although recently some have suggested it has only limited value in specifying radiation quality(13-15).]

For radiation protection purposes, the appropriate "RBE's" required would be those for chronic low-level exposures of humans. The biological effects of low-level exposures are not entirely known but probably include carcinogenesis, leukemia induction, life-span shortening and deleterious mutations. There are no data on these bio-

logical effects in humans exposed at sufficiently low doses and dose rates, and furthermore it seems unlikely that data will be directly obtained in the foreseeable future, since such human experiments are not feasible. Nor does it seem likely that epidemiological studies will greatly alleviate this situation, if the risks of somatic injury are of the magnitude estimated by the International Commission on Radiological Protection (ICRP)(16,17). Any values of RBE currently used in radiation protection are, therefore, extrapolations from epidemiological studies of humans acutely exposed or from animal experiments, and are essentially administrative in character.

The solution adopted by the ICRU/ICRP was to express the "RBE used in radiation protection" as the product of several modifying factors. Provision was made for several such factors including those which take account of LET (the Quality Factor), the nonuniform spatial distribution of absorbed dose, and differences in the absorbed dose rate(18). For external radiation exposure, however, only the Quality Factor (Q), which accounts for the difference in LET of ionizing radiations at the locations of interest, is defined. When ionizing radiation of more than one LET, L, is present at the point of interest, the dose equivalent at that point may be expressed by a modification of Equation 3.1 as (19)

$$H = \sum_{i=1}^{n} Q_i D_i \, . \qquad (3.2)$$

In practice, the ionizing particles producing the absorbed dose have a continuous distribution in L, and Equation 3.2 becomes(20)

$$H = \int_0^{L_{max}} Q(L) \cdot D(L)\, dL \qquad (3.3)$$

where D(L) is the absorbed dose per unit interval of LET due to particles with LET between L and L + dL. L_{max} is the maximum value of LET at the point of interest. Dose equivalent in high-energy environments is evaluated from a knowledge of the parameters of the radiation environment by calculating the D(L) distribution as a function of depth and using the relationship between Q(L) and L defined by the ICRP(21) Figure 3.1.

B. Dose-Equivalent–Depth Distributions

It is the current practice of regulatory organizations to set maximum permissible limits for the dose equivalent (MPD) in certain so-called "critical organs" such as the gonads, red bone marrow, thyroid, etc. For radiation protection purposes the dose equivalent in these critical organs must be calculated to determine whether those MPD's have been exceeded.

The quantity H, as defined by Equation 3.3 in principle may be calculated as a function of position in the human body, under any irradiation conditions. In practice, however, such detailed calculations, involving as they do complex details of geometry and nuclear interactions, require extensive computing facilities for their execution. Furthermore, even with the aid of large digital computers, certain simplifications have been necessary to make the calculations tractable.

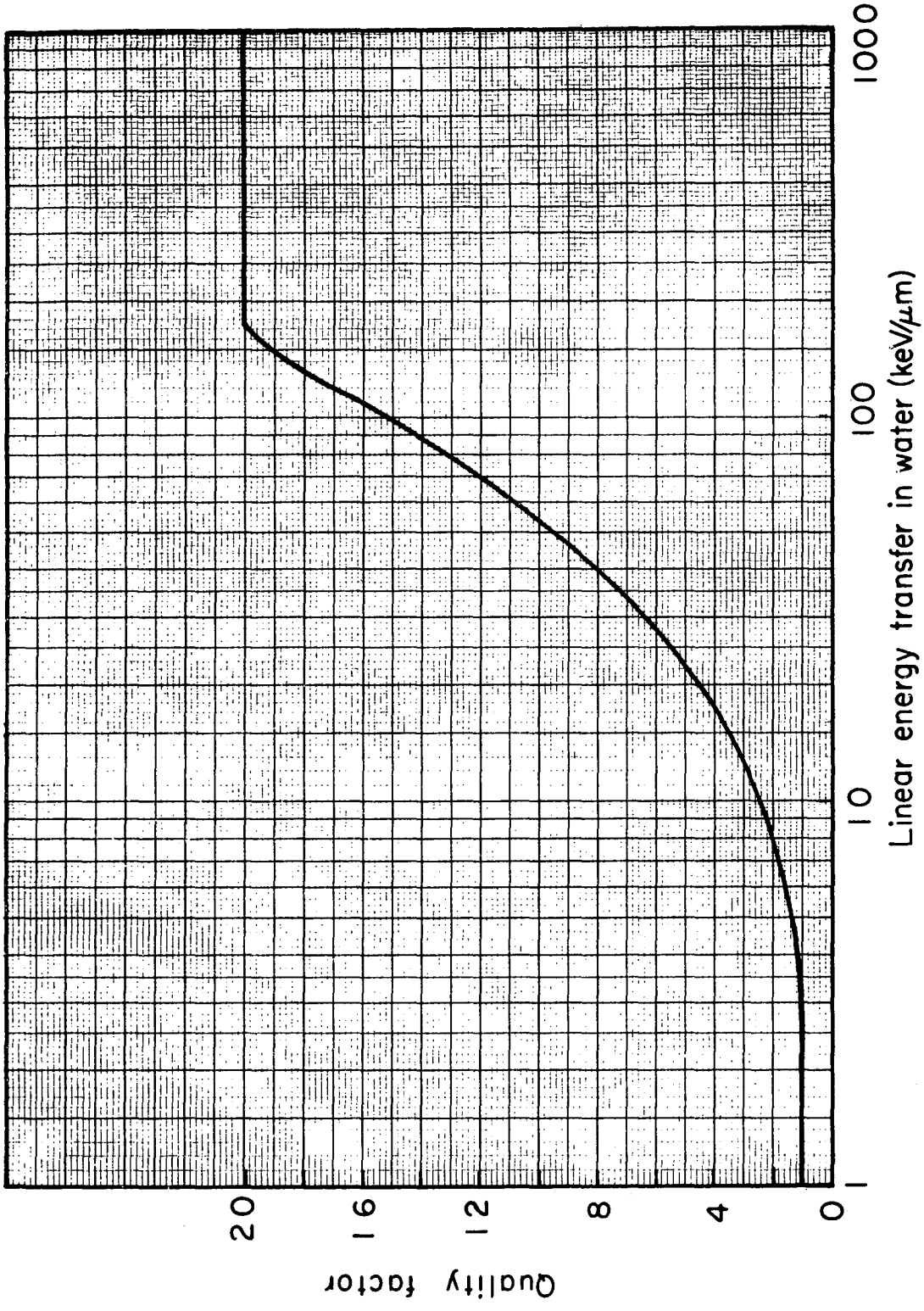

XBL733-2476

Fig. 3.1

At present most calculations have been made under limited radiation conditions for uniform, semi-infinite slabs of tissue-like material (e.g., water, polystyrene, "standard-tissue"), but an increasing number of calculations are being made for finite phantoms (parallelepipeds, cyclinders, elliptical cylinders). In addition, attention is being given to the effects of nonuniform body compositions(22). In the case of irradiation by neutrons, several summaries of these calculations have been published(23); comparison with experimental measurements indicates good agreement(24).

C. Conversion Factors

In selecting a single set of particle-flux-density to dose-equivalent rate conversion factors as a function of particle energy, it is conventional to choose those irradiation conditions that maximize the dose equivalent in the body. These generally occur for unilateral irradiation by a normally incident beam of particles. In addition, such conversion factors are derived from the maximum in the calculated dose-equivalent–dose distributions. Figure 3.2 shows conversion factors for electrons, neutrons, photons, and protons derived in this way by ICRP. In practice it is usually necessary to evaluate dose equivalent due to particles distributed over a range of energies.

The dose-equivalent rate $\dot{H}$ may be approximated by the equation

$$\dot{H} = \int_{E_{min}}^{E_{max}} \phi(E)dE/g(E), \qquad (3.4)$$

where g(E) is the appropriate conversion factor for particles of energy E, and E_{min}, E_{max} are the appropriate energy limits.

Because the conversion factors g(E) are derived from irradiation conditions which maximize the dose at each energy, the use of Equation 3.4 may overestimate the dose equivalent due to a continuous particle spectrum. Equation 3.4 expresses the sum of the maxima of the dose-equivalent depth curves at each energy rather than the maximum of the sum of the dose-equivalent distributions from each component of the spectrum(25).

For irradiation by particles extending over a wide energy range, Shaw et al (3) have suggested that the dose equivalent should be obtained by calculating the dose equivalent distribution in the body due to the entire spectrum. The maximum dose equivalent in the body (or the dose equivalent in the internal organs) may then be evaluated. They have reported such calculations for some typical accelerator neutron spectra (see Fig. 2.1 and showed that the use of Equation 3.4 with these spectra was accurate enough for practical purposes. This may be seen from Table 3.1 which compares effective conversion factors averaged over the entire energy range. In column 1 is given approximate values obtained using Eq. 3.4 [reported by Gilbert et al (2)]; Column 2 gives more precise values reported by Shaw et al (3). There is essential agreement between these two sets of values.

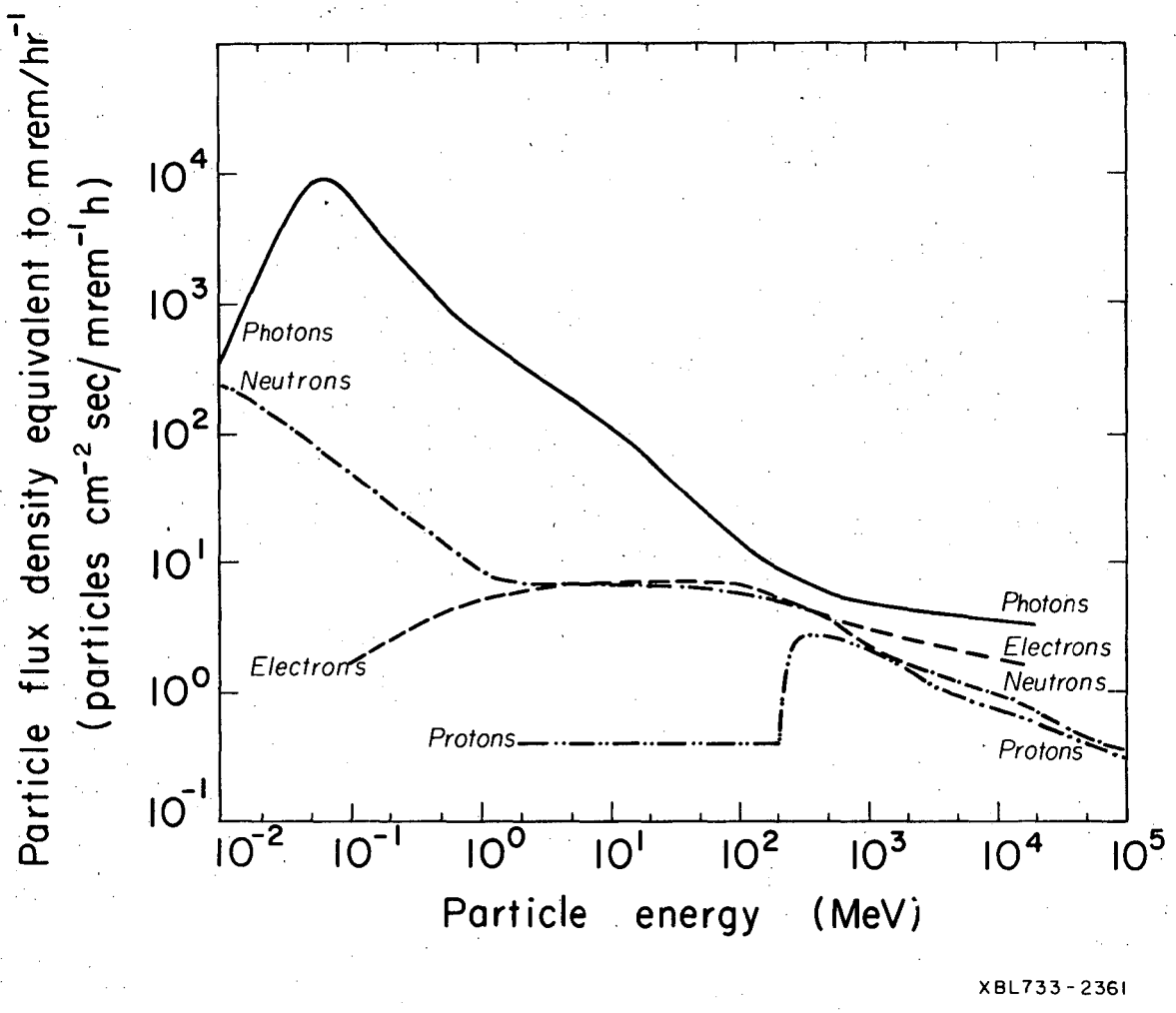

Fig. 3.2

Table 3.1. Effective conversion factors for neutron spectra

Spectrum	Effective neutron conversion factors $\left(\frac{n/cm^2\ sec}{mrem/h}\right)$	
	Gilbert et al (2)	Shaw et al (3)
Cosmic ray	12.1	14.1
Bevatron	8.8	11.9
CERN synchrotron bridge	7.3	12.1
CERN ringtop	4.3	5.1
1/E	4.7	6.4

3.3. Dosimetric Techniques at Research Accelerators

As we have seen, in many branches of health physics it has been customary to quantify radiation fields solely in terms of gross properties such as exposure, absorbed dose, and dose equivalent. This procedure is inadequate at accelerators. In order properly to perform the tasks required of a health physicist at an accelerator (such as personal dosimetry, the design and construction of radiation-measuring instruments, general radiation and particle beam dosimetry, shielding design or determination of induced activity), it is vital that the detailed composition of the radiation environments in terms of the energy spectra of their separate components is still in its early stages; techniques of measurement and data analysis are still being developed, and more extensive measurements are required.

Neutron spectrometry techniques

a. Nuclear emulsions. Lehman and Fekula (26) have summarized the neutron spectra determined at the Bevatron from the measurement of recoil protons in thick nuclear emulsions by saying that the general form of the stray neutron spectra (measured between 0.7 and 20 MeV) at eight locations near the Bevatron is a broad peak in the 0.5- to 2-MeV region, followed by a smooth 100-fold drop in value between the peak and 12 MeV. Figure 3.3 summarizes their data.

Unfortunately, proton recoil measurements in emulsions are unreliable above about 20 MeV, because track loss corrections become difficult.

At higher neutron energy, nuclear emulsions may still be used to give some indication of the slope of a smooth neutron spectrum if the average number of grey prongs per star is determined. This was first done for cosmic rays (27), but the technique has been refined and used in accelerator radiation environments at Berkeley (28-30). Figure 3.4 relates the average number of grey prongs per star, $\bar{A}$, to spectrum slope, γ, and maximum spectrum energy in the spectrum.

Patterson et al. (30) have reported the use of this technique in several radiation environments, and their results are summarized in Table 3.2. The values of the spectrum slope, ranging from 1.5 to 1.8 for the proton synchrotrons, is consistent with threshold detector data.

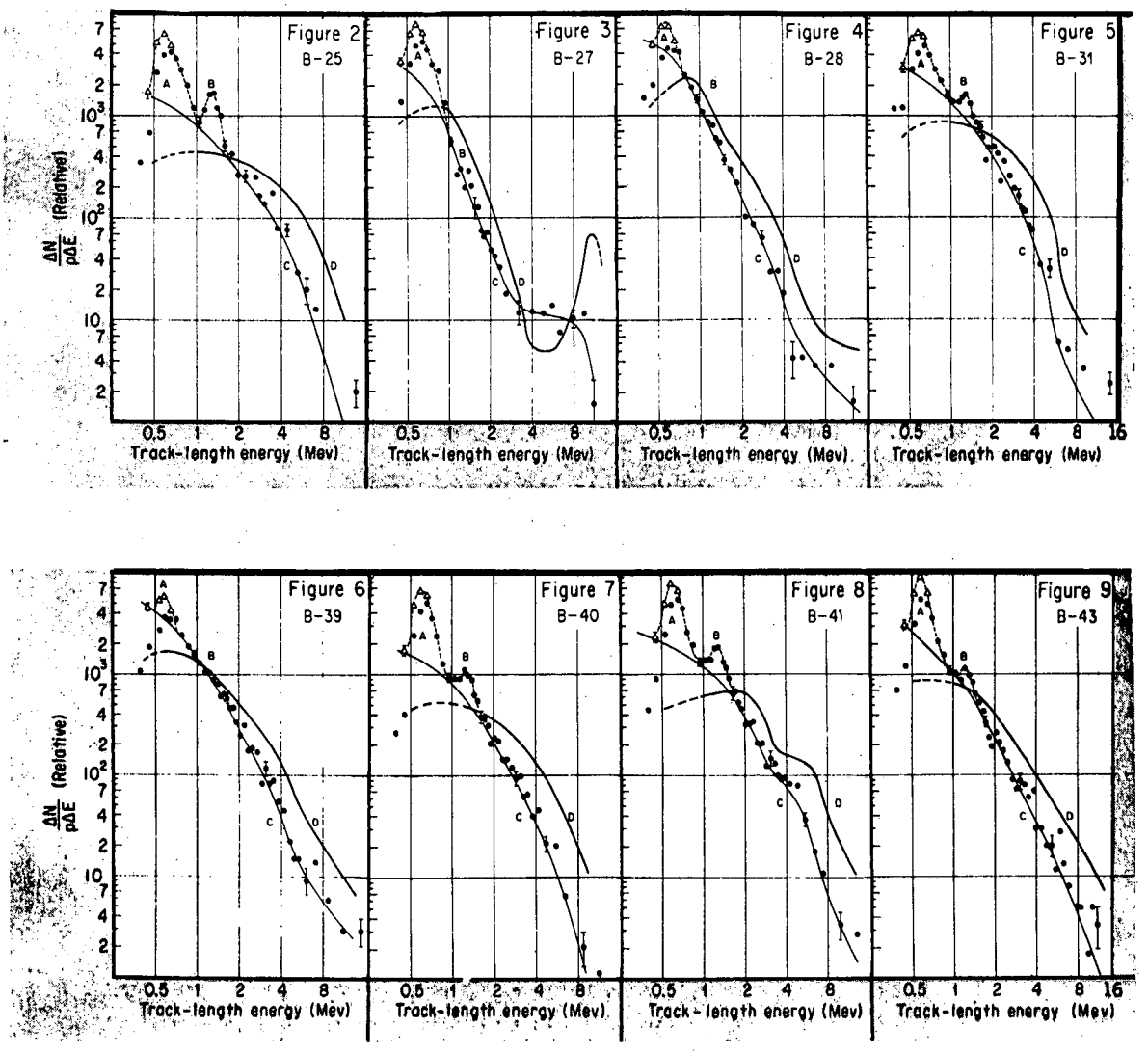

XBL 729-1911

Fig. 3.3

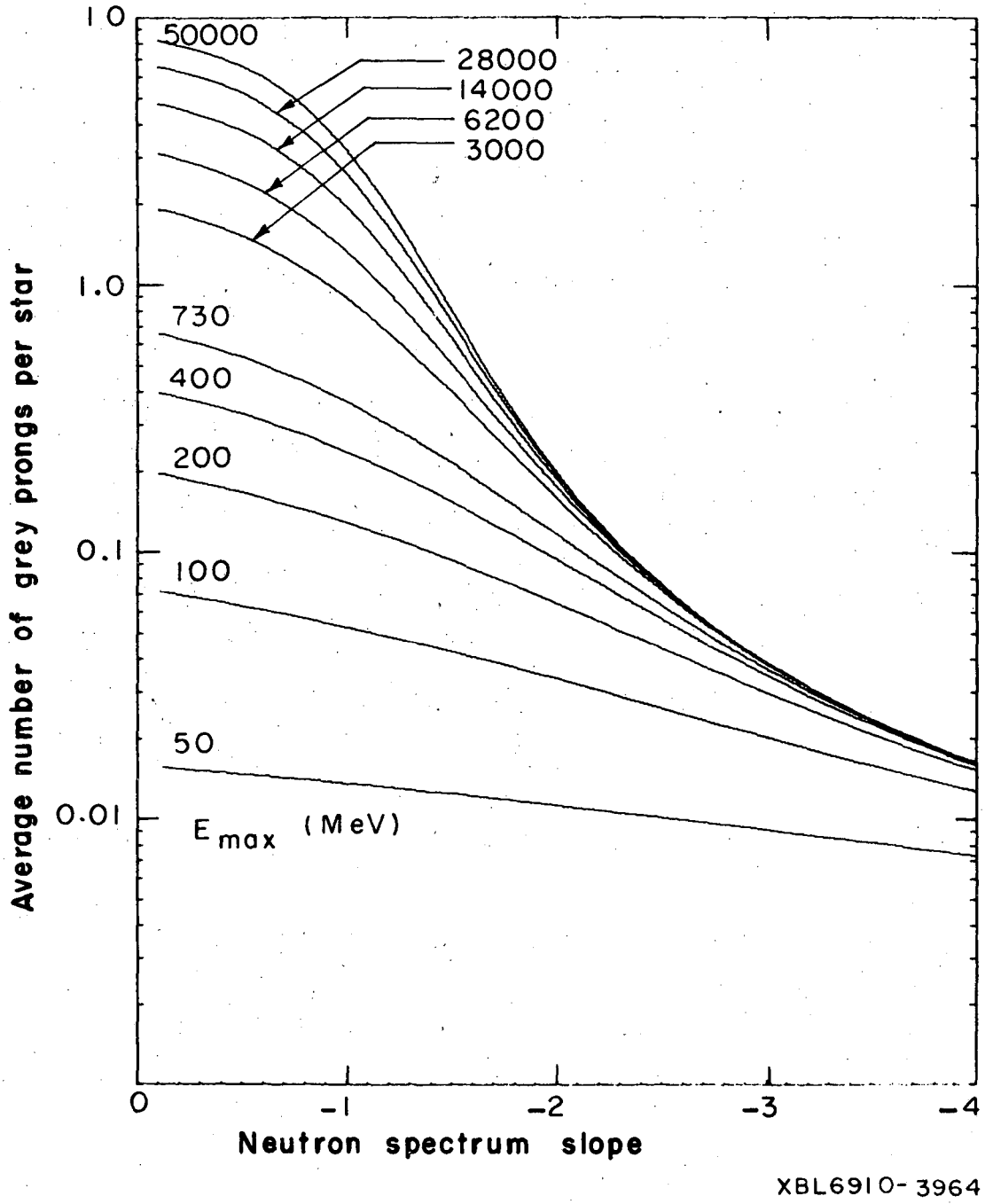

Fig. 3.4

Table 3.2. SPECTRAL INDICES OBTAINED FROM MEASURED VALUES OF THE AVERAGE NUMBER OF GREY PRONGS PER STAR

Location	E_{max} (MeV)	Spectral index, γ
184-inch cyclotron between Bays 10 and 11	730	0.75
Bevatron west tangent tank shielding wall (WTT)	6 200	1.50
Bevatron Col.7, main floor	6 200	1.68
Bevatron mezzanine	6 200	1.78
CERN PS	14 000	1.80
CERN PS	14 000	1.95
CERN PS	28 000	1.68
White Mountain, 12 000 ft altitude	(50 000)	1.32
White mountain, 14 000 ft altitude	(50 000)	1.35

b. Threshold detectors

The use of threshold detectors in neutron dosimetry is a well understood and universally accepted tehnique in radiation physics. Their use has found widespread application at most high-energy particle accelerators and has been described in several review articles (2,8,31-34).

Table 3.3 summarises some of the threshold reactions commonly used at accelerator laboratories. Column 5 indicates the typical sensitivity which may be readily achieved for these detectors. Sensitivity is, however, clearly a function of detector size and the precise experimental techniques employed, and the values indicated are intended only as a general guideline. They indicate the order of magnitude of minimum flux density that may be detected after a measurement lasting one hour. For precise details the reader is referred to the original sources. Furthermore, Table 3.3 is not intended to be comprehensive but to indicate the reactions in common use. Particular laboratories may have their own preferred specialities that they have perfected.

It may be seen from Table 3.3 that threshold detectors are available of high sensitivity over the entire energy range normally of interest at accelerators (0.1-100 MeV). No details of the shape of the neutron spectrum below about 1 MeV will be obtained using only one size of moderator with a thermal neutron detector but for radiation protection purposes detailed knowledge of the neutron spectrum in the energy range from thermal up to about 10 keV is rarely required because intermediate-energy neutrons are usually of little importance. In this energy region the dose equivalent per unit fluence is independent of energy and therefore a measurement of neutron fluence will usually be adequate. However, if detailed spectral information is required in the energy region, a set of moderators of different size -- known as Bonner spheres -- may be used. (See section on Bonner Spheres.) Fortunately this is not often required for two reasons: (1) because the dose-equivalent contribution is not large, and (2) because, below 10 keV, the dose equivalent per unit fluence is independent of neutron energy.

At high radiation intensities ($\leq$ 10 rem/h) several less sensitive reactions provide additional information. Figures 3.5 and 3.6 show the variation of sensitivity with energy for the reactions listed in Table 3.3.

In the future, we can confidently look forward to the refinement of the detection of ^{149}Tb produced in mercury so that unit flux density may be determined. The detection of spallation products in medium heavy targets offers interesting possibilities for a new type of threshold detector system (35). For example, the γ-rays resulting from the decay of more than 20 radionuclides produced in copper may be detected in a copper target. Simultaneous observation of several of these reactions would permit the determination of the neutron spectrum by one threshold detector, if the excitation functions for the reaction utilized were adequately known. Unfortunately, because of the small cross-sections of some of the reactions that would be utilized and the low detection efficiency, the technique will be limited to regions of high flux density.

Table 3.3. PROPERTIES OF SOME COMMONLY USED THRESHOLD DETECTORS

Detector	Reaction	Half-life	Energy range	Typical minimum flux density measurable $n \cdot cm^{-2} s^{-1}$ (a)	Remarks
BF_3 proportional counter	$^{10}B(n,\alpha)^{7}Li$	-	Thermal		
Gold foil	$^{197}Au(n,\gamma)^{198}Au$	2.7 days	Thermal	10^2	
Indium foil	$^{115}In(n,\gamma)^{116m}In$	54 min	Thermal	1	
Moderated BF_3 counter	$^{10}B(n,\alpha)^{7}Li$	-	Thermal - 15 MeV	10^{-2}	Energy range and sensitivity depends upon moderator size - 15 cm dia. values quoted.
Moderated gold foil	$^{197}Au(n,\gamma)^{198}Au$	2.7 days	Thermal - 15 MeV	10^2	
Moderated indium foil	$^{115}In(n,\gamma)^{116m}In$	54 min	Thermal - 15 MeV	1	
Thorium fission counter	Th(n, fiss.) fission products	-	> 2 MeV	1	
Sulphur	$^{32}S(n,p)^{32}P$	14.3 days	> 2.5 MeV	10^4	
Aluminium	$^{27}Al(n,\alpha)^{24}Na$	15 h	> 6 MeV	1	
Aluminium	$^{27}Al(n,spall.)^{22}Na$	2.7 yr	> 25 MeV	10^4	
Polystyrene: plastic scintillator	$^{12}C(n,2n)^{11}C$	20.4 min	> 20 MeV	1	
	$^{12}C(n,spall.)^{7}Be$	53.4 days	> 30 MeV	10^4	
Bismuth fission chamber	Bi(n, f) fission products	-	> 50 MeV	1	
Mercury	$Hg(n,spall.)^{149}Tb$	4.1 h	> 600 MeV	10	

(a) Based on 1 h measurement.

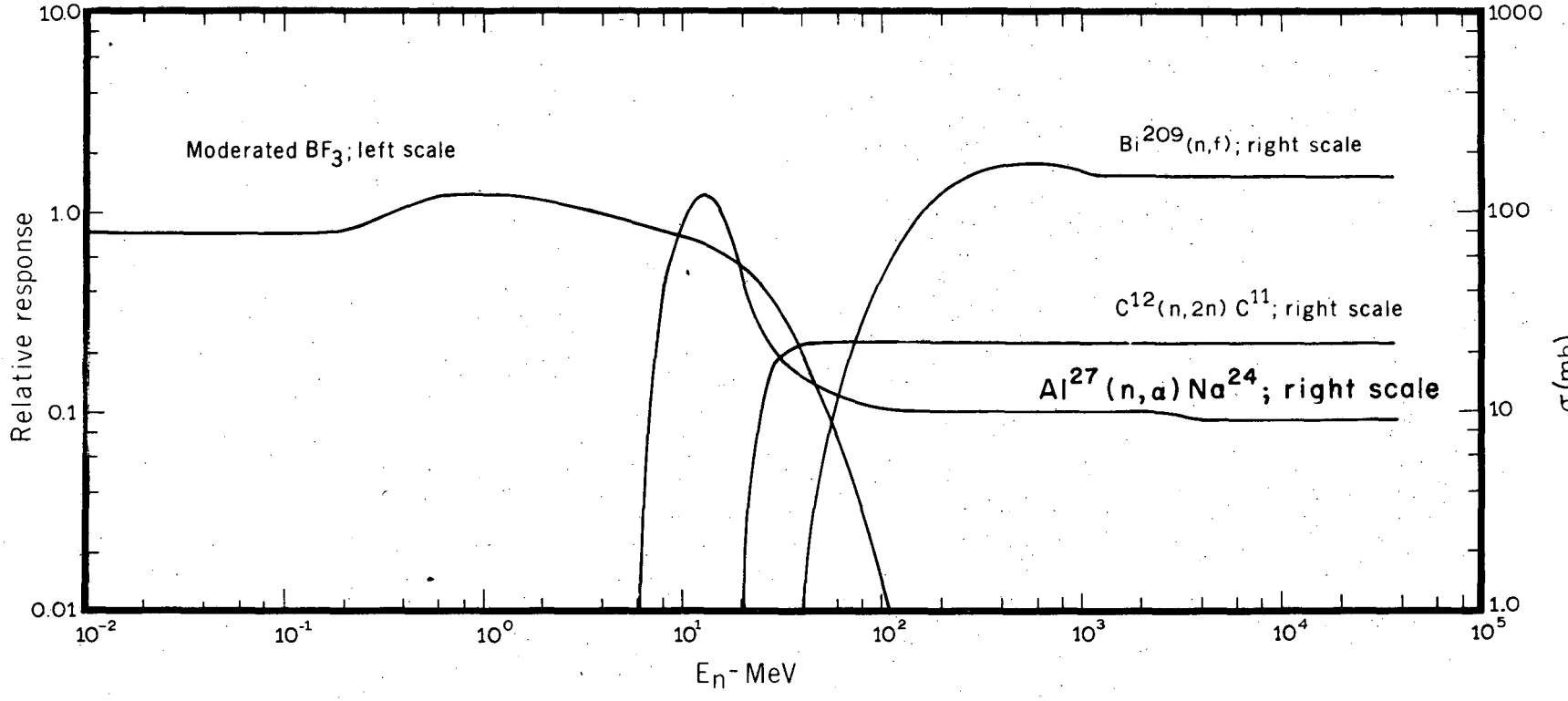

XBL 682 4491

Fig. 3.5

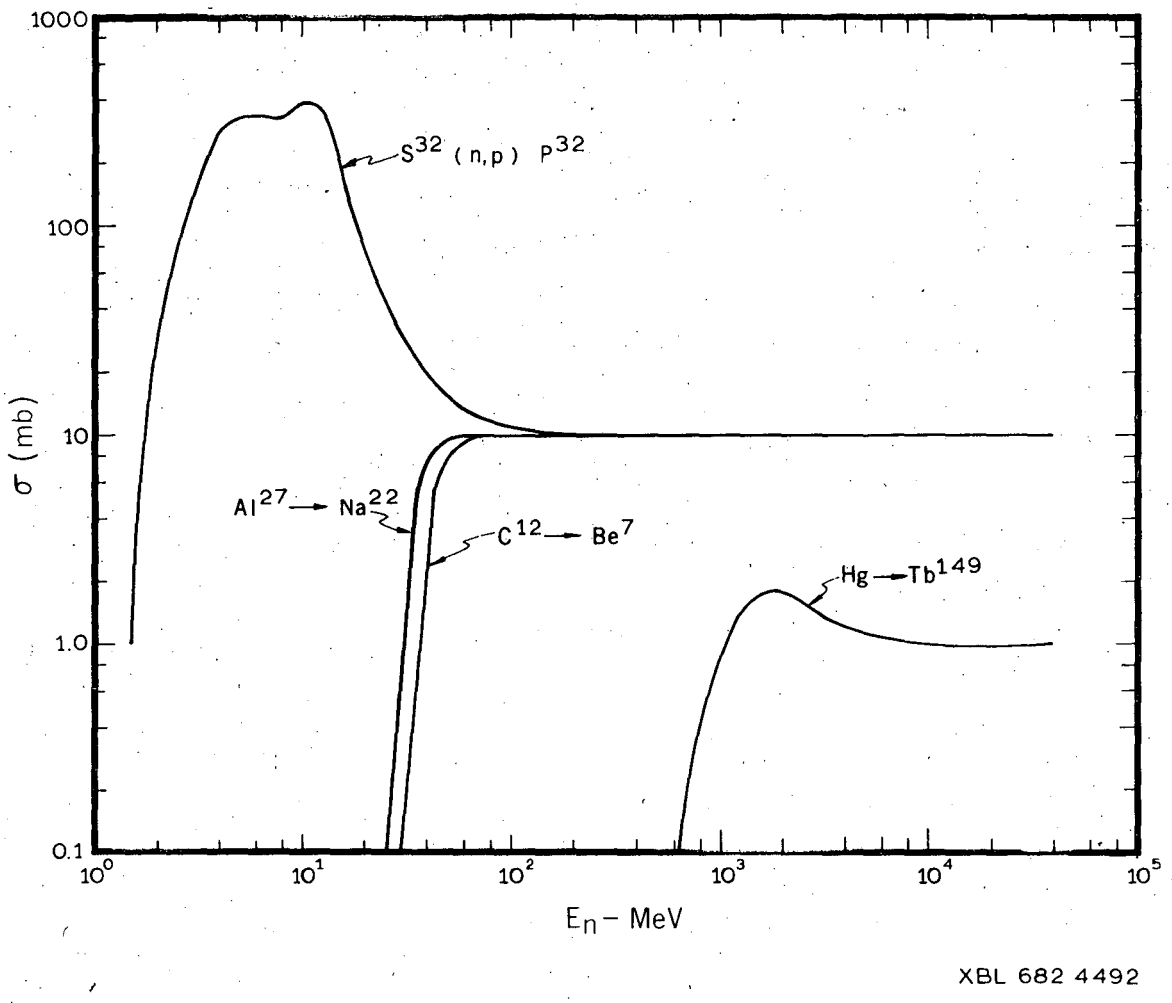

Fig. 3.6

C. Bonner Spheres

Bramblet et al.[36] first suggested the use of several moderating spheres of varying size to measure neutron radiation fields. These workers used a small cylindrical (4 mm high, 4 mm diam) lithium iodide scintillator (Eu activated) placed in the centers of polyethylene moderators of various diameters. Thermal neutrons arriving at the center of moderator interacted in the scintillator predominantly via the $^{6}Li\ (n,\alpha)^{3}H$ reactions, producing a 4.79-MeV α particle which is stopped in the crystal. The scintillator was coupled to a photomultiplier tube by a 0.5-in.-diam polystyrene light pipe, and the output of the photomultiplier therefore gave a measure of the thermal neutron flux density at the center of the moderator assembly.

Bramblett et al. calculated the response of polyethylene spheres of diameter 2,3,5,8, and 12 in. at some discrete energies to neutrons in the energy range 50 keV to 15 MeV. (Such spheres have subsequently been generally referred to as "Bonner Spheres," after the senior author of the original paper.) The largest of these moderators has a diameter comparable with that of the human trunk, and the variation with energy of its response to neutrons is therefore similar to that of the human body.

When detailed information of the shape of the neutron spectrum in the intermediate energy region is needed, the use of Bonner spheres is extremely useful.

Recently Bonner spheres have been successfully used in conjunction with activation detectors to measure accelerator and cosmic-ray neutron spectra.[37-39]

D. Spectrum Determination

Measurements with several activation detectors and Bonner spheres whose response functions are known provides information on the energy distribution of the neutron flux density.

One of the earliest successful attempts at spectrum determination was based on an extension of the idea, first proposed by Smith[33], of comparing the measured response of the threshold detectors with their anticipated response in hypothesized spectra. This technique does not require extensive computing facilities, but it is nevertheless greatly facilitated if they are available.

Specifically, a solution for the neutron spectrum $\phi(E)$ is sought from a set of activation equations of the form

$$A_j = C_j \int_{E_{min}}^{E_{max}} \sigma_j(E)\phi(E)dE \quad \text{for} \quad j = 1, 2, \cdots m \qquad (3.5)$$

where A_j is the saturation activity of the j^{th} detector,

$\sigma_j(E)$ is the cross section for the appropriate reaction at energy E,

C_j is a normalizing constant between activity and flux density,

E_{min}, E_{max} are the minimum and maximum neutron energies in the spectrum.

Gilbert et al. [2] have described the use of an iterative technique that employs on-line facilities of a CDC-6600 computer for the determination of neutron spectra from a few threshold detectors—TELLY. The operator indicates to the computer his best estimate of the neutron spectrum which will match his experimental data. This is done by drawing the spectrum with a light pen on the screen of a CRT display. The computer then calculates the detector responses and presents them for comparison with the experimental data. The operator then systematically modifies his suggested spectra to the computer until, after a few iterations, the detector responses are matched with an accuracy reflecting the experimental errors. TELLY was found to work well, avoiding many of the pitfalls of more "sophisticated" methods of spectrum analysis. Its only drawback is that it is somewhat difficult to use in a systematic manner when many detectors with overlapping regions of sensitivity are used.

Equation (3.5) is a degenerate case of a Fredholm integral of the first kind. Formal methods of solution are not applicable when, as is the case with activation detectors, the A_j's or σ_j's are known only as a set of discrete points. [40]

Routti [40] has critically reviewed the numerical techniques commonly used for solution of such first-order Fredholm equations, and the interested reader is referred to his paper for a detailed account.

Early attempts to obtain neutron spectra from activation detector data were frustrated by difficulties such as non-uniqueness or an oscillatory (and even negative) character to the solutions to the Fredholm equations. Some of these problems arise from the mathematical characteristics of the equations to be solved, while others are related to the specific method of solution adopted.

Routti suggests that a suitable method of solution must be able to combine the information contained in the measured data with any already existing information of the neutron spectrum. Such prior information is almost always available on physical grounds. Thus, for example, the solution must be non-negative and zero beyond a given maximum energy. In addition the spectrum of radiation penetrating thick shields constructed of a complex material such as concrete may be assumed to be smooth. Some information on intensity or shape may be available from previous measurements. It is important that all this prior information be properly taken into account in the solution technique selected. However, care must be taken to ensure that the

consequent additional constraints imposed on the spectrum do not prevent it from matching the measured responses or from assuming any physically acceptable shape.

Any appropriate solution must fulfill two basic measurements:

a. The neutron spectrum which is found to be a solution to the activation equations must accurately match the detector responses.

b. If many solutions are found that fulfill condition (a) there should be a flexible way to apply physical prior information on the solution so that the most appropriate solution may be selected.

It is important that any solution method be tested to ensure that it meet all these requirements. This is most conveniently done by computing the response of the system to test spectra. The resolutions of the system and the influence of experimental errors or uncertainties in the detector response functions may then be systematically studied.

Routti has applied a generalized least-squares method to solve the activation equations. In his technique the solution is forced to be non-negative, and prior information on the spectrum can be incorporated in a very flexible way. The technique and the computer program LOUHI, written to perform the analysis have been subjected to the tests described in the previous paragraph. These tests show that the method meets the two basic requirements for an appropriate solution.

Considerable experience has now been obtained with LOUHI and it has been found to be extremely reliable and capable of calculating neutron spectra with adequate accuracy for radiation protection purposes.

A desirable feature of LOUHI is that, in addition to activation detector data, it may be used to determine neutron spectra from Bonner sphere or nuclear emulsion data.

Examples of some neutron spectra obtained using threshold detectors have already been discussed in the section on accelerator radiation environments.

Rem-Meters

Under the conditions that prevail at research accelerators, the initial use of "rem-meters" is usually inappropriate because the design and construction of practical rem-meters requires some prior information of the radiation environment in which they are to be used.

The truly universal "rem-meter" —an instrument that determines dose-equivalent in any radiation field with good accuracy—is not theoretically feasible but even granted it were, there are still strong arguments for pursuing fundamental studies of accelerator radiation environments.

A dose-equivalent meter has been developed at Brookhaven National Laboratory which may be used in accelerator radiation environments.[42] It is basically a Rossi-type LET spectrometer[43] with a modified electrode system. The detector consists of a 0.6 cm thick spherical shell approximately 20 cm in diameter constructed of tissue equivalent plastic. The spectrometer has filling consists of the usual "tissue-equivalent" mixture of 66% methane, 3% nitrogen and 31% carbon dioxide at a pressure of 10 torr. Under these conditions the detector simulates a tissue sphere approximately 3 μ in diameter Measurements of cosmic-ray produced radiation using this instrument and a comparison with other techniques have been described by Hewitt et al.[39]

References

Section 3

1. MOYER, B. J., Practical control of radiation hazards in physics research, Ann. Rev. Nucl. Sci. 8 (1958) 327.
2. GILBERT, W. S., et al., CERN-LRL-RHEL Shielding Experiment at CERN, Lawrence Radiation Laboratory Report UCRL-17941, Sept. 1968.
3. SHAW, K. B., STEVENSON, G. R., and THOMAS, R. H., Evaluation of dose equivalent from neutron energy spectra, Health Phys. 17 (1969) 459.
4. PATTERSON, H. W., ROUTTI, J. T., and THOMAS, R. H., What quality factor?, Health Phys. 20 (1971) 517.
5. RINDI, A., and THOMAS, R. H., "Absorbed dose—An unfortunate red herring in radiation protection," in Proc. Sixth Annual Health Physics Society Mid-Year Topical Symposium, Richland, Washington, Nov. 1971, Columbia Chapter, Health Physics Society, Richland, Washington (1971).
6. RINDI, A., and THOMAS, R. H., Povera e Nudá Vai, Dosimetria, Health Phys. 23, 715 (1972).
7. MOYER, B. J., Neutron physics of concern to the biologist, Rad. Res.1 (1954) 10.
8. SULLIVAN, A. H., "The present status of instrumentation for accelerator health physics," in Proc. Second International Conference on Accelerator Dosimetry and Experience Stanford, California, Nov. 1969, CONF-691101, p. 625.
9. Pszona, S., Direct Evaluation of Dose Equivalent in Mixed Radiation Fields, IEEE Trans. Nucl. Science, NS-23, No. 4, 1368 (1976).
10. Thomas, R.H., Neutron Dosimetry at High Energy Particle Accelerators - A Review, Proc. IAEA Symp. on Neutron Monitoring for Radiation Protection Purposes, IAEA, Vienna 1973, p. 322.
11. Rindi, A., Thomas, R. H., op cit. ref. 5, p. 465.
12. Boag, J. W. et al., Brit. J. Radiol. 45, 314 (1972).
13. Rossi, H. H. 1969. In Proc. Symp. Neutrons in Radiobiol., Oak Ridge, CONF-691106.
14. Katz, R. 1971. Proc. Biophysical Aspects of Radiat. Quality, 11. Vienna: IAEA.
15. Katz, R., Sharma, S. C., Homayoonfar, M., Irradiation Equivalence, Health Physics 23, 740 (1972).
16. ICRP 1969. ICRP Publication #14. Oxford: Pergamon.

17. Patterson, H. W., Thomas, R. H., Proc. Berkeley Symposium, Math. Statistics, and Probability, 6th, 6, 313, Berkeley, Univ. Calif. Press (1970).

18. RBE Committee, Health Phys. 9, 357 (1963).

19. Neary, G. J., Phys. Med. and Biol. 7, 419 (1963)

20. ICRP 1970. ICRP Publication #15, Para. 13. Oxford: Pergamon

21. ICRP, Data for Protection Against Ionizing Radiation from External Sources (Oxford) (1973), Publication 21.

22. Figerio, N. A., Coley, R. F., Branson, M. H., Phys. Med. Biol. 18, 53 (1973).

23. See for example, Auxier, J. A., Snyder, W. S., Jones, T. D. 1968. Radiat. Dosimetry, eds. F. H. Attix, W. C. Roesch, Chap. 6. New York: Academic Press.

24. See for example, Fuller, E. W., Eustace, R. C., in Proc. Int. Congress Radiation Protection of Accelerators and Space Radiation p. 344; or Armstrong, T. W., Bishop, B. L. 1971. ORNL-TM-3304.

25. Patterson, H.W., Thomas, R.H., Accelerator Health Physics, Academic Press, New York (1973), Chapt. 2.

26. LEHMAN, R. L., and FEKULA, O. M., Energy spectra of stray neutrons from the Bevatron, Nucleonics 22 11 (1964) 35.

27. ROSSI, B., High Energy Particles. Prentice-Hall, New York (1954), p. 488.

28. REMY, R., Neutron Spectroscopy by the Use of Nuclear Stars from 20 to 300 MeV (M. S. thesis), Lawrence Radiation Laboratory Report, UCRL-16325, Aug. 1965.

29. OMBERG, R. P. and PATTERSON, H. W., Application of the Stars Produced in Nuclear Emulsions to the Determination of a High Energy Neutron Spectrum, Lawrence Radiation Laboratory Report UCRL-17063, Feb. 1967.

30. PATTERSON, H. W., HECKMAN, H. H., and ROUTTI, J. T., New measurements of star production in nuclear emulsions and applications to high energy neutron spectroscopy, op. cit. Ref. 8, p. 750.

31. Tardy-Joubert, P., Methods and Experience of Dosimetry Around Saturne in Proc. 1st. Symposium on Accelerator Dosimetry, Brookhaven National Laboratory, Nov. 1965. USAEC Report CONF-651109, p. 117.

See also: "Les Principaux rayonnements recontres aupres des grands accelerateurs" in Progress in Radiobiology 2 (Proc. XI Int. Congress of Radiology, Rome, Aug. 1965), Excerpta Medica Foundation, Amsterdam 1967, p. 1849.

32. Perry, D.R., Neutron Dosimetry Methods and Experience on the 7 GeV Proton Synchrotron, Nimrod, in "Neutron Monitoring" (Proc. Symp. Vienna, 1966). IAEA Vienna (1967) p. 355.

33. Smith, A. R., Threshold Detector Applications to Neutron Spectroscopy at the Berkeley Accelerators, op. cit. Ref. 31, p. 226.

34. SMITH, A R., Some experimental shielding studies at the 6.2 BeV Berkeley Bevatron, op. cit. Ref. 31, p. 365.

35. ROUTTI, J. T., High Energy Neutron Spectroscopy with Activation Detectors, Incorporating New Methods for the Analysis of Ge(Li) Gamma-ray Spectra and the Solution of Fredholm Integral Equations, Lawrence Radiation Laboratory Report UCRL-18514, April 1969.

36. BRAMBLETT, R. L., EWING, R. I., and BONNER, T. W., A new type of neutron spectrometer, Nucl. Instr. Methods 9 (1960) 1.

37. Aleinikov, V.E., et al., Comparison of Dosimetry Methods and Instruments in the Radiation Fields of Proton Accelerators at the Joint Institute of Nuclear Research, in Neutron Monitoring for Radiation Purposes, Vol. 2., IAEA Vienna, p. 363.

38. Distenfeld, C., Improvements and Tests of the Bonner Multisphere Spectrometer, Brookhaven National Laboratory Report BNL-21293.

39. Hewitt, J.E. et al., Ames Collaborative Study of Cosmic Ray Neutrons, National Aeronautics and Space Administration report, NASA TM X-3329, January 1976.

40. Routti, J.T., Mathematical Considerations of Determining Neutron Spectra from Activation Measurements, in op cit. Ref. 8, p. 494.

41. Routti, J.T., Ph.D. Thesis, University of California, Berkeley, Published as Lawrence Berkeley Laboratory internal report, UCRL-18514 (1969).

42. Kuehner, A.V., Chester, J.D., and Baum, J.W., Portable Mixed Radiation Dose Equivalent Meter for Radiation Protection Purposes, in Neutron Monitoring for Radiation Protection Purposes, Vol. 1, IAEA Vienna (1973), p. 223.

43. Rossi, H.H. and Rosenzweig, W., Measurements of Neutron Dose as a Function of Linear Energy Transfer, Rad. Res. 2, 417 (1955).

4. Shielding

4.1. Introduction

The successful design of the shield for a high-energy particle accelerator essentially depends on a good understanding of the nuclear processes that occur in the shield, and the transport of the resulting interaction products through the shield and outside. In the twenty five years following World War II our understanding of nuclear physics and high-energy interactions has advanced to the point where, with the exception of the highest energies, shield design is no longer an "art" as it was described by Jaeger in 1960[1] but rather an exact science.

Space does not permit any discussion of the historical development of accelerator shielding, but this has been described in several review articles[2,3] which also include descriptions of the most important accelerator shielding experiments.

In recent years the development of computational techniques suitable for operation with large digital computers for the calculation of source terms and radiation transport in complex geometries has facilitated shield design.[4]

Useful as the computer programs are for shielding computation, they are of little didactic value. In order to understand the physical principles of accelerator shield design, it is still useful to examine the semi-empirical techniques developed over the past 20 years for shielding calculation. The most important of these is the so-called "Moyer Model."

4.2. Phenomenological Models

Consider an effective point source produced by protons interacting in a thick target (Figure 4.1. The radiation level on the outside surface of a shield may be written, by analogy with the corresponding photon shielding problem, as

$$H = \frac{1}{r^2} \int F(T)\, B(T) \exp\left(\frac{-d(\theta)}{\lambda(T)}\right) \cdot \frac{d^2 n(T, \theta)}{dT\, d\Omega}\, dT, \qquad (4.1)$$

where r is the distance from the source,

T is the neutron energy,

F is a factor which converts fluence to dose equivalent,

d is the shield thickness,

λ is the effective removal mean-free path,

B is a buildup factor, and

$\frac{d^2 n}{dT\, d\Omega}$ is the yield of neutrons per unit solid angle between T and T + dT at angle θ. (See Figure 4.1.)

De Staebler(5) wrote Equation 4.1 as:

$$H = \frac{1}{r^2} \sum_i B_i F_i \exp\left(\frac{-d}{\lambda_i}\right) \cdot \left(\frac{dn}{d\Omega}\right)_i \qquad (4.2)$$

where the subscript i denotes a range of neutron energies for which B, F, and λ are fairly constant and the definition of $(dn/d\Omega)$ is obvious.

Moyer(6,7) made an extremely important contribution when he recognized that Equation 4.2 may be approximated by a single energy group because the nature of the radiation field outside the shield of a high-energy proton accelerator will be determined by neutrons with energy greater than about 150 MeV. Neutron attenuation lengths above 150 MeV are roughly independent of energy, but diminish rapidly with energy below about 100 MeV. Consequently, the greater yields of low-energy, as compared to high-energy neutrons, at the primary interaction, will be more than compensated for by the greater attenuating action of the shield for these

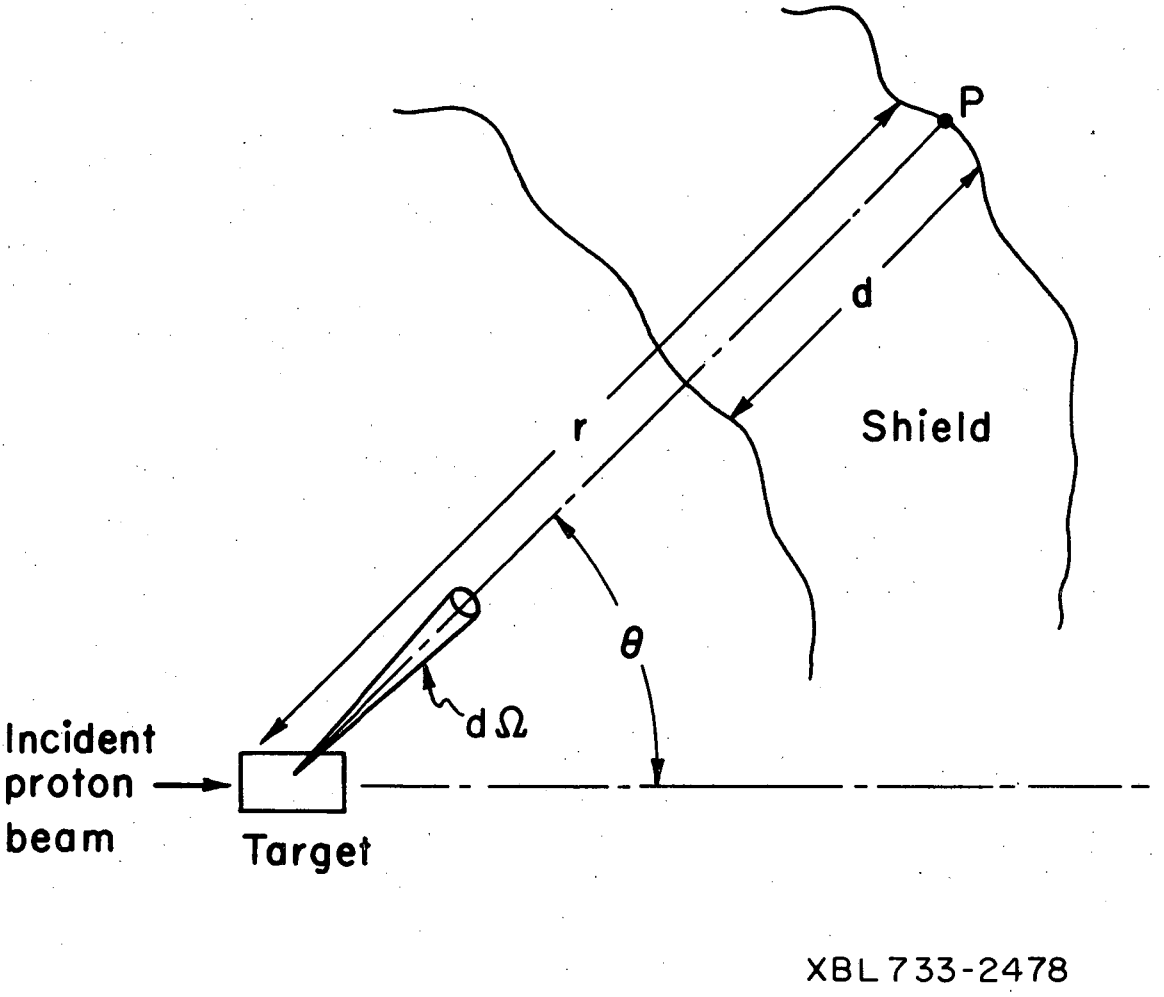

Fig. 4.1. Schematic Diagram of Typical Shielding Geometry.

neutrons. Deep in the shield, high-energy (E > 150 MeV) neutrons regenerate the cascade but are present in relatively small numbers. At a shield interface the radiation field observed consists of these "propagators," born close to the primary radiation source, accompanied by many particles of much lower energy born near the interface. Equation 4.2 therefore becomes

$$H \propto \frac{N g(\theta)}{r^2} \cdot \exp(-d/\lambda) \qquad (4.3)$$

where N is the proton intensity incident on the target,

θ is the angle subtended to the beam direction,

$g(\theta)$ is the angular distribution of high energy particles at the source,

d is the shield thickness, and

λ is the effective attenuation length of high-energy neutrons.

The total neutron flux density (and consequently the dose-equivalent rate) will be proportional to the high-energy neutron flux density. Because the low-energy components are produced by interaction of the high-energy propagators, their intensity decreases through the shield in an exponential manner with effectively the same attenuation length for all directions through the shield.

Moyer(6,7) generated appropriate parameters to be used in Equation 4.3 in calculating shielding for the Bevatron. Smith(8) has described the excellent agreement between measured radiation levels outside the Bevatron shield and those predicted by Moyer.

Many shielding experiments have subsequently confirmed Moyer's basic assumptions. For example, Smith et al (9) used threshold detectors to measure the spatial variation of flux density produced in concrete bombarded by 6-GeV protons. Figure 4.2 shows the relative flux density distribution, measured by the $^{27}Al \rightarrow {}^{24}Na$ reaction (threshold 6 MeV) along paths drawn at several angles to the incident beam direction. The transmission curves are seen to be exponential and essentially parallel, within the limits of experimental accuracy. Similar results were obtained with detectors utilizing the $^{12}C \rightarrow {}^{11}C$ reaction (threshold 20 MeV). In addition, Smith et al demonstrated the existence of an equilibrium spectrum by calculating the ratio of the response of the carbon and aluminum activation detectors. Figure 4.3 shows that this ratio becomes constant both in the beam direction and transverse to it. Equilibrium is evidently much more rapidly attained in the transverse direction than in the beam direction.

In the past five years effort has been devoted to obtaining optimum values of λ and $g(\theta)$ for use in Equation 4.3.

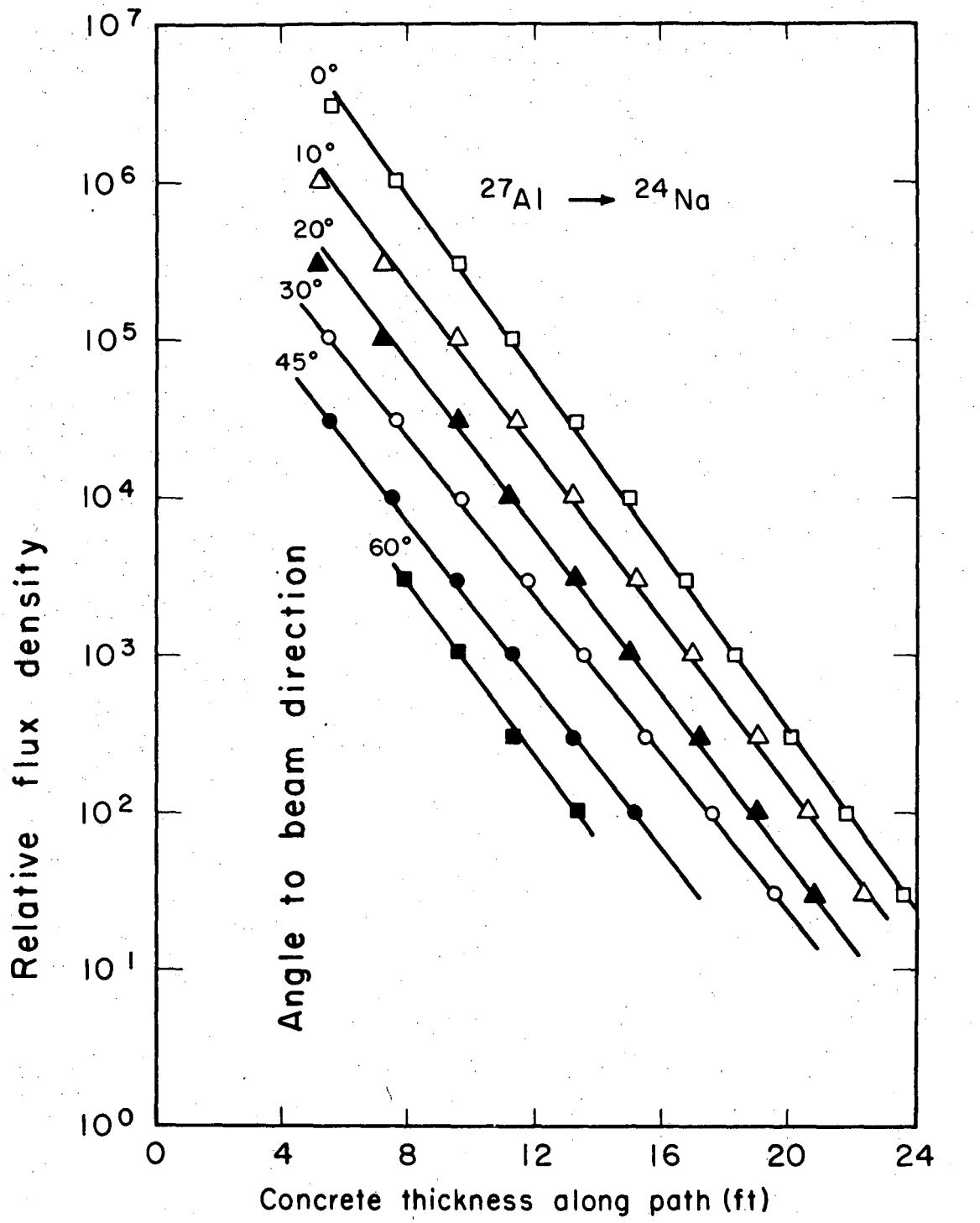

MUB-4051A

Fig. 4.2

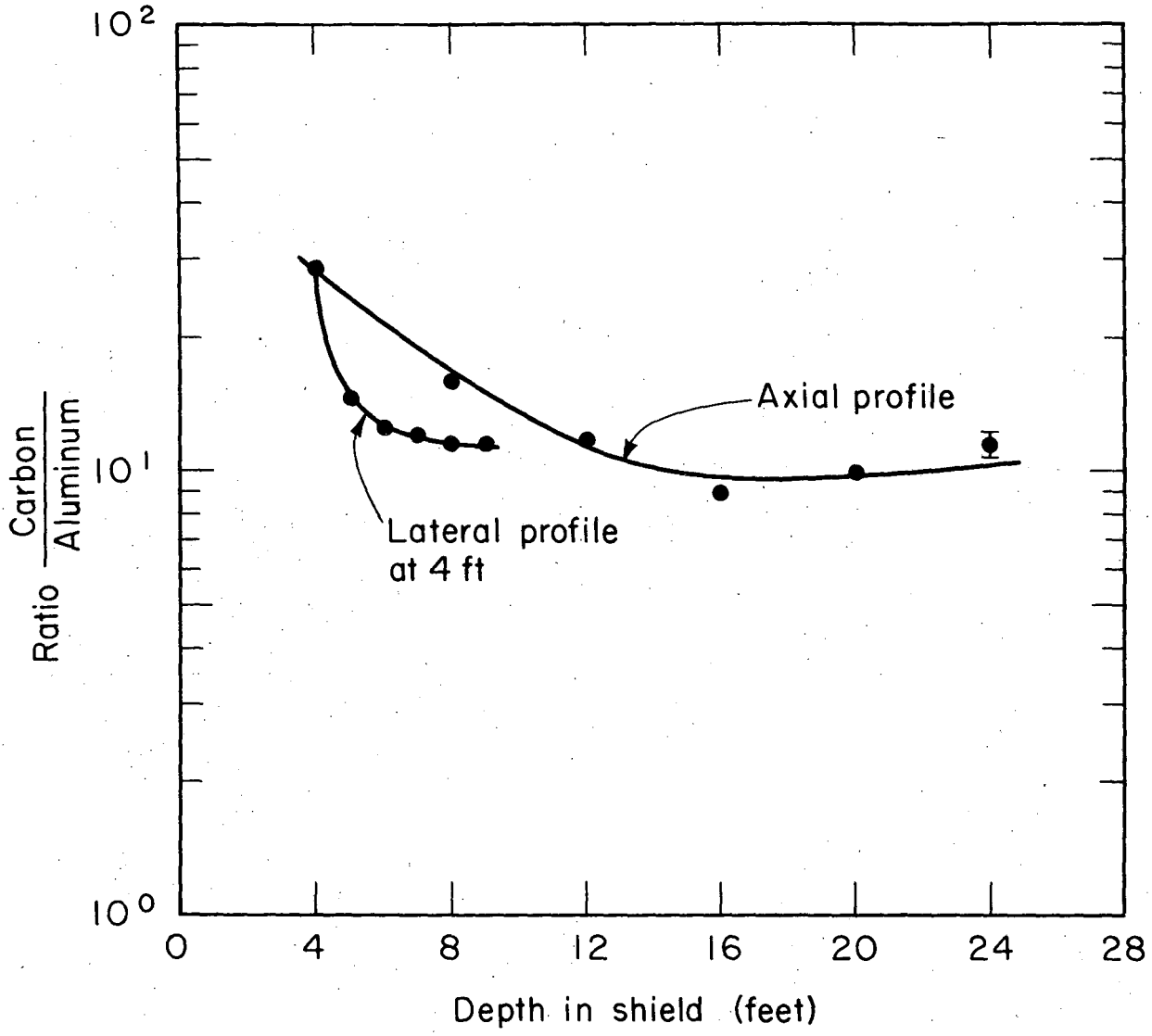
10^2
10^1
10^0
Ratio Carbon / Aluminum
Axial profile
Lateral profile at 4 ft
0
4
8
12
16
20
24
28
Depth in shield (feet)
MUB-8448

Fig. 4.3

High Energy Attenuation Length

As we have seen in the section on accelerator radiation environments, neutrons are the principal radiation component outside the shield of high intensity, high energy particle accelerators. Our prime concern in shield design must therefore be adequate neutron attenuation.

Neutron attenuation is determined by the inelastic cross sections of the shield material, which at high energies are essentially independent of energy. Figure 4.4 shows the variation of σ_{in} with energy for several materials. Since the high-energy attenuation length is inversely related to cross section:[3]

$$\lambda_{atten} = \frac{1}{N \sigma_{in}} \qquad (4.4.)$$

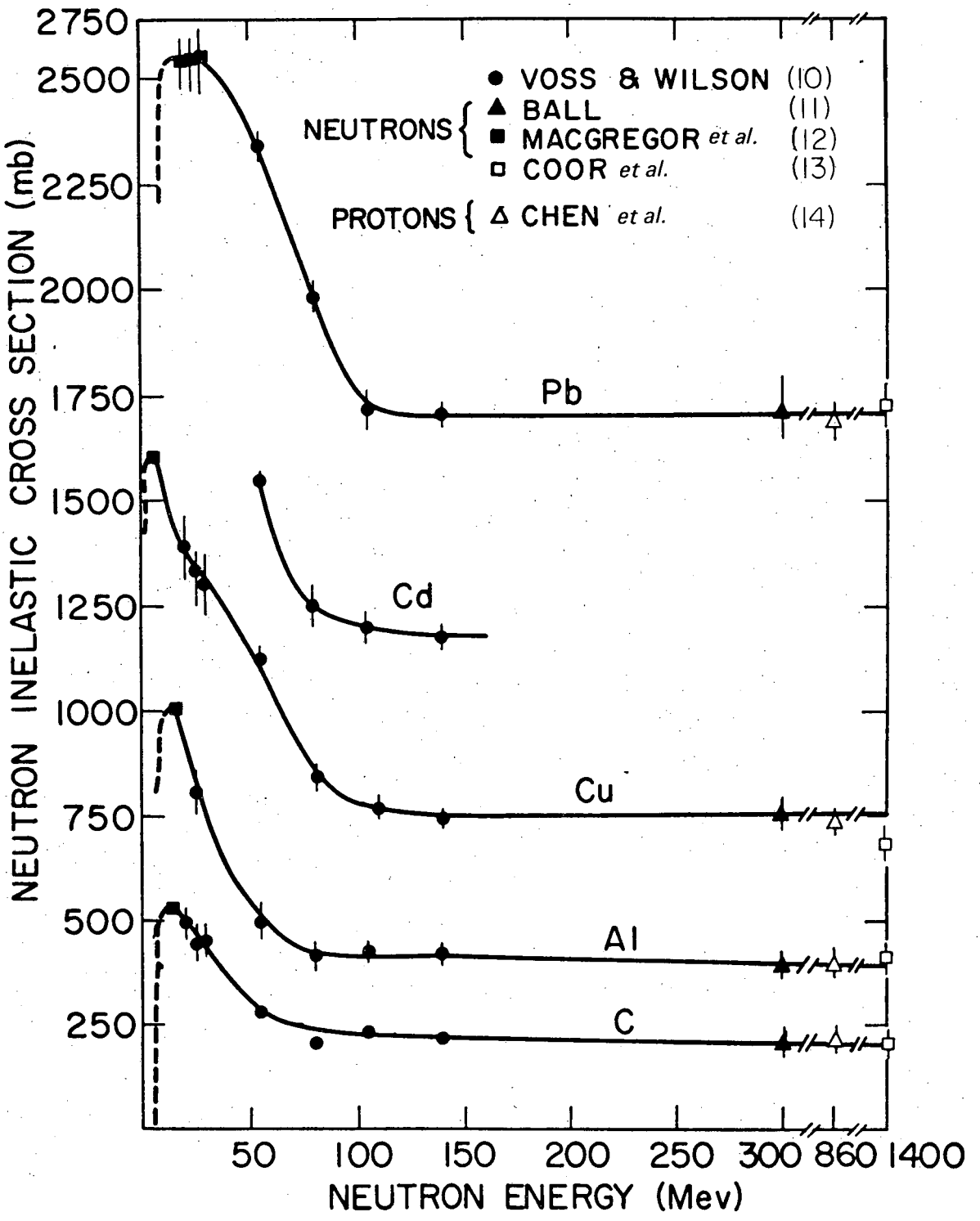

XBL 709-6581A

Fig. 4.4

this behavior of the cross sections explains the experimental observation that attenuation length is independent of energy for neutron energies above about 100-150 MeV. Figure 4.5 shows an early comparison (1957) between calculated and measured values of neutron attenuation lengths in concrete due to Patterson and his co-workers.[15] Although the absolute magnitude of the attenuation length for high energy neutrons in concrete is now known to be somewhat smaller, this figure clearly shows the presence of a rather sharp "knee" in the attenuation length curve at an energy of about 100-150 MeV.

At high energies then, if we assume the inelastic cross section is responsible for attenuation processes and using equation 4.4, since

$$\sigma_{in} = \pi R^2 \tag{4.5}$$

where R is the nuclear radius given by:

$$R = R_0 A^{1/3} \tag{4.6}$$

we might expect

$$\rho\lambda = 38\, A^{1/3} \text{ g cm}^{-2} \tag{4.7}$$

where a value of 1.2×10^{-13} cm has been taken for the nuclear radius, r_0.

Over the past fifteen years many shielding experiments have been performed, some of which are summarized in Table 4.1, but accurate data are still limited.[16]

As may be noted from an inspection of Table 4.1, which summarizes high energy shielding measurements in concrete and steel made up to 1965, there is a wide range in the value of attenuation lengths reported.[16] These variations are due to three sources:

i. Differing interpretations of the term "attenuation length" -- particularly in the earlier literature.

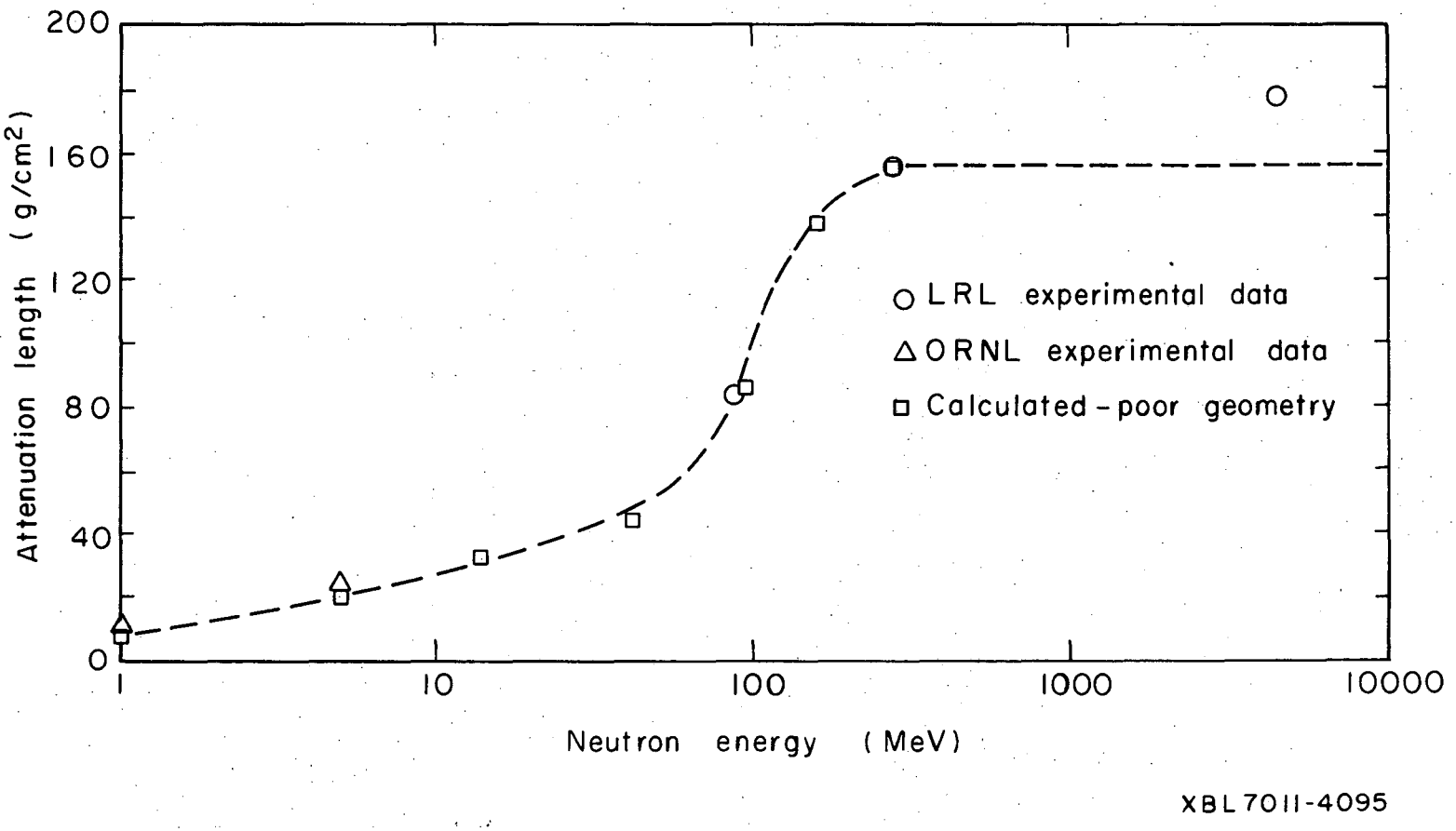
200
160
120
80
40
0
Attenuation length (g/cm²)
1
10
100
1000
10000
Neutron energy (MeV)
○ LRL experimental data
△ ORNL experimental data
□ Calculated - poor geometry
XBL 7011-4095

Fig. 4.5

Table 4.1 Summary of high-energy shielding measurements (up to 1965). After Thomas

Laboratory	Incident particle	Beam energy [GeV]	Shield material	Shield density [g/cm^3]	Detector	λ_{atten} [g/cm^2]
LBL	n	0.09	concrete	2.3	BF	81
LBL	n	0.27	concrete	2.3	BF	152
Princeton	n	0.30	concrete	3.85	MC	145 ±10
BNL	p	1.5	concrete	4.0–4.3	CT	130 ±15
BNL	p	2.5	concrete	4.0–4.3	CT	169 ±32
LBL	n	4.5	concrete	2.3	BF	172
BNL	π	4.5	concrete	2.3	CT	118 ±8[a]
BNL	π	4.5	steel	7.8	CT	155 ±11[a]
BNL	π	6	concrete	2.3	CT	121 ±8[a]
BNL	π	6	steel	7.8	CT	155 ±11[a]
LBL	p	6.2	concrete	2.4	^{11}C	108 ±20[b]
LBL	p	6.2	concrete	2.4	^{27}Al	112 ±20[b]
LBL	p	6.2	concrete	2.4	^{198}Au	116 ±20
R.L.	p	6.2	concrete	2.4	^{32}S	123 ±10
LBL	p	6.2	concrete	2.4	G5	160 ±20[c]
BNL	π	9	concrete	2.3	CT	129 ±9[a]
BNL	π	9	steel	7.8	CT	179 ±12[a]
RL, ORNL	p	10	concrete	3.65	G5	164 ±20
RL, ORNL	p	10	steel	7.8	G5	119 ±10
CERN	p	10	steel	7.8	^{11}C	145 ±15
CERN	p	10	steel	7.8	IC	155 ±16
DESY, SLAC, CERN, etc.	p	20	concrete	3.65	G5	132 ±5[d]
DESY, CERN, SLAC	p	20	steel	7.8	G5	137 ±10
CERN	P	20	steel	7.8	^{11}C	170 ±17[b]
CERN	p	20	steel	7.8	IC	155 ±16
CERN	p	24	concrete	2.4	G5	145 ±10
			concrete and earth	3.65 1.5		

Key:
BF Bismuth fission chamber
CT Counter telescope
MC Monte Carlo calculation
^{11}C, ^{32}S, ^{37}Al Activation detectors,
G5 Nuclear emulsion,
IC Ionization chamber.

[a] DeStaebler's estimate of error
[b] Thomas's estimate of error
[c] Unpublished data.
[d] Weighted mean of results from DESY, CERN, RL, and Stanford

ii. Imprecise knowledge of shield density.

iii. Measurements in region of the shield where the radiation spectrum had not recorded equilibrium and the attenuation was consequently not truly exponential.

Since the data summarized in Table 4.1 were taken, a series of carefully designed shielding experiments have been performed at the Brookhaven National Laboratory[17] and the European Centre for Nuclear Research (CERN).[18]

The data reported by Gilbert et al.,[18] taken at CERN with the complex geometry which obtain under actual operating conditions were analyzed to give a value of attenuation length of 117 ± 2 g cm^{-2} in earth, which is close to the value predicted by equation (4.7).

The data reported by Bennet et al. for the steel backstop irradiated by 28 GeV protons support the basic premise of the Moyer Model. At depths beyond $\sim$ 150 gm cm^{-2} into the back-stop the flux density of neutrons greater than 20 MeV in energy is attenuated exponentially with an attenuation length which is independent of angle to the incident beam direction. Reasonable agreement is obtained between the experimental data and the Monte-Carlo calculations of Ranft.[4]

While our understanding of high-energy processes is not yet perfect, the use of attenuation lengths calculated from equation (4.7) is certainly consistent with available experimental determinations of attenuation length.

4.2. Angular Distribution of Secondary Particles

The exact nature of the angular distribution function $g(\theta)$ that should be used in Equation 4.3 is not immediately obvious. One approach is to deduce angular distribution from measurements of particle flux density within the shield around the radiation source. Using such an approach, Gilbert et al (18) found that an angular distribution of the form

$$g(\theta) = a \exp(-b\theta) \quad 60° \leq \theta \leq 120° \qquad (4.8$$

well represented the flux density data measured in the earth shield of the CPS. In these measurements a thin Be-Al target was bombarded by 14.6 or 26.4 GeV/c protons. In their experiment the parameter b did not seem to be strongly dependent upon primary proton energy. Values of b in the range 2.1-2.4 radian^{-1} were reported by Gilbert et al consistent with values of b around 2.5 reported by Stevenson et al (19), using a similar technique, for a primary proton energy of 7 GeV.

The angular distribution of secondary hadrons determined from measurements around fairly thin targets is of more fundamental interest. Such data are needed to test the validity of Monte Carlo and other transport model calculations, which are used increasingly to estimate the magnitude of a variety of radiation phenomena such as radiation damage, induced radioactivity, and radiation intensity. Measurements of momentum-integrated secondary-particle yields around internal targets are difficult because of poorly defined source geometry(18,20). Recently some careful measurements of the angular dependence of hadron yields from various target materials bombarded by 3-GeV(21), 7-GeV and 23-GeV(22) protons have been reported. Levine et al(22) conclude from their measurements that the shape of the angular distribution measured with any particular detector is independent of primary proton energy and, within the range $60° \leq \theta \leq 120°$, is consistent with the form suggested

by Gilbert et al(18) (Equation 4.8). Table 3 summarizes values of the parameter b obtained at 7 GeV, from which it may be concluded that b is strongly dependent upon the energy threshold of the radiation detector. Comparison with the 3-GeV data of Awschalom and Schimmerling(21) indicates no strong dependence of b upon primary proton energy. Figure 7 shows the data of Table 4.2. (A range for threshold energy is indicated because different hadrons may produce the radioactive species observed.)

In using the Moyer model to calculate transverse shielding for proton accelerators, the appropriate angular distribution $g(\theta)$ is assumed to be that of particles with energies greater than about 150 MeV(6). Extrapolation of the data of Fig. 4.6 gives a value of b of 2.3±0.3 at 150 MeV. This value is in surprisingly (and perhaps fortuitously) good agreement with the values of b in the range 2.1-2.5 extrapolated from measurements deep in the shield.

The absolute yield of secondary hadrons depends both upon target material and primary proton energy. At large angles the yields appear to be dominated by contributions from the intranuclear cascade and are not inconsistent with a variation proportional to $A^{1/3}$(22). If the yield y, is expressed in the form

$$y = \text{constant} \cdot E^n \cdot g(\theta) \tag{4.9}$$

n lies in the range 0-0.5, depending upon the detector used, over the angular range $30° \leq \theta \leq 80°$.

Comparison of the experimental with the integrated momentum spectra of secondary particles predicted by a modification of the semi-empirical Trilling production formula(23,24) indicates good <u>absolute</u>

Table 4.2. Values of relaxation parameters

Detector	Assumed reaction threshold	Relaxation parameter b, radians^{-1}				
		7-GeV data			3-GeV data	
		"W"	Cu	Al	Pb	Fe
HPD* & TLD		1.65 ± 0.1	1.36 ± 0.05	1.25 ± 0.05		
^{32}S-^{32}P	3.0 ± 0.5 MeV	0.29 ± 0.03	0.39 ± 0.04	0.50 ± 0.06	0.23 ± 0.07	0.30 ± 0.08
^{27}Al-^{24}Na	6.0 ± 0.5 MeV	0.51 ± 0.02	0.65 ± 0.04	0.71 ± 0.04		
^{19}F-^{18}F	11 ± 1 MeV	0.73 ± 0.05	0.90 ± 0.05	1.05 ± 0.07		
^{12}C-^{11}C	22 ± 3 MeV	1.28 ± 0.05	1.34 ± 0.03	1.32 ± 0.05	1.10 ± 0.12	1.35 ± 0.16
^{12}C-^{7}Be	35 ± 5 MeV	1.6 ± 0.1	1.7 ± 0.1	1.4 ± 0.2		
^{27}Al-^{18}F	35 ± 5 MeV	1.6 ± 0.1	1.7 ± 0.1	1.4 ± 0.2	0.84 ± 0.14	1.07 ± 0.13
Au fission	90 ± 10 MeV	2.1 ± 0.3	2.1 ± 0.3	2.1 ± 0.3		

*Hydrogen pressure dosimeter.

agreement at angles less than 30°. At larger angles there is a divergence between the experimental data and theoretical predictions for two reasons: Firstly, this Trilling formula does not correctly describe the production of particles with high tranverse momentum. Secondly, the production of particles in the intranuclear cascade and by evaporation processes must be correctly accounted for. Recently Ranft and Routti have described suitable empirical formulae which predict angular distributions in good agreement with available experimental data at all angles(25).

4.2.3. Accuracy of the Moyer Model

Use of the Moyer model with appropriate input data, and under fairly simple geometrical conditions, leads to estimates of radiation levels usually accurate to better than a factor of two. Figure 4.7 indicates the accuracy possible when experimental data are fitted to a Moyer-type equation. Calculated and measured neutron flux densities in the earth shield of the CPS are shown(26). Fluxes are plotted as a function of longitudinal distance from an internal target for five different depths in the shield. Flux densities were measured utilizing the $^{27}Al(n, \alpha)^{24}Na$ reaction in aluminum. In this particular example, flux densities are predicted to about 20%, over a range of five orders of magnitude. Estimates of dose-equivalent rate follow from a knowledge of neutron flux density and spectrum.

For the calculation of shield thicknesses transverse to a proton beam, for uniform beam loss, the Moyer model takes a particularly simple form. Substituting for $g(\theta)$ using Equation 4.8 and using experimental data from the CPS it may be shown that

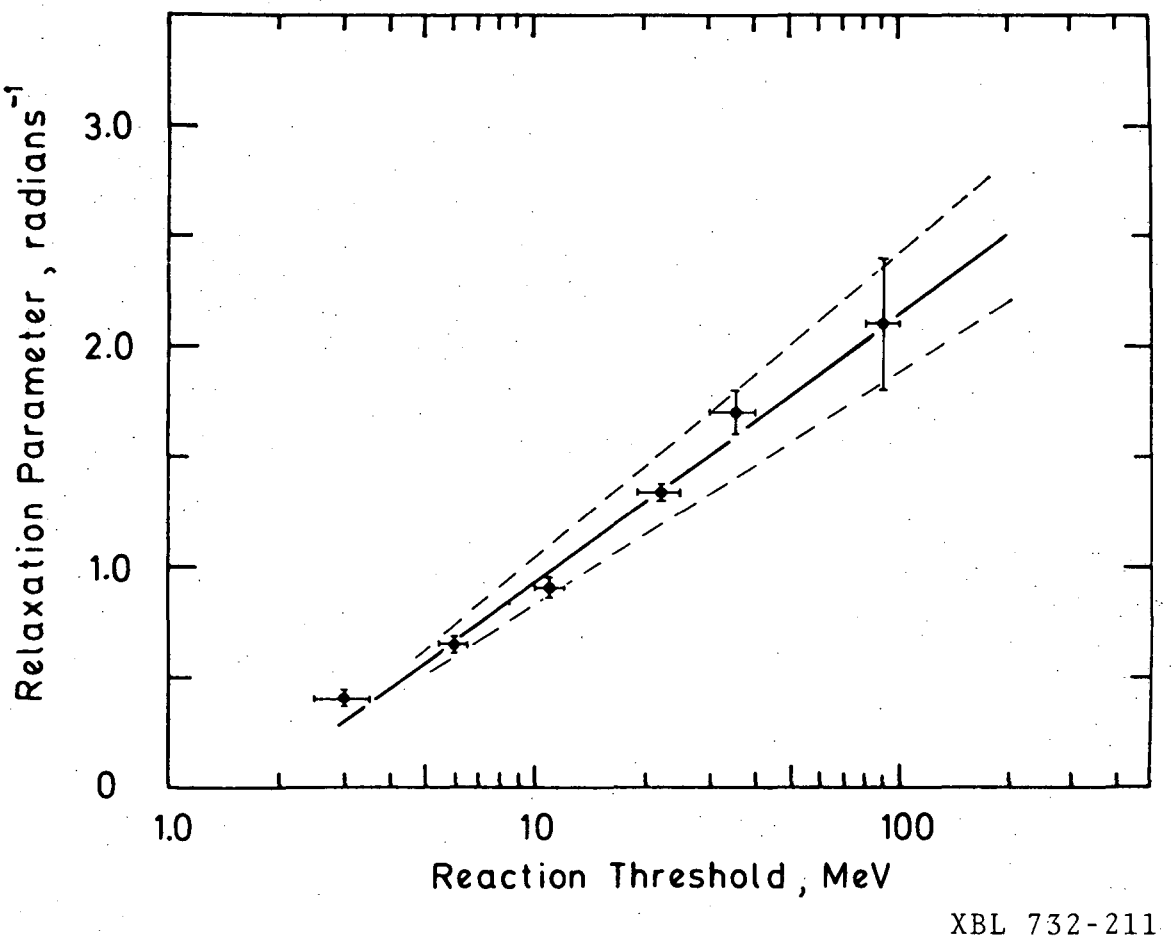
Relaxation Parameter, radians^{-1}
3.0
2.0
1.0
0
1.0
10
100
Reaction Threshold, MeV
XBL 732-211

Fig. 4.6

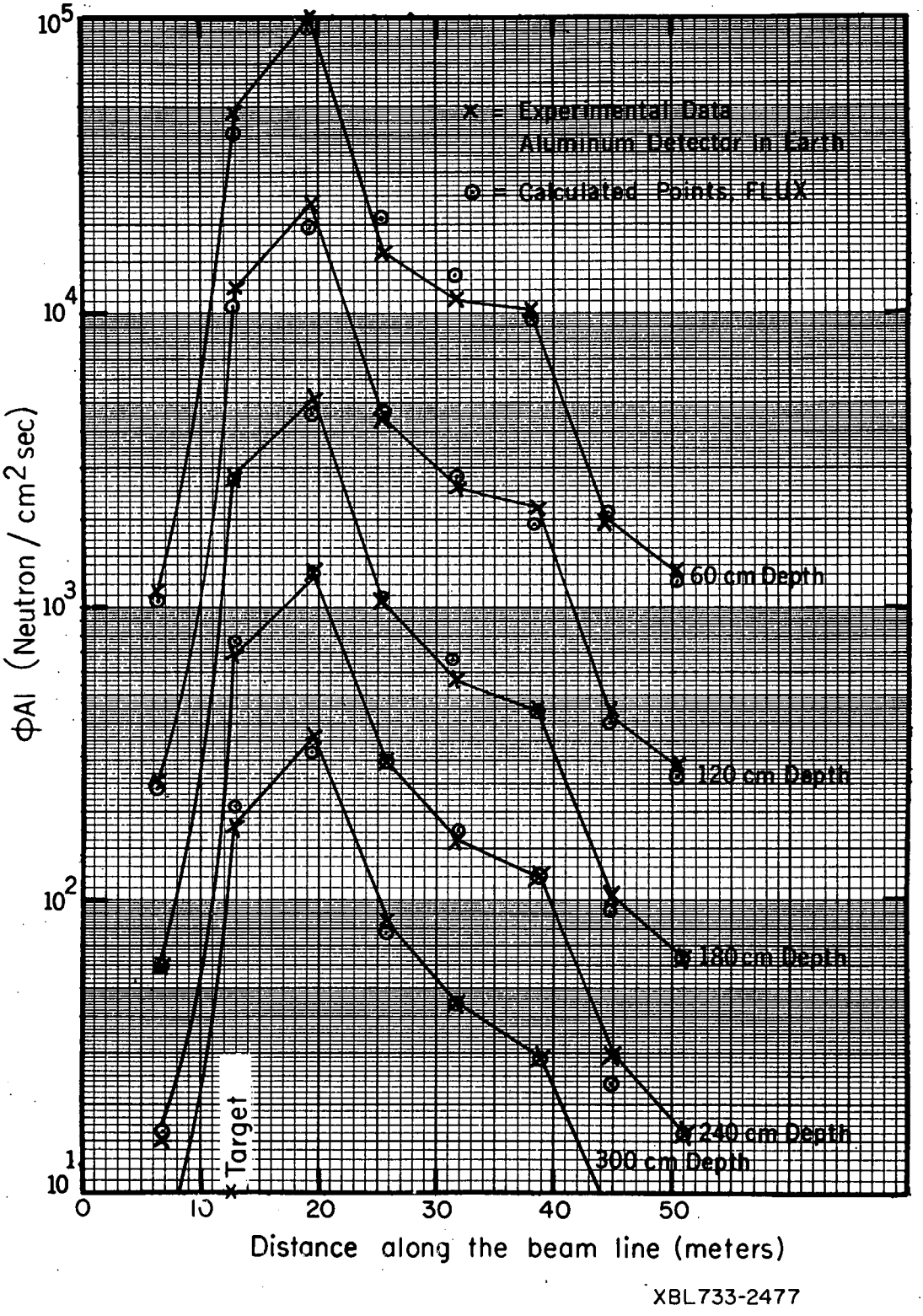
× = Experimental Data
Aluminum Detector in Earth
⊙ = Calculated Points, FLUX
60 cm Depth
120 cm Depth
180 cm Depth
240 cm Depth
300 cm Depth
× Target
ΦAl (Neutron / cm² sec)
Distance along the beam line (meters)
10⁵
10⁴
10³
10²
10¹
0
10
20
30
40
50
XBL733-2477

Fig. 4.7

$$\dot{H} = \frac{0.11\,L}{(a+d)} \int_0^{\pi} \exp(-2.3\theta)\, \exp\left(-\frac{d}{\lambda}\,\mathrm{cosec}\,\theta\right) d\theta, \qquad (4.10)$$

where $\dot{H}$ is measured in mrem/h,

L is the beam loss in units of GeV/cm sec,

a is the accelerator tunnel radius in meters,

d is the shield thickness in meters, and

λ is the attenuation length.

Integrals of the form appearing in Equation 4.10 have been tabulated in the region of physical interest by Routti and Thomas(27).

Phenomenological models permit simple, rapid, and fairly accurate shield estimates. Furthermore, they provide a valuable physical insight into the problems of shielding. Such models are, however, necessarily limited by operational experience.

4.3. Monte Carlo Calculations

One of the most important advances in the study of accelerator radiation environments over the past ten years has been the development of Monte Carlo techniques to calculate electromagnetic and hadronic cascade phenomena. These calculations have recently been reviewed by Ranft(4), and space does not permit a complete discussion here. Accurate and reliable calculations of radiation phenomena at accelerators have required development of an understanding not only of the interaction of primary particles with internal targets and machine components, but also of particle production resulting from primary particle interaction, the transport of these primary and secondary particles together with

their interaction products through matter and, finally, the conversion from the calculation of particles transported to observable phenomena. Ranft has reported good agreement with experimental data in such diverse areas as induced radioactivity, radiation doses, radiation heating, and shielding.

A good example of the agreement between theoretical and experimental data is the recent calculation of the neutron spectrum in the earth's atmosphere by Armstrong et al (28). These workers used a Monte Carlo code to compute the production of protons, charged pions, and neutrons by the incident galactic protons, and the subsequent transport of these particles down to energies of 12 MeV. The production of neutrons of energy $\leq$ 12 MeV as calculated by the Monte Carlo code, was used as input to a discrete-ordinates code to obtain the low-energy neutron spectrum. Figure 4.8 shows the results of these calculations and an absolute comparison with the experimental data of Hess et al (29) at atmospheric depths of 200 and 1033 g/cm^2. The calculated and measured spectra differ somewhat at lower energies but are in good agreement at high energies. The increasing number of such examples of good agreement between calculated and experimental data is extremely encouraging.

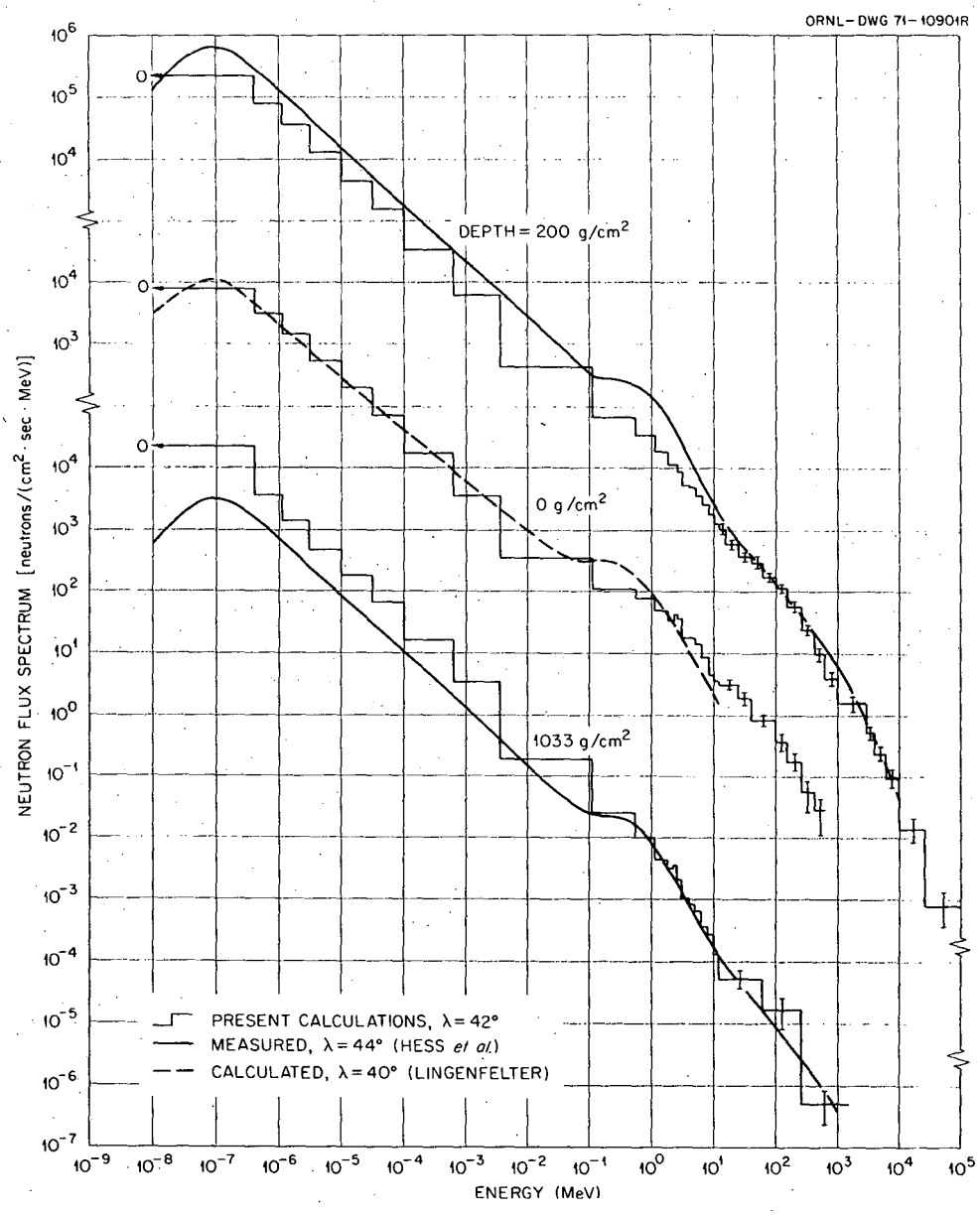

XBL 729-1939

Fig. 4.8

References

Section 4

1. Jaeger, T., "Grundzeuge der Strahlenshutztechnick," Springer-Verlag, Berlin (1960).
2. Patterson, H. W. and Thomas, R. H., Experimental Studies at High Energy Proton Accelerators -- A Review, Particle Accelerators 2, 77 (1971).
3. Patterson, H. W. and Thomas, R. H., "Accelerator Health Physics," Chapter 6, Academic Press, New York (1973).
4. Ranft, J., Particle Accel. 3, 129 (1972).
5. DeStaebler, H., Transverse Radiation Shielding for the Stanford Two-Mile Accelerator, SLAC Report SLAC-9 (1962).
6. Moyer, B. J., Evaluation of Shielding Required for the Improved Bevatron, Lawrence Berkeley Laboratory internal report UCRL-9769 (1961).
7. Moyer, B. J., Proc. Premier Colloq. Int. Prot. aupres des Grandes Accel. Paris: Presses Univ. de France, p. 65 (1962).
8. Smith, A. R., Some Experimental Studies at the 6.2 BeV Berkeley Bevatron, Proc. First Symposium on Accelerator Dosimetry, Brookhaven National Laboratory, USAEC Report CONF-651109, p. 224 (1965).
9. Smith, A.R., et al., Radiation Field Inside a Thick Concrete Shield for 6.2 GeV Incident Protons, op. cit. ref. (8), p. 365.
10. Voss, R. G. P. and Wilson, R., Analysis of High-Energy Neutron Cross Sections, Proc. Roy. Soc. (London), A236, 41 (1956).
11. Ball, W. P., Nuclear Scattering of 300 MeV Neutrons, Ph.D. Thesis, Lawrence Berkeley Laboratory internal report UCRL-1938 (1956).
12. MacGregor, M. H., Ball, W. P. and Booth, R., Neutron Inelastic Cross Sections at 21.0, 25.5, and 29.2 MeV, Phys. Rev. 111, 1155 (1958).
13. Coor, T., Hills, D. A., Hoonyak, W. F., Smith, L. W., and Snow, G., Nuclear Cross Sections for 1.4 BeV Neutrons, Phys. Rev. 98, 1369 (1955).
14. Chen, F. F., Leavitt, C. P. and Shapiro, A., Attenuation Cross Sections for 860 MeV Protons, Phys. Rev. 99, 857 (1955).
15. Patterson, H. W., Proc. Conf. on Shielding of High Energy Accelerators, New York, April 11-13, p. 199.
16. Thomas, R. H., The Proton Synchrotron as a Source of Radiation, in Engineering Compendium on Shielding 1, 67 (1968), Springer-Verlag, New York.

17. Bennet, G. W., Brown, H. N., Foelsche, H. V. J., Fox, J. D., Lazarus, D. M., Levine, G. S., Toohig, T. E., Thomas, R. H., and Kostoulus, J., Particle Distribution in a Still Beam Stop for 28 GeV Protons, Particle Accelerators 4, 229 (1973).
18. Gilbert, W. S. et al., 1966 CERN-LRL-RHEL Shielding Experiment at the CERN Proton Synchrotron, Lawrence Berkeley Laboratory internal report UCRL-17941 (1968).
19. Stevenson, G. R., Shaw, K. B., Hargreaves, D. M., Lister, L. P., and Moth, D. A., Rutherford Laboratory Report RHEL/M/48 (1969).
20. Charalambus, S., Goebel, K., and Nachtigall, D., CERN internal report DI/HP/97 (1967).
21. Awschalom, M. and Schimmerling, W., Nuovo Cimente A64, 871 (1969).
22. Levine, G. S. et al., Particle Accelerators 3, 91 (1972).
23. Ranft, J., Nucl. Instrum. and Methods 48, 133 and 261 (1967).
24. Ranft, J. and Borak, T., National Accelerator Laboratory report NAL-FN-193 (1969).
25. Ranft, J. and Routti, J. T., Particle Accel. 4, 101 (1967).
26. Gilbert. W. S., Proc. Int. Conf. High Energy Accel. 9th, Cambridge, Mass., p. 221 (1967).
27. Routti, J. T. and Thomas, R. H., Nucl. Instrum. Methods 72, 157 (1969).
28. Armstrong, T. W., Chandler, K. C., and Barish, J., Neutron Phys. Div. Ann. Rep. ORNL-4800, p. 63 (1972).
29. Hess, W. N., Patterson, H.W., and Wallace, R., Phys. Rev. 116, 445 (1959).

5. Induced Radioactivity

5. Induced Radioactivity

The development and transport of the electromagnetic and hadronic cascades also result in the production of radioactivity in accelerators and their surroundings. Accelerator shielding and accelerator components such as targets, vacuum chamber, magnets and rf cavities, cooling water or ground water close to the accelerator buildings, and air in the accelerator room may all become radioactive to some degree.

Barbier (1) has summarized the mechanism for the production of radioactivity at high-energy accelerators. In principle, all the nuclides which have atomic mass and atomic number equal to, or less than, the sum of the numbers of the target plus projectile nuclei can be produced. Many of the radionuclides that can be produced have half-lives so short that they need not be considered in protection problems.

5.1. Radioactivity of Accelerator Components and Other Solids

The number of radionuclides which might be produced is potentially very large. Fortunately the materials used in accelerator construction are limited in number, the most important being iron, several stainless steels, copper, aluminum, aluminum alloys, and several plastics. Charalambus and Rindi (2) have reported a table of all the main radionuclides that can be produced at a typical proton accelerator. They considered only radionuclides with a half-life longer than one hour and show that about 70% of them are γ-emitters. However, even shorter half-lives may be of concern for protection purposes if they are produced in large quantities.

Table 5.1 summarizes the radionuclide commonly identified in materials used in accelerators; those with half-lives of less than 10 minutes are excluded. Most of the radionuclides listed are produced by simple nuclear reactions such as (n, xn), (p, xn), (p, pn) etc., but some result from spallation, fragmentation, or capture reactions.

Several measured cross sections for high-energy reaction have been reported by Bruninx (3-5). Rudstam (6) has proposed a very useful empirical formula for their calculation, while Bertini (7) has reported intranuclear cascade calculations of these cross sections.

Because the number of radionuclides produced in accelerator components is large and accelerator operation often variable, the production and decay of gross radioactivity is a complex function of time. Notwithstanding, for radiation protection purposes it may be necessary to have some estimate of the dose rate, and its variation with time.

The decay of dose rate near the 600-MeV CERN synchrocyclotron has been reported by Baarli (8) and Rindi (9). Reliable experimental data of this type are few because of the difficulty of obtaining them at most accelerators. During periods of accelerator shutdown, gross changes in the remnant radiation field may result from structural changes in the accelerator and its shielding. What data are available, however, show that beginning a few minutes after the shutdown, the dose rate decays by about a factor of two in the first two hours and by about another factor of two within the next 50 hours. This is in agreement with measurements at all the accelerators at the Lawrence Berkeley Laboratory (10), and elsewhere (11). Indeed it seems confirmed by general experience that the gross features of the decay of induced activity near accelerators

Table 5.1. Radionuclides commonly identified in solid materials irradiated around accelerators

Irradiated material	Radionuclides
Plastics, oils	^{7}Be, ^{11}C
Concrete, aluminum	As above, plus ^{22}Na, ^{24}Na, ^{32}P, ^{42}K, ^{95}Ca
Iron, steel	As above, plus ^{44}Sc, ^{44m}Sc, ^{46}Sc, ^{47}Sc, ^{48}V, ^{51}Cr, ^{52}Mn, ^{52m}Mn, ^{54}Mn, ^{56}Mn, ^{57}Co, ^{58}Co, ^{60}Co, ^{57}Ni, ^{55}Fe, ^{59}Fe
Copper	As above, plus ^{65}Ni, ^{61}Cu, ^{64}Cu, ^{63}Zn, ^{65}Zn

Table 5.2. Radionuclides identified in the air of different accelerators

Radionuclide	Where identified	Explanation of previous symbol and reference
^{7}Be	A	A = Saclay 560-MeV electron linac (20)
^{11}C	A, B, C, D, E, F	
^{13}N	A, B, C, D. E, F, G, H	B = CERN 600-MeV proton synchrocyclotron (21)
^{14}O	D	C = CERN 28-GeV proton synchrotron (22)
^{15}O	A, C, D, E, G. H	
^{16}N	E	D = PPA 3-GeV proton synchrotron (23)
^{24}Na	A, D	
^{37}S	D	E = RHEL 7-GeV proton synchrotron (24)
^{38}Cl	A, H	
^{39}Cl	A	F = BNL 30-GeV proton synchrotron (25)
^{41}A	A, B, C, D, F	
^{34m}Cl	D	G = RPI 50-MeV electron linac (26)
		H = Frascati 300-MeV electron linac (27)

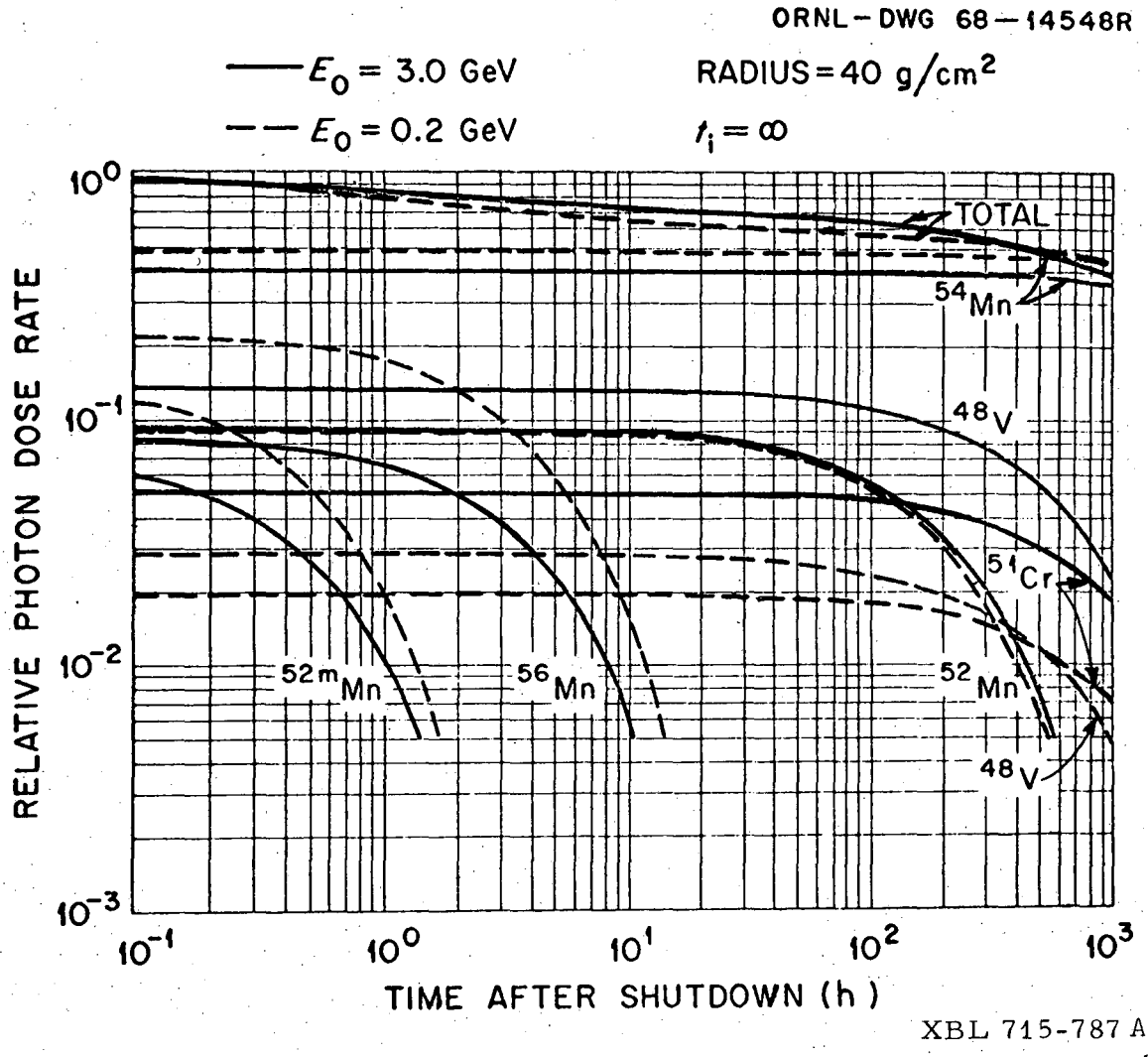

Fig. 5.1. Relative contribution to photon dose rate.

that have been in operation for several years, are nearly independent of the type of particles accelerated and their maximum energy.

Sullivan and Overton(12) have shown that the dose-rate decay may be approximated by an equation of the form

$$D(t) = B\phi \ln\left(\frac{T+t}{t}\right) \qquad (5.1)$$

where $D(t)$ is the dose rate at time t after irradiation ceases, ϕ is the flux density of high-energy primary particles, T is the irradiation time and B is a parameter which depends on several variables but is a constant for any given set of irradiation, target and geometrical conditions. Equation (5.1) is in good qualitative agreement with the form of the build-up and decay of dose rates observed in an accelerator environment, and in a recent paper Sullivan(13) has reported values of B for heavy materials that give reasonably good absolute agreement with observation. More accurate calculations require detailed Monte Carlo techniques of the type used in shielding calculations. Armstrong et al (14,15) have calculated the dose rate resulting from the irradiation of steel by 200-MeV, 3-GeV, and 200-GeV protons. For long irradiation times they find that ^{52m}Mn(21 min), ^{56}Mn(2.6 h), ^{52}Mn(5.6d), ^{48}V(16 d), ^{51}Cr(27.8 d), and ^{54}Mn(280 d) are the dominant radionuclides (Fig. 5.1). These calculations are supported by recent observations at the 76-GeV proton synchrotron in Serpukhov(16).

At electron accelerators, too, only few nuclides are dominant. For example, Saxon(17) reports that at the 4-GeV electron synchrotron NINA, ^{56}Mn, ^{52}Mn, and ^{48}V are dominant in steel. Similar results have been reported by Wyckoff(18) from exposure to the 100-MeV

bremsstrahlung beam of the NBS linac. De Staebler(19) has estimated the gross production of radioactivity by a high-energy electron accelerator as some 34 Ci at saturation per kW of beam power.

5.2. Radioactivity of Air

Radioactive gases are produced by the interaction of primary and secondary particles with the nitrogen, oxygen, argon, and carbon nuclei of air circulating in the accelerator vaults. In Table 5.2 we show the radionuclides which have been found in the air at different accelerators. Radionuclides with half-lives less than one minute are of no concern, decaying to negligible activities before personnel can enter the accelerator room or before the air can reach populated areas around the accelerator. Long-lived activities, on the other hand, may be discounted because of their low production rate. Such arguments, supported by the measurements cited in Table 5.2, suggest that at existing accelerators only four radionuclides need be considered: ^{15}O, ^{13}N, ^{11}C, and ^{41}A. A further increase in the energy or in the intensity of the accelerators however, could cause the production of amounts of ^{7}Be and ^{3}H which may be important.

Presently, the concentrations of radioactive gases measured in the accelerator room a few minutes after shutdown, may range between 10 and 30 times the MPC for continuous inhalation(21). However, the air is quickly mixed with inert air and the radioactivity decays rapidly so that the associated dose rate is negligible compared to that from the solid machine parts.

5.3. Radioactivity of Water

Radioactivity induced in cooling water circuits of high-intensity accelerators is potentially of concern for the following reasons: high dose rates around pipes carrying this water, radioactive contamination resulting from spills, and disposal problems. Rose et al (28) reported that external radiation levels as high as 100 mrem/h were found at various regions close to the cooling system of the Harwell 150-MeV cyclotron when it was operated with an internal beam of about 1 μA. Warren et al (29) have reported dose rates of between 0.5 and 4 mrem/h from cooling water circuits along the accelerator structure of the Stanford 20-GeV electron linear accelerator. Considerably higher levels are found from heat exchangers for high-power beam dumps – rates up to 120 mrem/h being observed.

Distenfeld(25) has concluded from measurements at the Brookhaven AGS that with a proton beam intensity of 10^{13} protons/sec the external radiation hazard from induced activity in cooling water would be trivial. However, the dose rate from large volumes of water, such as heat exchangers or storage tanks, would be measurable during accelerator operation. Some rough experimental studies of the production of radionuclides in water from typical high-energy neutron spectra(30) have confirmed ^{11}C, ^{7}Be, and ^{3}H as the most important ones produced. The ratio of the specific activities of tritium and ^{7}Be extrapolated at saturation in samples of water irradiated under several different conditions varied between 1.3 and 5.8. Disposal of irradiated water to streams would generally be controlled by the tritium content, since ^{7}Be is strongly absorbed in the mixed bed resins used for

demineralizing the waters(31). Careful studies of the radioactivity produced in water irradiated by high-energy electrons (29) have identified ^{15}O, ^{11}C, and ^{7}Be as the most important radionuclides.

References

Section 5

1. Barbier, M., Induced Radioactivity, Amsterdam: North Holland, (1969).
2. Charalambus, S., Rindi, A., Aerosol and Dust Radioactivity in the Halls of High Energy Accelerators, Nucl. Instrum. Methods 56:125 (1967).
3. Bruninx, E., High Energy Nuclear Reaction Cross Sections, Vol. 1, CERN Report 61-1 (1961).
4. Bruninx, E., High Energy Nuclear Reaction Cross Sections, Vol. 2, CERN Report 62-9 (1962).
5. Bruninx, E., High Energy Nuclear Reaction Cross Sections, Vol. 3, CERN Report 64-17 (1964).
6. Rudstam, G., Systematics of Spallation Yields, Zeit Naturforsch, 21A: 1027 (1966).
7. Bertini, H. W., Calculations of Nuclear Reactions for Incident Nucleons and π-Mesons in the Energy Range 30-2700 MeV, in Proc. Second International Conf. on Accelerator Dosimetry, Stanford, California, November 5-7, 1969. USAEC Report CONF-691101, p. 42.
8. Baarli, J., Induced Radioactivity in the CERN Accelerators, in First International Conference on Shielding Around High Energy Accelerators, Paris, France, January 1962. Presses Universitaires de France, Paris (1962), p. 123.
9. Rindi, A., Colloq. Intern. sur la Dosimetrie des Irradiations dues a des Sources Externes, Paris, France, Vol. 2:153 (1964).
10. Boom, R.W., Toth, K.S., Zucker, A., Residual Radiation of the Lawrence Radiation Laboratory 184-Inch Cyclotron, Oak Ridge National Laboratory Report ORNL-3158, June 1961.
11. Awschalom, M., Larsen, F.L., Sass, R.E., The Radiation Measurements Group at the Princeton-Pennsylvania 3-GeV Proton Synchrotron, in Proc. First Symposium on Accelerator Dosimetry, Brookhaven, November 5-7, 1965, USAEC Report CONF-65119, p. 57.
12. Sullivan, A.H., Overton, T.R., Health Physics. 11:1101 (1965).
13. Sullivan, A.H., Health Physics 23:253 (1972).

14. Armstrong,T.W., Barish, J.
    a. Calculation of the Residual Photon Dose Rate Induced in Iron by 200 MeV Protons.
    b. Calculation of the Residual Photon Dose Rate Due to the Activation of Concrete by Neutrons from a 3-GeV Proton Beam.
    Both in Proc. Second International Conf. on Accelerator Dosimetry, op. cit. ref. (7) pp. 63-90.
15. Armstrong, T.W., Alsmiller, R.J., Nucl. Sci. Eng. 38:53.(1969).
16. Golovachik, V.T., Britvich, G.I., Lebedev, V.N., IFVE-69-76, Transl. ORNL-tr-2328 (1969).
17. Saxon, G., DNPL Rep. P8, Daresbury, England (1969).
18. Wyckoff, J., Radioactivity Produced by a Linac, IEEE Trans. Nucl. Sic. 14(3) 990 (1967).
19. De Staebler, H., SLAC Report TN-63-92, Stanford, California (1963).
20. Vialettes, H., Gas and Dust Activation in the Target Room of the Salcay Electron Linac, in Proc. Second Internal Conf. on Accelerator Dosimetry, Stanford, California Nov. 5-7, 1969, USAEC Report CONF-691101, p. 121.
21. Rindi, A., Charalambus, S., Nucl. Instrum. Methods 47:227 (1967).
22. Höfert, M., Radiation Hazard of Induced Activity in Air as Produced by High-Energy Accelerators, op cit. Ref. 20, p. 111.
23. Awschalom, M., Larsen, F., Schimmerling, W., Health Phys. 14:345; idem 1969. Nucl. Instrum. Methods 75:93.
24. Shaw, K. B., Thomas, R. H., Problems Associated with a High Energy Proton Beam, Health Physics 13:1127 (1967).
25. Brookhaven National Laboratory, BNL Report 7956, p. 225 (1964).
26. George, A.C., Breslin, A.T., Haskins, T.W., Ryan, R.M., op cit ref. 11, p. 513 (1965).
27. Ladu, M., Pelliccioni, M., Roccella, M., Giorn, Fis. San. Minerva Fis. Nucl. 11(2):112 (1967).
28. Rose, B. et al., Radioactivity of Cyclotron Cooling Water, AERE NP/R- 2768, Harwell, England (1958).
29. Warren, G.J., Busick, D.D., McCall, R.C., Radioactivity Produced and Released from Water at High Energies, in op cit ref. 20, p. 99.

30. Stapleton, G.B., Thomas, R. H., Rutherford Laboratory Report, RHEL RP/PN/45 (1967).

31. Busick, D. D., Warren . G.T., Operational Health Physics Associated with Induced Radioactivity at the Stanford Linear Accelerator Center, in op. cit. ref. 20, p. 139.

6. Environmental Impact of High-Energy Accelerators

6.1. Prompt Radiation Field Outside High-Energy Accelerator Shields.

6.2. Transport of Radionuclides into the Environment

6.3. Environmental Monitoring at Accelerators

6.3.1. The Lawrence Berkeley Laboratory and its Location

6.3.2. Environmental Monitoring of Penetrating Radiation

General inaccuracies in reported dose equivalent due to neutron-fluence to dose equivalent conversion.

Inaccuracies in determination of dose equivalent due to uncertainties in natural background.

References

6. Environmental Impact of High-Energy Accelerators

The radiological impact of high-energy accelerators on the environment is different in character from most other types of nuclear installation.[1]

At high energy accelerators the predominant source of radiation exposure to the general public is due to the "prompt radiation field" produced during operation, rather than due to the leakage of radionuclides into the environment.

6.1. Prompt Radiation Field Outside High-Energy Accelerator Shields. As we have seen, the radiation field outside the shielding of high energy, high intensity accelerators is dominated by neutrons. This is true for both proton and electron accelerators and -- although no data are yet available -- will be true for high-energy heavy-ion facilities such as the Bevalac. As an example, Fig. 6.1 shows observations of gamma and neutron dose equivalent rates at one of the Stanford Linear Accelerator Monitoring Stations, some hundred meters from the accelerator.[2] The data, which include natural background, clearly show the periods of accelerator operation where significant external radiation was produced. The dominance of neutrons of the accelerator-produced radiation is evident even though electrons are the primary particles accelerated.

High-energy accelerators, even when adequately shielded for reasons of radiation protection and to permit their experimental utilization, may nevertheless be significant sources of neutrons. The total area of the shielding of the larger facilities available for neutron leakage may be extremely large (see introduction), and thus the leakage flux integrated over the shield surface can be large, even if the flux density is small. As an example, $\sim 10^{9}$ n sec^{-1} leak from the Bevatron roof shield when protons are accelerated. Neutron sources of this intensity can be detected at distances up to 1000 meters and it is therefore important to understand the transport of these neutrons through the atmosphere.

Our present experimental and theoretical understanding of neutron transport in the atmosphere has recently been summarized by Rindi and Thomas.[3] Figure 6.2 shows measurements reported in the literature of neutron flux density at distances greater than 100 meters from six

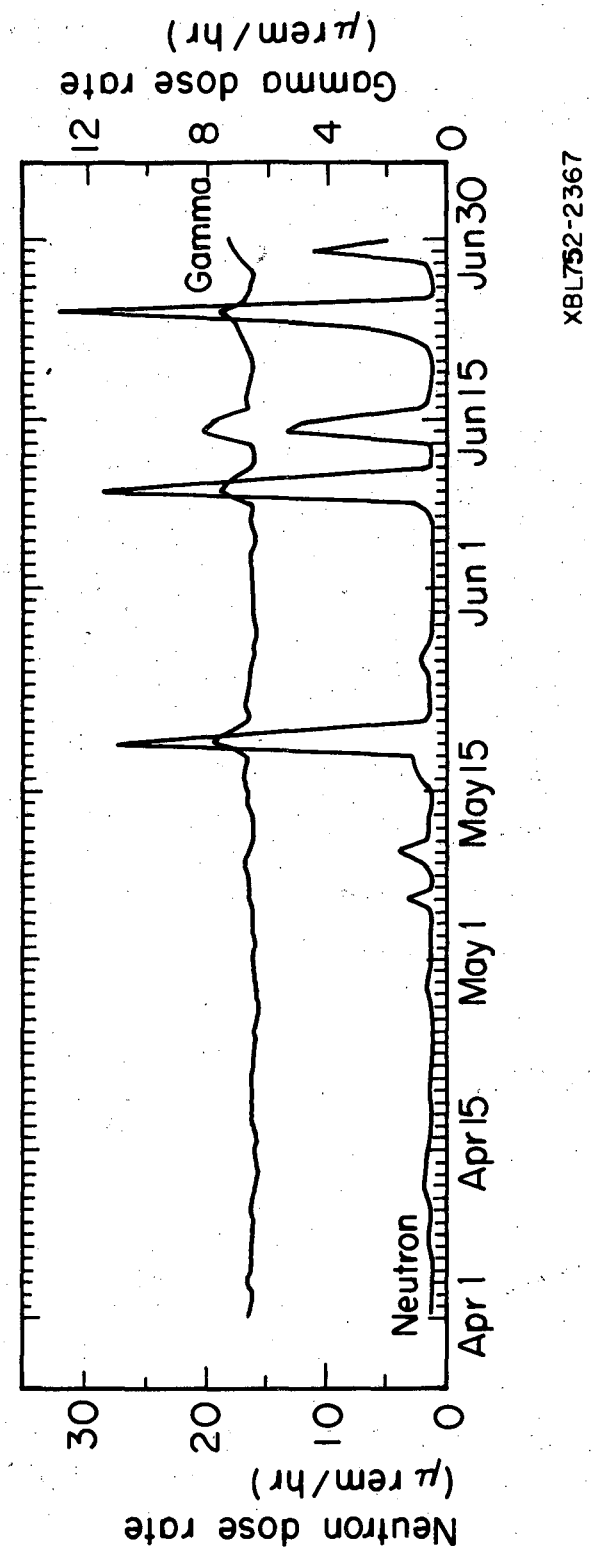

Fig. 6.1.

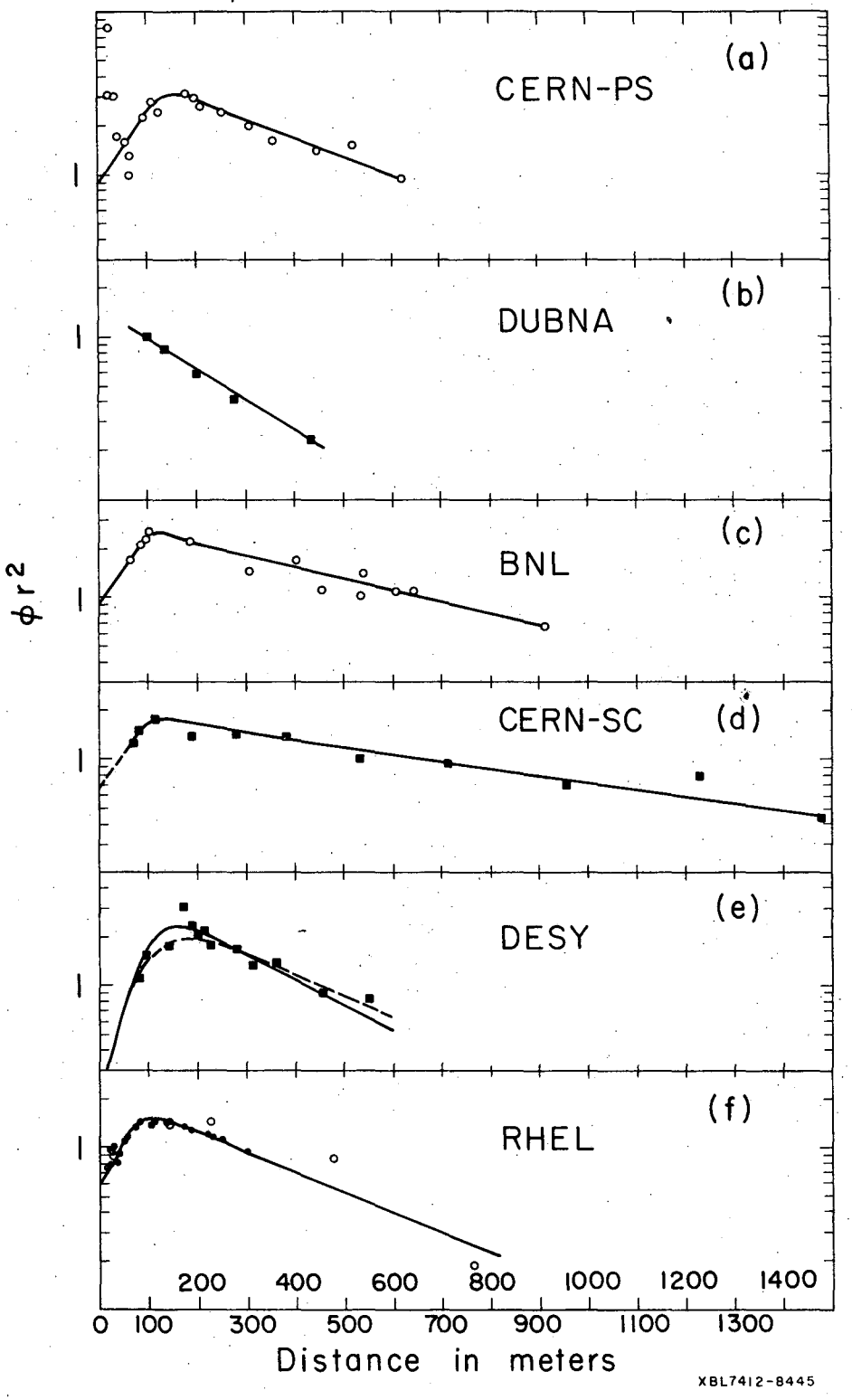
(a)
CERN-PS
(b)
DUBNA
(c)
BNL
(d)
CERN-SC
(e)
DESY
(f)
RHEL
φr2
0 100 300 500 700 900 1100 1300
200 400 600 800 1000 1200 1400
Distance in meters
XBL7412-8445

Fig. 6.2

TABLE 6.1

Summary of some experimental measurements

Laboratory	Primary Beam	Type of Measurement	Buildup factor	Buildup distance (in meters)	λ for expression (10) (in meters)	Reference
CERN-PS	29-GeV proton	Neutron fluence with a long counter	~3	150	395	4
Dubna	10-GeV proton	Neutron fluence with a long counter		< 100	230	5
BNL	30-GeV proton	Neutron fluence with Bonner sphere	2.8	125	610	6
CERN-SC	600-MeV proton	Neutron fluence with a long counter	2.7	140	990	7
DESY	4-GeV electron	Neutron fluence with a BF_3 counter and scintillators	6 or 7	150	330 or 270	8
RHEL	30-MeV proton	Neutron fluence with a long counter	2.5	110	303	9,10

high-energy accelerators as a function of distance. The ordinate shows the product of the measured flux density with the square of the distance from the accelerator. Smooth curves are drawn through the experimental points. On such a plot an inverse square law variation would be a horizontal line. These sets of data indicate an initial buildup followed by an approximately exponential attenuation of the parameter $r^2 \phi(r)$ at distances greater than about 200 meters from the accelerator. Thus we empirically find that:

$$\phi(r) \propto \frac{e^{-r/\lambda}}{r^2} \tag{6.1}$$

Table 6.1 summarizes the data plotted in Fig.6.1. The values of attenuation length obtained are seen to vary between 230 m and 990 m. Rindi and Thomas tentatively explain these variations in observed attenuation length in terms of leakage spectrum from the accelerator shield.

At well-shielded accelerators the leakage neutron spectrum reaches equilibrium within the accelerator shield: this equilibrium is controlled by neutrons of energy greater than about 100 MeV and the characteristics of their interaction with matter. The nature of the equilibrium achieved is determined by the nuclear properties of the shield. At the interface between the shield and air small changes in the equilibrium spectrum -- most noticeably in the neutron resonance region -- are initiated. An equilbrium determined by the nuclear properties of air will be reestablished after passage through two to three interaction mean free paths, corresponding to several hundred meters. Rindi and Thomas conclude that many measurements reported in the data are limited to this transition region and large variation in reported values are to be expected. A lower limit for λ would be that measured for fission neutrons of $\lambda \approx 225$ meters[11] while an upper limit consistent with the inelastic cross section of nitrogen, and the attenuation of strongly interacting particles in extensive air showers, would be $\lambda \approx 850$ meters.[3]

Rindi and Thomas suggest that many of the published data are consistent with this suggestion. Measurements made at low energy accelerators or where the shield leakage spectrum was rich in low energy neutrons give values of λ in the region ~250 m. At accelerators where the leakage spectrum is dominated by high-energy neutrons, higher values of λ are to be expected and, indeed, observed. Rindi[7] has reported $\lambda \approx 990$ meters at the CERN synchrocyclotron, while Distenfield[6] has measured a value of 610 meters at the Brookhaven alternating gradient synchrotron. There are data, however, which do not fit with this general hypothesis[12] and continuing study of high-energy neutron transport problems is needed.

In summary, from their review of the available experimental data, Rindi and Thomas conclude:

1. The radiation intensity decreases at least as fast as does the inverse of the square of the distance from the source.

2. At large distances from accelerators, neutrons are the dominant component of the radiation field.

3. For well-shielded accelerators in the GeV region, the neutron spectrum emerging from the shield is in equilibrium. At lower energies or at accelerators with inadequate overhead shielding, hardening of the spectrum with distance is observed.

4. The empirical relation

$$\phi(r) \approx \frac{\alpha Q e^{-r/\lambda}}{4\pi r^2}$$

is a simple but adequate expression for the skyshine intensity around most accelerators. Value of λ reported in the literature vary between 267 m and 850 m. At large distances (several thousand meters) from our understanding of high-energy hadron cascades , we would expect λ to approach the value of ~ 100 g cm^{-2}.

Transport of Radionuclides into the Environment.

a. Water Supplies. The possible contamination of the ground water close to a high energy laboratory was first theoretically studied at the Stanford Linear Accelerator Center by Nelson[13] who concluded that there would be no detectable increase in the radioactivity in ground water due to operation of the SLAC 200 GeV electron accelerator. This conclusion has been

subsequently confirmed by a program of measurements of the radioactivity of ground water over the past 12 years at Stanford.[14] There have, in fact, been no reports in the literature of significant ground water contamination from radionuclides produced by accelerator operation.

There is, however, a theoretical protential for ground water contamination at the larger high energy accelerators such as the 20 GeV electron linear accelerator at Stanford, or the strong-focussing synchrotrons at Batavia, Brookhaven, (USA); Geneva (Switzerland); or, Serpukhov (USSR); because these accelerators are buried underground. It is therefore possible for substantial particle flux densities to be generated in the earth and water in the shield, with the concommitant production of radionuclides in the environment. As, an example, a flux density of fast neutrons of $\sim 10^5$ n cm^{-2} sec^{-1} will produce tritium, by spallation reactions of the oxygen in water, at a specific activity (at saturation) equivalent to the maximum permissible concentration..

Stapleton and Thomas[15,16] have estimated the total quantities of radionuclides that are produced in the earth shield of a large proton synchrotron, such as that at the Fermi National Accelerator Laboratory at Batavia, and conclude the magnitude to be of the order of tens of curies. In the specific case of tritium, the quantity produced in the environment by a high energy accelerator is thus comparable to the quantity released to the environment by a boiling-water nuclear power reactor.

Hoyer[17] has reported measurements of several radionuclides in the earth shield of the CERN 25 GeV proton synchrotron and identified ^{22}Na and ^{45}Ca in drainage water taken from the earth shield. He finds fair agreement (within a factor of about three) between his measured data and values calculated from measured value neutron flux density distribution within the earth shield.[18] In all cases the measured values are lower than those calculated and Hoyer tentatively ascribes this fact to the migration of the radionuclides induced in the earth away from the accelerator. It is this migration of radionuclides from the shield that theoretically might be a source of contamination of water supplies and deserve consideration and has been the subject of some research.

A detailed study of this possibility would be extremely complex, but it is possible to understand its magnitude by the use of the sample model shown in Fig. 6.3, where it is assumed that radionuclides produced in the activation zones around the accelerator are washed downward by rainfall to the water table, where they are moved horizontally to the edge of the accelerator laboratory. In this movement they are mixed with the ground water and diluted. This water might then be available for public use, in which case it would have a specific activity S, in units of MPC, given by:

$$S_i = D \sum_i \frac{\varepsilon_i \, Q_i \left(1 - e^{-T_i/\tau_i} \right) e^{-t_i/\tau_i}}{M_i} \qquad (6.2)$$

where there are i radionuclides produced and:

D is a dilution factor.

ε_i the fraction of activity produced that migrates from the site of its production.

Q_i is the total quantity of the ith radionuclide produced at saturation.

T_i is the residence time in the activation zone.

τ_i is the mean life of the ith radionuclide.

t_i is the transport time from reaching the water table to reaching the laboratory perimeter.

M_i is the MPC of the ith radionuclide.

Equation (6.2) permits a crude assessment of the magnitude of the problem. The maxium rate of release of activity occurs at small residence times (T = 0), when all the activity produced migrates (ε = 1) and the transport time to the site boundary is very short (e^{-t_i/τ_i} = 1) when:

$$S_{MAX} = D \sum_i \frac{Q_i}{M_i \, \tau_i} \qquad (6.3)$$

At the accelerator site where the water table is not disturbed by pumping, the out-flow of water would equal the inflow from rainfall and the radioactivity released would be diluted in a volume of water equivalent to the rainfall on the site.

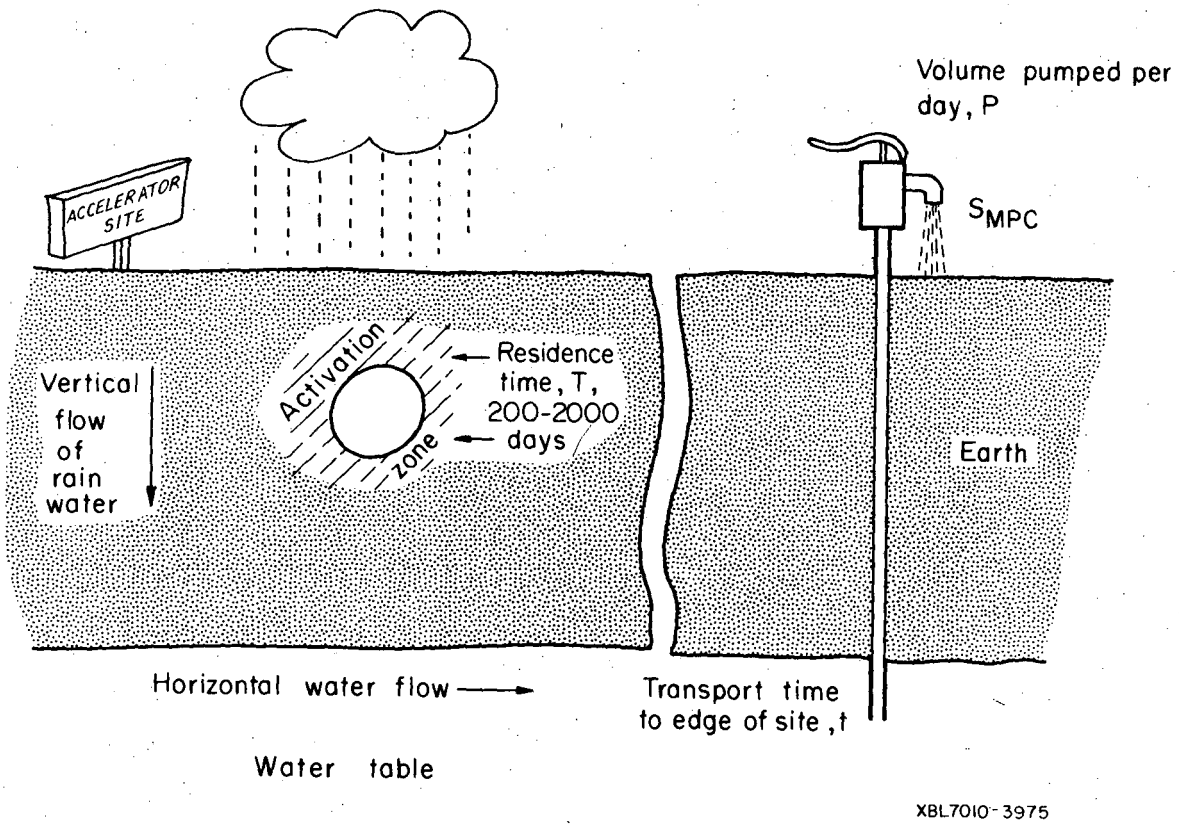
Volume pumped per day, P
ACCELERATOR SITE
S_{MPC}
Activation zone
Residence time, T, 200-2000 days
Vertical flow of rain water
Earth
Horizontal water flow
Transport time to edge of site, t
Water table
XBL7010-3975

Fig. 6.3

Equation (6.2) permits a crude assessment of the magnitude of the problem and Fig. 6.4 gives an example of the concentration of several radionuclides as a function of residence time, for a particular accelerator.[15] This example assumed a 500 GeV proton sychrotron, situated on a site similar to that at the CERN accelerator, losing 10^{12} protons per second to the shield. It was assumed that all the radionuclides produced in the earth and water in the shield were released directly to the ground water and transported to the site boundary in a short time (7 days) and diluted with a quantity of water equivalent to the net rainfall on the accelerator site. (10^{10} ml/day.) Inspection of Fig. 6.4 shows that even under these extremely conservative assumptions the specific activity of the water would never exceed 0.03 MPC and that this value is rather insensitive to residence time up to periods of 1000 days. This crude treatment shows that the problem is not likely to be a serious one, but in actual practice its magnitude is likely to be much smaller.

Although the number of radionuclides produced in the earth and ground water in an accelerator shield is potentially very large, only a few can actually be produced in maximal quantities in ground-water systems.

Equation 6.2 shows that radionuclides of greatest concern

a. are produced in large quantities, and (or)
b. have a low MPC,
c. pass efficiently into the ground-water system,
d. do not decay significantly in being transported to a public water supply.

Nuclides with short half-lives will decay so rapidly as to be of no potential hazard by the time they reach a public water supply. Conversely, if the half-life is long the production rate will be too small and the nuclides will not appear in significant quantities. Knowledge of the hydrogeology of the accelerator site being studied will indicate the range of raidoactive half-lives that are of interest. It is usually reasonable to study radionuclides with half-lives in the range 10 hours $< T <$ 100 years, but detailed investigation of site conditions will identify the appropriate range to be investigated. Those nuclides in this range of half-life that also satisfy conditions (a), (b), and (c) are fortunately few in number.

Furthermore, not all the radionuclides produced move freely in the ground water. Chemical sorption inhibits the migration of several of the radionuclides produced into the ground water. This has been most extensively studied for reactor produced radionuclides buried underground.[19]

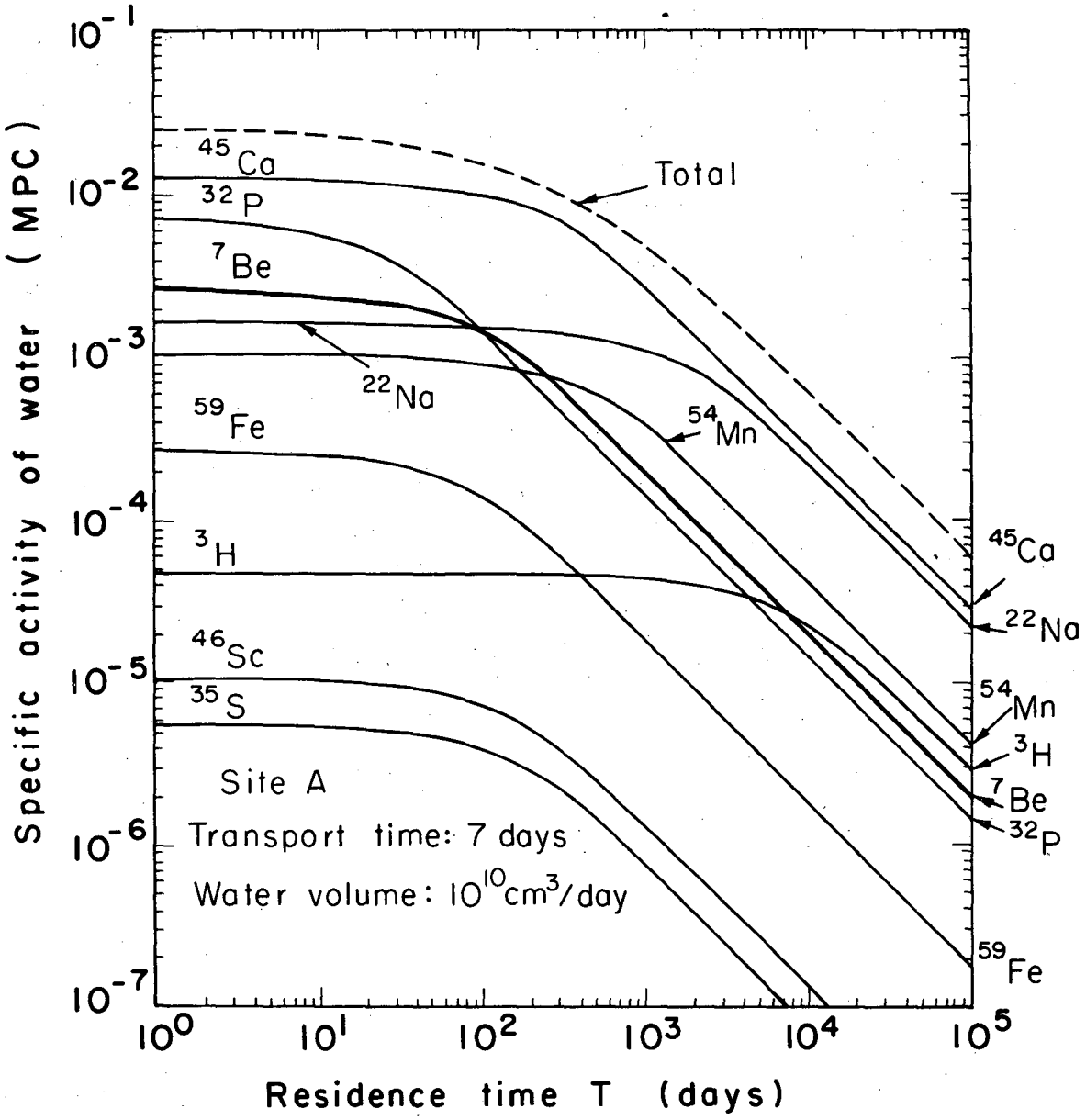
Specific activity of water (MPC)
Residence time T (days)
Total
45Ca
32P
7Be
22Na
59Fe
54Mn
3H
46Sc
35S
Site A
Transport time: 7 days
Water volume: 10^10 cm^3/day
XBL7010-4056

Fig. 6.4

6.3. Environmental Monitoring at Accelerators

In a climate of increasing public apprehension of environmental pollution by nuclear facilities it is necessary that the radiological impact be carefully monitored.

At research installations there is no "proper" way of doing this and monitoring systems must be adopted to the specific needs of the facility.

The environmental monitoring programe of the Lawrence Berkeley Laboratory is typical of installations at many research accelerator laboratories and will be described in some detail.

6.3.1. The Lawrence Berkeley Laboratory and its Location

The Lawrence Berkeley Laboratory (LBL) of the University of California is situated on the western slope of the most westerly range of hills parallel to the eastern side of San Francisco Bay. Elevation of the site varies between 400 ft. and 800 ft. above sea level. The Laboratory area is enclosed on the north and south sides by sparsely populated residential areas of the cities of Berkeley and Oakland. The major part of the Berkeley Campus of the University of California lies on the west side of the Laboratory. Higher up on the hills to the east are the Lawrence Hall of Science and Space Sciences Laboratory; beyond them lies uninhabited land and the Tilden Regional Park. The geographical setting is shown in the map (Fig. 6.5), **and a good impression of the location of the Laboratory may be obtained from** Fig. 6.6, **which shows a general view of the western side of the Berkeley Hills with the Lawrence Berkeley Laboratory lying at the foot of the hills. The Berkeley Campus of the University of California is in the center of the photograph, while the city of Berkeley surrrounds the Campus and Laboratory in the foreground and to the right and left of the picture. Almost the entire urban population of the San Francisco Bay Area (∿4 million people) lies within 80 kilometers of the Laboratory.* More importantly, as we shall show later when we discuss the estimates of population exposure,**

***It is conventional to estimate population dose contributed by a nuclear installation out to a distance of 80 kilometers from the facility.** (see Section 7.)

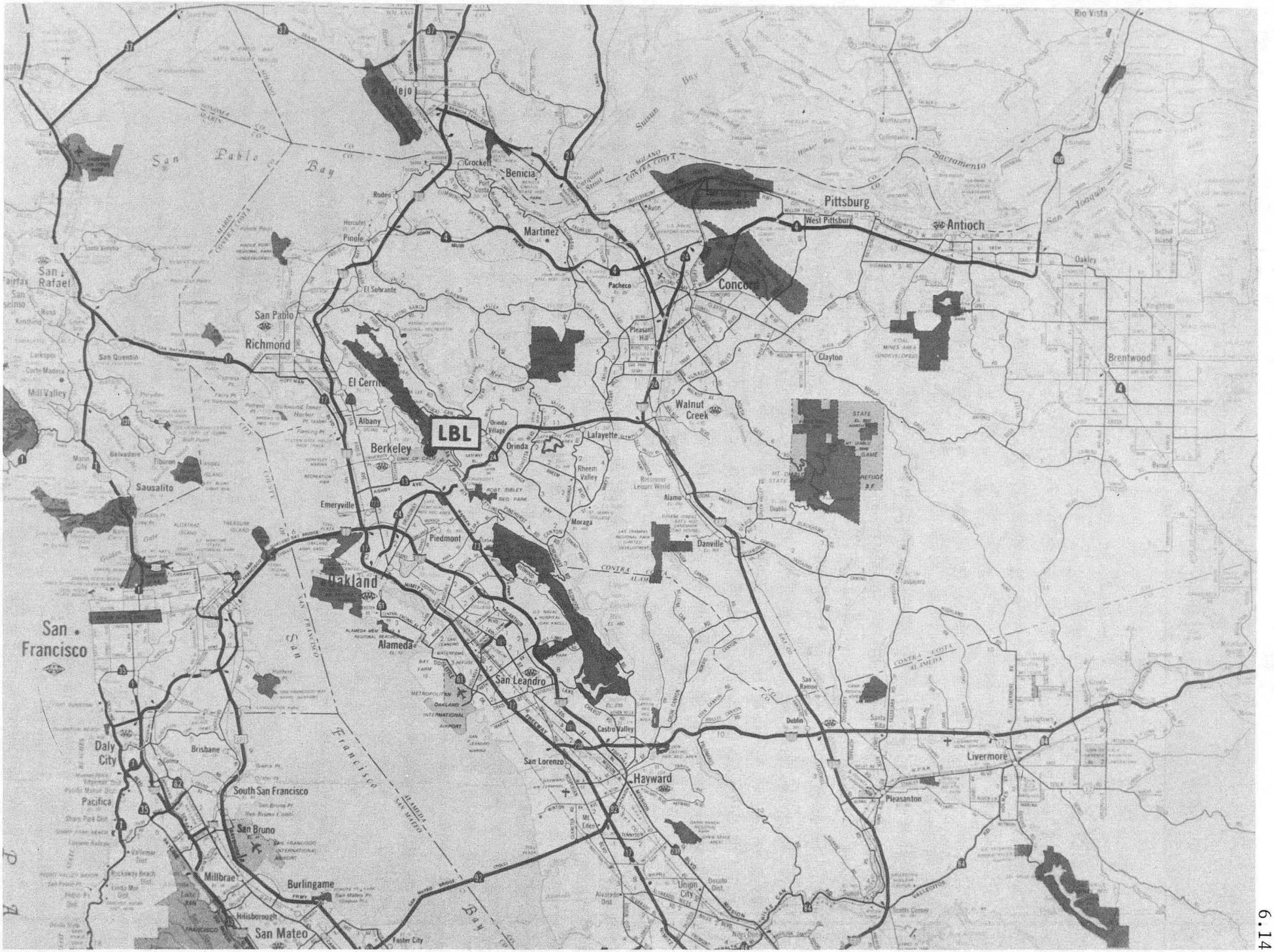

Fig. 6.5

XBC 7412-6205

XBB 673-1730

Fig. 6.6

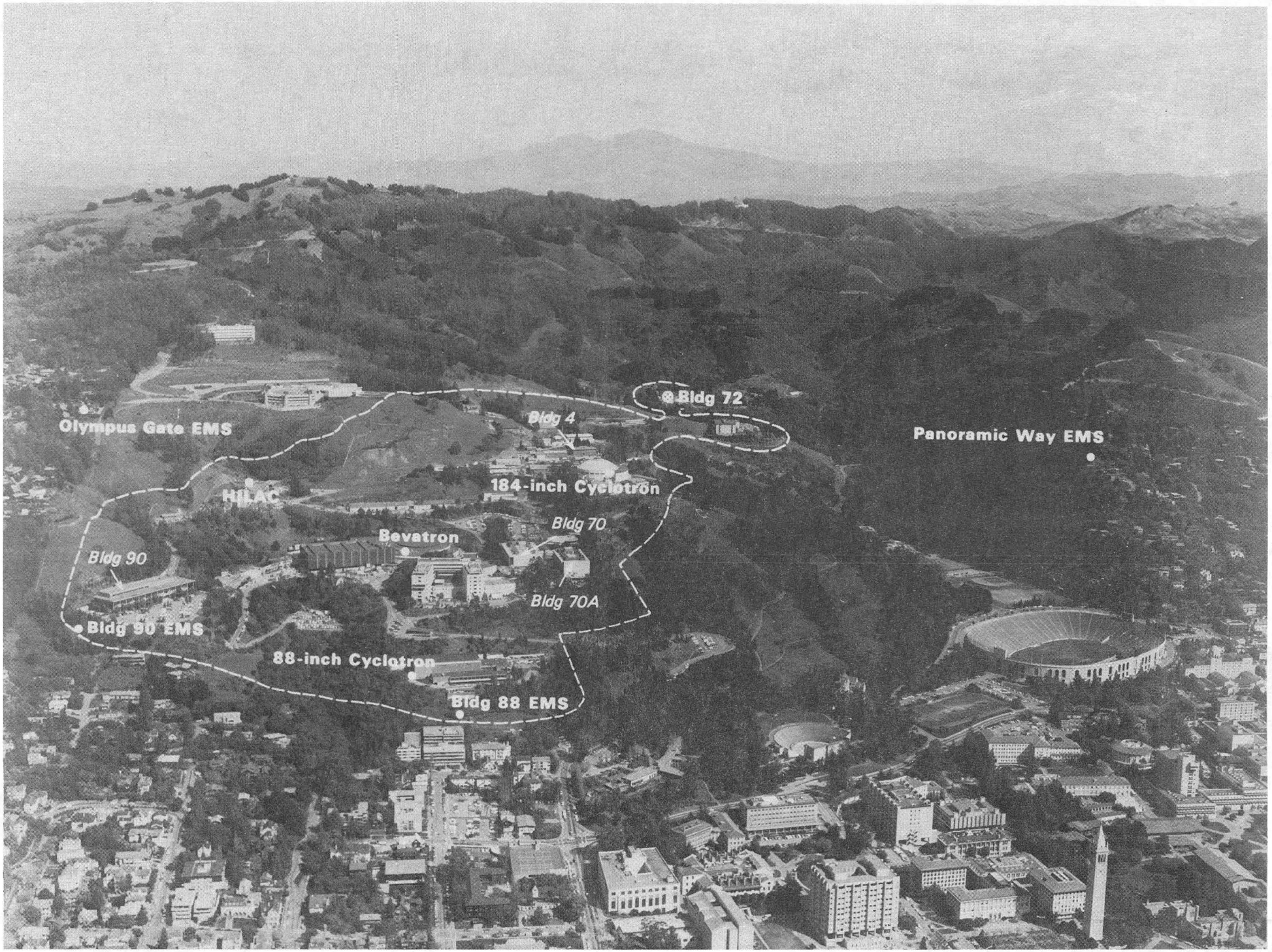

XBB 733-1830

Fig. 6.7

it is estimated that the equivalent of 329,000 live or work within 8 kilometers of the Laboratory perimeter. This proximity of a large population to the Laboratory results in a population dose due to Laboratory operations comparable in magnitude to the collective dose of radiation workers.** For example, in 1973 the population dose was reported as <60 man rem[20], while the collective dose to Laboratory personnel was 90 man rem. These facts have led to special attention being given at LBL to population exposure since 1959.

The major source of radiation exposure, both to the general population and Laboratory personnel, is the operation of four particle accelerators engaged in fundamental research. These accelerators are: the Bevatron, a 6 GeV proton synchrotron; the SuperHILAC, a heavy ion linear accelerator, producing heavy ion beams up to 8 MeV/amu in energies; and the 184-inch and 88-inch cyclotrons. Because these accelerators are used in research, they present many new and novel radiation problems--their radiation environments are themselves to some extent a subject of research. Such studies have always formed an integral part of accelerator development at the Lawrence Berkeley Laboratory.[21-23]

** This occurs because a large number of people in the general population receive very small average exposures due to LBL operations, whereas a comparatively smaller number of LBL employees and visitors receive a somewhat larger exposure. For example, in 1973 the average exposure to members of the general population (329,000 people) within 5 km of LBL was <0.18 millirem, while the average exposure to 4703 Lab visitors and employees was 21 millirem.

The simultaneous operation of four particle accelerators leads to a complex variation of radiation intensity, both with time and distance from the Laboratory. This complexity is compounded by the flexibility in modes of accelerator operation demanded by a research program. Different experiments may require radiation intensities which vary by three orders of magnitude or more. For example, large bubble chambers or spark chambers require neutron flux densities between one and two orders of magnitude below that required on radiation protection considerations alone. On the other hand, some experiments may require prolonged high intensity runs--with consequent high ambient radiation levels. A recent example of such an experiment at Berkeley was the production and identification of Element 106 at the SuperHILAC.[24] Flexibility in experimental facilities -- including radiation shielding--are essential if a successful research program is to be carried out around high energy particle accelerators.

The radiation phenomena at a research laboratory such as LBL are constantly changing and therefore, of necessity, under continuous review. The problems presented are always new and their solution requires constant alertness. For the past twenty years studies at Berkeley have principally centered around proton accelerators. Just at the time the radiation phenomena of such accelerators has become fairly well understood, the Laboratory's interests have changed direction with an increasing interest in high-energy, heavy-ion research. A whole new set of problems which require identification and solution is thus being presented to the health physicist.

6.3.2. Environmental Monitoring of Penetrating Radiation

General

The presence of a large urban area contiguous with the Laboratory's boundaries led to an early interest in environmental studies at the Lawrence Berkeley Laboratory. When it became apparent

that the Bevatron was an intense neutron source, radiation intensities were first measured within the Laboratory.[25] These studies led to the establishment of a permanent environmental monitoring program (see Fig. 6.7).

Estimates of the contribution of dose equivalent at the Laboratory boundary due to accelerator operation have been made for many years. Figures 6.8 - 6.11 show reported site boundary penetrating radiation levels at the location on the Laboratory boundary. Radiation levels have been consistently below the maximum permissible dose-equivalent for non-occupational exposure.

Under certain operating conditions, any one of the Laboratory's accelerators may have a stray radiation field which can be detected at distances as far as a few thousand feet. The radiation intensity at a given location and time may consist of contributions from any one or all of these accelerators. Attempts to understand and predict the Laboratory's stray radiation field have in the past required combinations of stationary detectors and counting equipment that could not be read simultaneously. Many series of measurements were made with mobile counting equipment; each series lasted for a few hours and was scheduled during the infrequent times when only one of the accelerators was operating at a constant beam level. These measurements facilitated understanding of the contribution to the radiation environment of each accelerator and of the selection of permanent environmental monitoring locations.

Since 1964 radiation levels at ten locations have been continuously monitored (Fig. 6.7).[26] These locations were strategically selected to monitor the radiation output of the Laboratory's accelerators, both close to each accelerator and at the Laboratory perimeter. Two environmental monitoring stations (situated at the Olympus Gate and adjacent to the 88-inch cyclotron) are specifically located to record the highest radiation levels at the Laboratory boundaries, while two others--those at

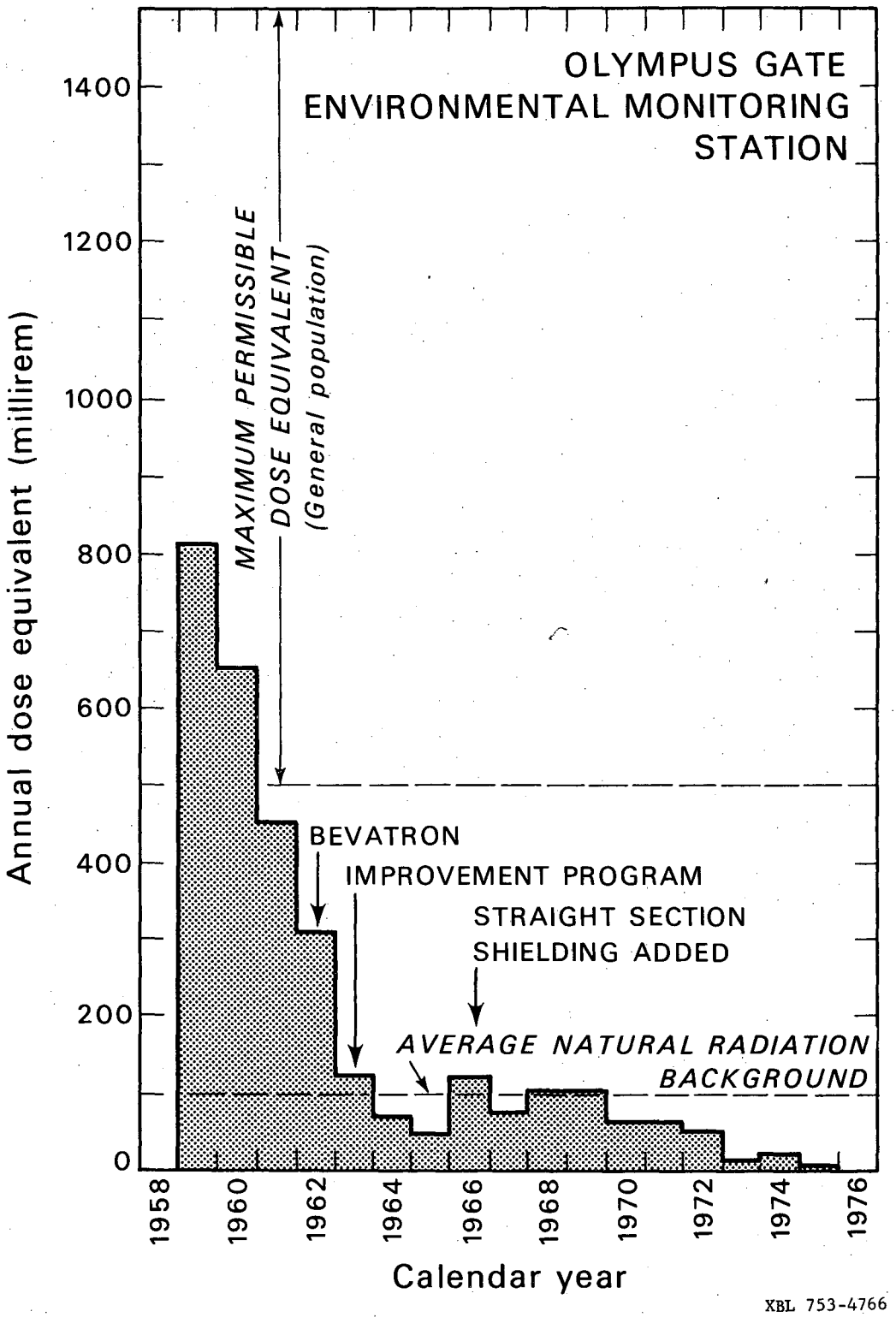
OLYMPUS GATE
ENVIRONMENTAL MONITORING
STATION
MAXIMUM PERMISSIBLE
DOSE EQUIVALENT
(General population)
BEVATRON
IMPROVEMENT PROGRAM
STRAIGHT SECTION
SHIELDING ADDED
AVERAGE NATURAL RADIATION
BACKGROUND
Annual dose equivalent (millirem)
0
200
400
600
800
1000
1200
1400
1958
1960
1962
1964
1966
1968
1970
1972
1974
1976
Calendar year
XBL 753-4766

Fig. 6.8

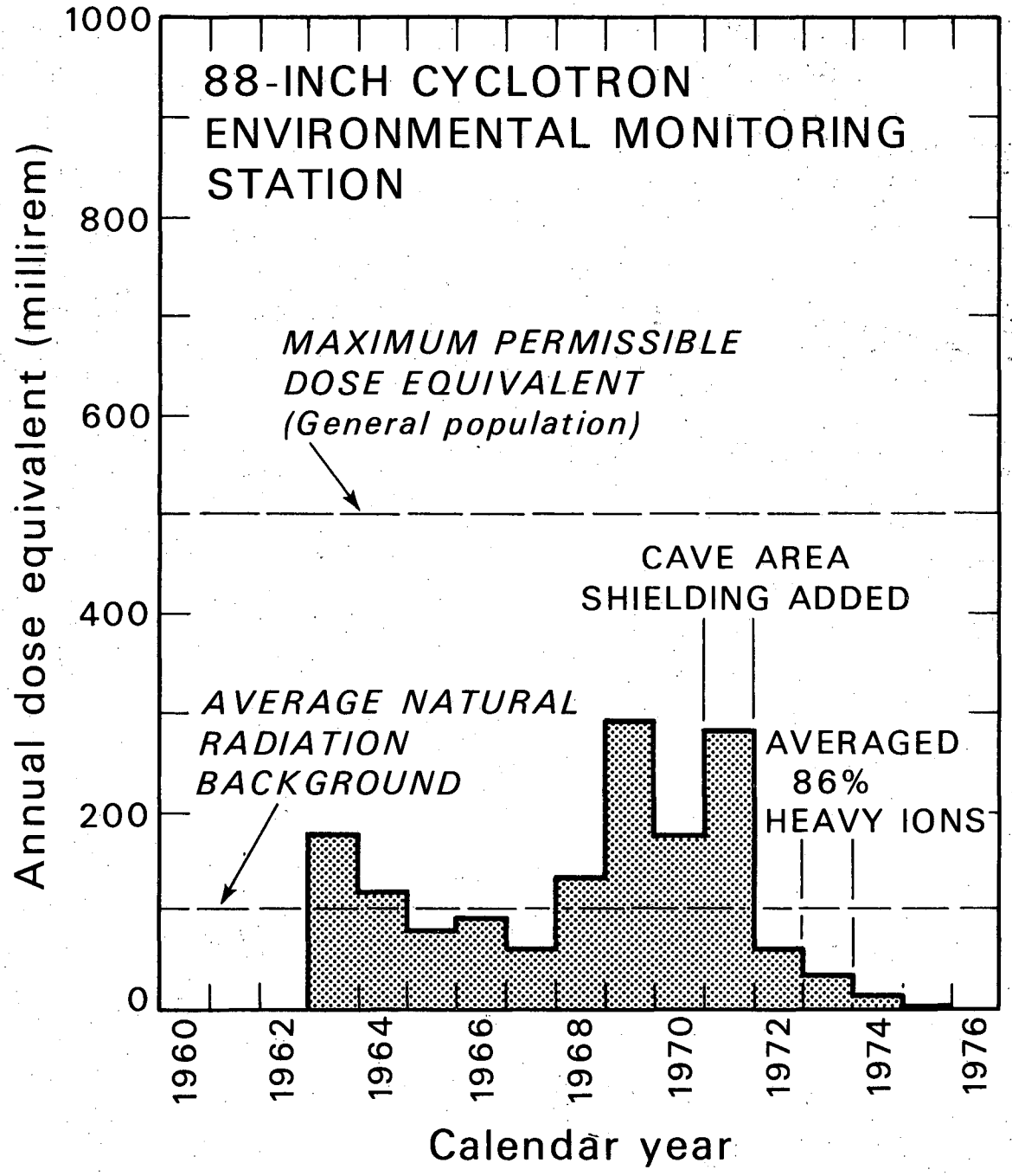

Fig. 6.9

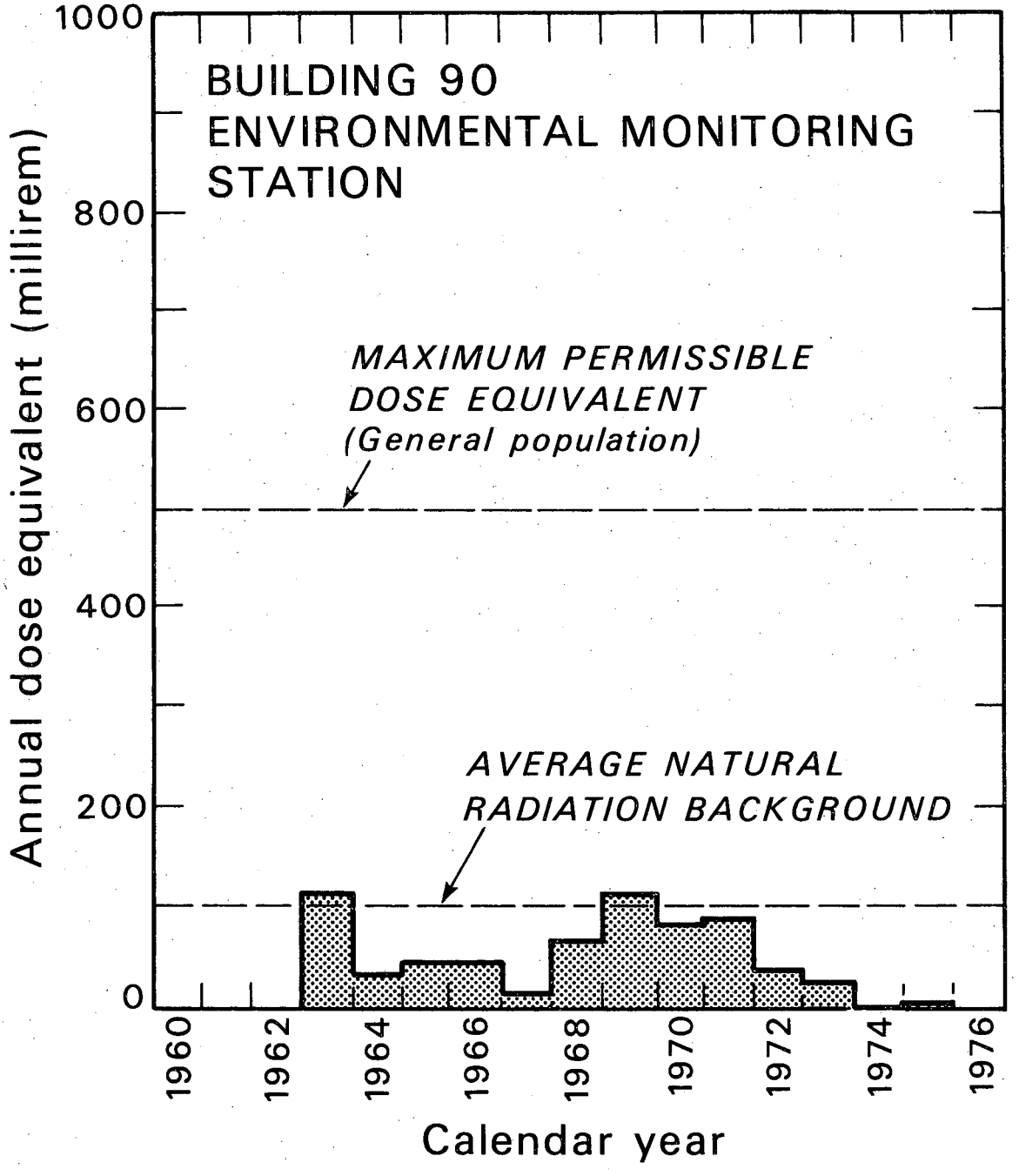

XBL 753-4768

Fig. 6.10

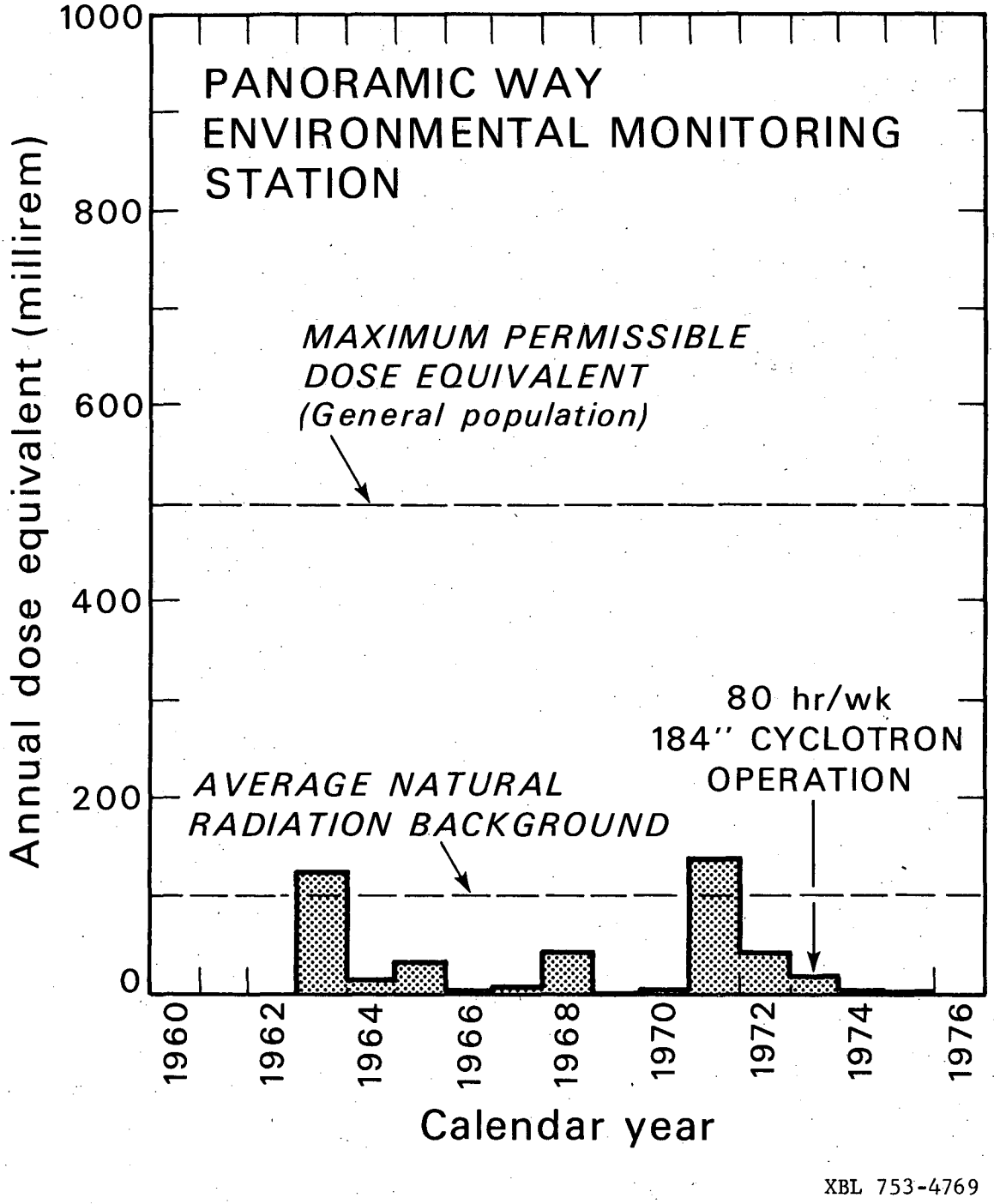

Fig. 6.11

Building 90 and at Panoramic Way--respond to skyshine from the Bevatron and the 88-inch cyclotron and to direct radiation from the 184-inch cyclotron respectively.

Radiation levels are continuously monitored and recorded at a central location by means of a telemetry system. Both the rate and time-integrated intensity of radiation exposure are monitored.

Neutrons are detected by means of a moderated BF_3 proportional counter. Moderator thicknesses are chosen to provide a flat energy response over the range of neutron energies from 0.25 to 20 MeV.[27] Neutron energies have been measured by a variety of techniques. These include proton recoil proportional counters,[28] threshold detectors, and fission counters.[29] An energy compensated Geiger-Müller counter is used to detect and record gamma radiation.[30]

The monitoring system also provides a means for determining the relative contributions of each of the several accelerators to the total radiation environment by studying radiation levels during maintenance shutdown periods when radiation levels at remote locations are produced by different combinations of accelerator operating conditions.

In general, the response of each monitoring station is a complex function of the mode of operation of each and all the Laboratory's accelerators. With all accelerators operating simultaneously, it is not possible, at the present time, to assign accurately to particular accelerators their relative contributions to the radiation level at each station. Without more detailed study, only approximate assignments may be made.

Radiation Levels at the Laboratory Boundary, 1959-1973

The maximum permissible annual dose equivalent to which members of

the general population at the boundary of a laboratory such as Lawrence Berkeley Laboratory may be exposed is 500 millirem/year (MPD). It has been Laboratory policy to place considerable effort toward maintaining radiation levels well below this limit.

The environmental monitoring program of the Laboratory showed that approximately 80% of the accelerator produced radiation in 1972 was due to the operation of the Bevatron when accelerating protons.[31]

The Bevatron has a long history--having been in operation since 1954. During the past 19 years substantial changes have occurred in accelerator intensity, mode of operation, and shielding. Figure 6.8 shows the number of protons accelerated in the Bevatron each year in the period 1954-1973.[32,33] During this period the beam intensity of the accelerator, and, therefore, the potential radiation source, increased by a factor of more than 10,000. Radiation levels around the Bevatron have been controlled primarily by the addition of shielding, but also by improved techniques in beam control, extraction, and beam dumping into well shielded locations.

Figures 6.9-6.12 show the annual dose equivalent reported for the four environmental stations as a function of time.

Radiation levels at the Olympus Gate Station have shown a steady decline since 1959 when estimates were first made. The Olympus Gate Station is in direct view of the Bevatron and most directly influenced by that accelerator. During late 1962 and early 1963 the Bevatron underwent a substantial modification and was out of operation for a significant time. This shutdown was, however, only partially responsible for the falling radiation level recorded. This falling trend continues through 1964 and 1965 because of the addition of shielding and improvements in accelerator operation--particularly the development of an extracted proton beam.

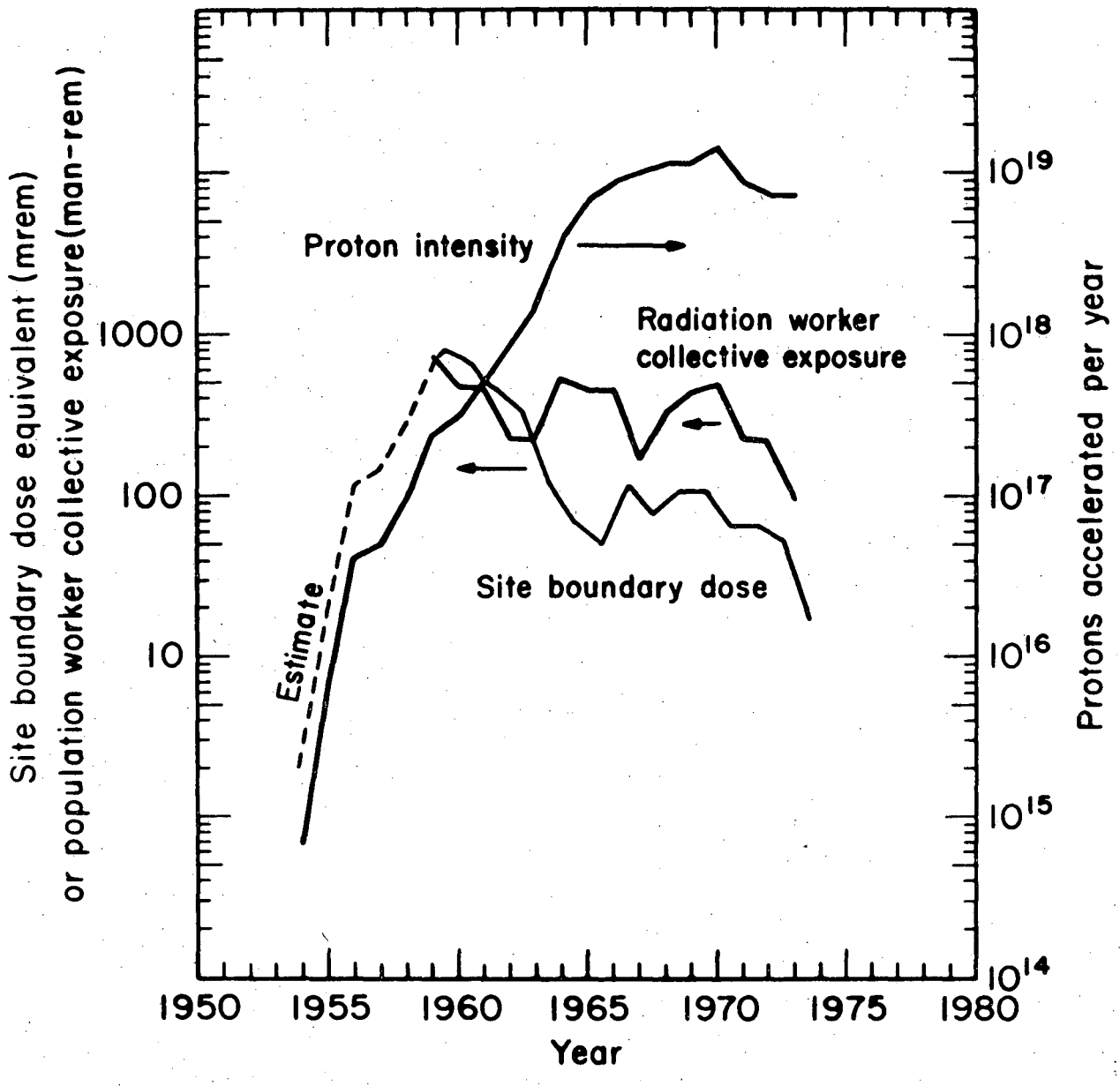
Site boundary dose equivalent (mrem)
or population worker collective exposure(man-rem)
1000
100
10
Proton intensity
Radiation worker
collective exposure
Site boundary dose
Estimate
10^{19}
10^{18}
10^{17}
10^{16}
10^{15}
10^{14}
Protons accelerated per year
1950
1955
1960
1965
1970
1975
1980
Year
CBB 752-1175

Fig. 6.12

Radiation levels through 1966 showed an increase due to increasing circulating proton beam intensity, but the decrease observed in 1967 was because of the installation of extra shielding to the straight sections of the Bevatron. Since 1970 radiation levels have declined due to increasing use of the Bevatron to accelerate heavy ions, and this trend is expected to continue.

The monitoring station adjacent to the 88-inch cyclotron responds to radiation from both the Bevatron and the 88-inch cyclotron. The 88-inch cyclotron was completed in 1961 and the first external beam obtained in 1962. During the period 1962-1966 the radiation levels observed at this station closely reflect the operation of the Bevatron (see Figs. 6.8 and 6.9). In 1967, however, the increasing intensity at the 88-inch cyclotron is reflected in the higher radiation levels recorded at this station. The addition of new shielded eaves to the roof during the latter part of 1970 resulted in a dramatic reduction in the radiation levels for 1971, and the 88-inch cyclotron is now so well shielded that its adjacent monitoring station now principally responds to the Bevatron.[34]

The station situated at Panoramic Way is in direct view only of the 184-inch cyclotron and responds principally to that accelerator. High readings at this station may usually be directly attributed to unusual experimental conditions at the 184-inch cyclotron. Reduced use of this accelerator will result in a decline in readings at this station. The residual levels measured will be largely due to skyshine radiation from the Bevatron.

Radiation levels recorded at the Building 90 environmental monitoring station are principally caued by skyshine from the Bevatron and 88-inch cyclotron (compare Figs. 6.8, 6.9, 6.10

When the maximum dose equivalent is considerably less than the MPD, an uncertainty of as much as a factor of three in estimation of the dose equivalent is acceptable.[35] However, there is increasing tendency by regulatory agencies to require improved accuracy in the measurement of man-made radiation. Lowder and Gogolak[36] have clearly drawn attention to the implications of this requirement for increased accuracy:

> "The recent trend toward the quantitative definition of 'as low as practicable' guidelines pertaining to the release of radionuclides to the environment for nuclear facilities and the resulting dose places a significantly increased burden on environmental surveillance programs. It was previously believed that adherence to the admonitions of expert bodies such as the ICRP[37] to limit unnecessary radiation exposure was achieved by demonstrating that such exposure was well below the recommended 'maximum permissible' annual levels of 500 mrem to individuals or 170 mrem to a 'suitable sample'.[38] U.S. regulatory agencies are now preparing numerical limitations on environmental radiation dose to man from light-water power reactors and the nuclear power fuel cycle.[39, 40] The net effect of these limitations is to lower the 'maximum permissible' dose to off-site individuals by two orders of magnitude. While the merits of such a reduction in terms of public health and realistic benefit-risk assessment are arguable, the rationale for this change has been that practical, though costly, techniques for the treatment of nuclear facilities effluents will permit

plant operation within the limits.

"Questions immediately arise relating to how well the actual doses can be assessed and documented, given the fact that most existing environmental surveillance programs were designed to assure that critical population groups do not receive doses that are much higher than the proposed limits. If the public and regulatory agencies are to be assured that nuclear facilities are operating within their design specifications, both experimental and calculational methods are required to allow accurate dose assessment at the very low exposure levels that are expected to exist."(36)

This requirement for improved accuracy poses severe problems both of measurement and data interpretation at high energy accelerator laboratories.

The accuracy of environmental monitoring is primarily limited by two factors:

i. Inaccuracies in neutron fluence to dose equivalent conversion which may amount to 50% or more, and

ii. uncertainties in natural background.

Inaccuracies Due to the Neutron Fluence to Dose Equivalent Conversion

We have seen that the major component of accelerator-produced radiation is due to neutrons. Neutrons up to an energy of 20 MeV may be readily measured with a moderated BF_3 counter, and the neutron fluences at the site boundary in this energy region may be determined with good accuracy. Conversion of this measured fluence to dose equivalent is, however, of limited accuracy when the neutron spectrum and conditions of irradiation are not well known. Errors of 50% or more are possible when these parameters are poorly understood. This problem has been discussed in detail by several authors(41-44) and already summarized in section 2.

Inaccuracies in Dose Equivalent Due to Uncertainties in Natural Background

If man-made contributions to the radiation environment are to be known within a few millirem per year, natural background radiation levels must be extremely well understood.

As an example, natural background at the Lawrence Berkeley Laboratory amounts to between 70-110 millirem/yr made up as follows:

Natural radioactivity of surrounding earth:	approx. 40-80 millirem/y
Cosmic rays:	μ mesons - approx 30 millirem/yr
	neutrons - approx 3 millirem/yr
	Total - approx 70-110 millirem/yr

The components from natural radioactivity show fluctuations of more than a factor of two from place to place due to geological and human causes, e.g. outcrop of granitic rocks, presence of large buildings or paved roads. In addition to variations in the γ-component from place to place, the background at a particular place may show secular variations of as much as 30%, primarily due to variations in the water content of the soil.[45]

Measurements of radiation levels due to accelerator produced photons to an accuracy of better than about 30 millirem per year therefore requires an accurate assessment of natural background because of terrestrial radioactivity. This may be achieved by preoperational radiation surveys in the field, measurements during periods of accelerator shutdown, or by the laboratory radio-assay of soil samples taken in the field and the calculation of environmental exposure rates.[46] If the latter method is adopted, an estimate of average exposure rates will be limited in accuracy to about 30% until good data on seasonal fluctuations in background is obtained.

References

Section 6

1. Thomas, R.H., High Energy Accelerators and the Environment, Lawrence Berkeley Laboratory, University of California internal report LBL-4654, to be published.
2. Jenkins, T.M., Accelerator Boundary Dose and Skyshine, Health Physics 27, 241 (1974).
3. Rindi, A.R. and Thomas, R.H., Skyshine, Particle Accelerators 7, 23 (1975).
4. Ollendorff, A Study of Radiation Levels at the CERN Site, CERN Internal Report DI/HP/66 (1964).
5. Komochkov, M.M., The Dubna Synchrophasotron, in "Engineering Compendium on Radiation Shielding," edited by R.G. Jaeger (Springer-Verlag, Berlin, 1970, Vol. III, Sec. 10.7.32. See also: V.N. Lebedev, L.S. Zolin, and M. I. Salatskaya, Distrution of the Penetrating Radiation Field Over the Protective Zone of the 10 GeV Synchrophasotron, Joint Institute for Nuclear Research, USSR, Internal Report P-2177,(1965).
6. Distenfeld, C. and Colvett, Skyshine Considerations for Accelerator Shielding Design, Nucl. Sic. Eng. 26, 117 (1966).
7. Rindi, A. and Baarli, J., Scattered Radiation at Large Distances for the CERN 600 MeV Synchrocyclotron, CERN Internal Report DI/HP/19 (1966).
8. Bathow, G., Clausen, V., Freytag, E., and Tesch, K., Skyshine-Messungen und ihr Vergleich mit Abschatzungen, aus der diffusionstheorie, Nukleonic 9, 14 (1967). (Available in English translation as Stanford Linear Accelerator Center internal report SLAC-Trans-42).
9. Thomas, R.H., Shaw, K.B., Simpson, P.W., and MacEwan, J.F., Neutron Surveys Around the Rutherford Laboratory 50-MeV Proton Linear Accelerator, Rutherford Laboratory Internal Report NIRL/M/30 (1962).
10. Simpson, P.W. and Laws, D., Rutherford Laboratory Internal Report, Addendum to NIRL/M/30 (see Ref. 9).
11. Stephens, L. and Aceto, H., Variation of a Fission-Neutron Flux and Spectrum from a Fast Reaction Measured Over Large Distance, in Neutron Dosimetry, IAEA Vienna (1963), p. 535.
12. Höfert, M. and Hanon, J.M., The Influence of the PS Operation on Stray Radiation Levels at the CERN Site, CERN Health Physics Internal Report HP-73-121 (1973); and, Höfert, M., Coninckx, F., Hanon, J.M., and Roubaud, G., Environmental Implications of the Operation of the Present Neutrino Facility with Beam Intensities Exceeding 5×10^{12} Per Pulse, CERN Health Physics Internal Report HP-74-136 (1974).

13. W.R. Nelson, "Radioactive Ground Water Produced in the Vicinity of Beam Dumps." Stanford Linear Accelerator Center Internal Report SLAC TN, July 1965 (unpublished).

14. D. Busick, A Three Year Summary of Environmental Radiation Measurement at SLAC. To be published.

15. R.H. Thomas, Possible Contamination of Ground Water System by High Energy Proton Accelerators, in Proceedings of the Symposium on Health Physics Aspects of Nuclear Facility Siting, Idaho Falls, November 3-6, 1970.

16. G.B. Stapleton and R.H. Thomas, Estimation of the Induced Radioactivity of the Ground Water System in the Neighborhood of a Proposed 300-GeV High Energy Accelerator Situation on a Chalk Site. Health Physics 23, 689 (1972).

17. F. Hoyer, Induced Radioactivity in the Earth Shielding on Top of High Energy Particle Accelerators. CERN 68-42, December 9, 1968.

18. Gilbert, W.S. et al., CERN-LRL-RHEL Shielding Experiment 1966, Lawrence Berkeley Laboratory Internal Report, UCRL-17941 (1968).

19. C.A. Mawson, Consequences of Radioactive Disposal into the Ground in Health Physics, Vol. 2, Pt. I, Edited by A.M.F. Duhamel, Pergamon Press, Oxford (1969).

20. Wallace, R. (Ed.), Annual Environmental Monitoring Report (for Calendar Year 1973), Lawrence Berkeley Laboratory, University of California, in Environmental Monitoring at Major U.S. Atomic Energy Commission Contractor Sites, Calendar Year 1973, Vol. 2, p. 1173, WASH-1259 (1973).

21. Freytag, E., Radiation Protection at High Energy Accelerators (in German), G. Braun, Karlsruhe (1972).

22. Patterson, H.W. and Thomas, R.H., 1973, Accelerator Health Physics, Academic Press, New York.

23. Zaitsev, L.N., Komochkov, M.M. and Sychev, B.C., The Basis of Accelerator Shielding (in Russian), Atomizdat, Moscow (1971).

24. Ghiorso, A., et al., Element 106, Lawrence Berkeley Laboratory-2988, September, 1974.

25. Patterson, H.W., The Effect of Shielding on Radiation, Proc. of the First International Conference on Shielding Around High Energy Accelerators, Paris, January, 1962 (Presses Universitaires de France), p. 95.

26. Stephens, L.D. and Dakin, H.S. A High Reliability Environmental Radiation Monitoring System, in Proc. of the VIth International Congress of the Society Francaise de Radioprotection, Bordeaux, France, March 27-31, 1972, p. 753.

27. Yamashita, M., Stephens, L.D., Smith, A.R., and Patterson, H.W., Detection Efficiency of Bare and Moderated BF_3 Gas-Filled Proportional Counters for Isotropic Neutron Fluxes, UCRL-16103, January 12, 1966.

28. Moyer, B.J., Survey Methods for Neutron Fields, Lawrence Berkeley Laboratory Report UCRL-1635, 1952.

29. Smith, A.R., The Stray Radiation Field of the Bevatron, UCRL-8377 (1958).

30. Jones, A.R., Pulse Counter for γ-Dosimeters, Health Physics 8, p. 9 (1962).

31. Stephens, L.D. and Thomas, R.H., 1974a, Radiation Levels at the Site Boundary of the Lawrence Berkeley Laboratory, Lawrence Berkeley Laboratory Internal Report, HPN-6, February 11, 1974.

32. Everette, W., Lawrence Berkeley Laboratory, Private Communication, October, 1974.

33. Hartsough, W.D. and Lothrop, F.H.G., Bevatron Monthly Report for January, Lawrence Berkeley Laboratory Internal Report BeV-2003, February 2, 1971.

34. Gleiter, M.E., A Preliminary Determination of Environmental Radiation at Large Distances Due to LBL Operation, Lawrence Berkeley Laboratory Internal Note HPN/5, December 1973.

35. International Commission on Radiation Units and Measurements, Radiation Protection Instrumentation and Application, ICRU Report 20, Section I, C.6., Washington, D.C. (1971).

36. Lowder, W.M. and Gogolak, C.V., Experimental and Analytical Radiation Dosimetry Near a Large BWR IEEE Trans, Nucl. Sci. NS-21, No. 1, 423 (1974).

37. International Commission on Radiological Protection (ICRP) Publication 6, (As amended 1959 and revised 1962), 1964 (Oxford: Pergamon Press).

38. Federal Radiation Council Report No. 1 (1960). Background Material for the Development of Radiation Protection Standards.

39. Federal Register 36, 111 (1971). Code of Federal Regulations Title 10, Part 50, Appendix I.

40. Environmental Radiation Protection Requirements for Normal Operations of Activities in the Uranium Fuel Cycle, Notice of Proposed Rulemaking, U.S. Environmental Protection Agency (1973).

41. Shaw, K.B., Stevenson, G.R. and Thomas, R.H., Evaluating Dose Equivalent from Neutron Energy Spectra, Health Physics 17, 459 (1969).

42. Patterson, H.W., Routti, J.T., and Thomas, R.H., What Quality Factor? Health Physics 20, 517 (1971).

43. Stevenson, G.R., Hofert, M., Neufeld, J., Rindi, A., Routti, J.T., and Pretre, S., Proposal for Standardizing the Fluence to Dose Equivalent Conversion Factors for Whole Body Neutron Exposure, in Proc. of IAEA Symp. on Neutron Monitoring, Vienna, Dec. 11-15, 1, 177 (1972).

44. Gilbert, W.S., Keefe, D., McCaslin, J.B., Patterson, H.W., Smith, A.R., Stephens, L.D., Shaw, K.B., Stevenson, G.R., Thomas, R.H., Fortune, R.D., and Goebel, K., CERN-LRL-RHEL Shielding Experiment at the CERN Proton Synchrotron, Lawrence Berkeley Laboratory Report UCRL-17941 (1968).

45. dePlanque-Burke, G., Variation in Natural Environmental Gamma Radiation and its Effect on the Interpretability of TLD Measurements made Near Nuclear Facilities. (Health and Safety Laboratory preprint July 1974 -- submitted to Health Physics.)

46. Wollenberg, H.A., Patterson, H.W., Smith, A.R., and Stephens, L., Natural and Fallout Radioactivity in the San Francisco Bay Area, Health Physics 17, 313 (1969).

7. Population Dose Equivalent Calculation

7. Population Dose Equivalent Calculation

7.1. Definition of Population Dose Equivalent

The population dose equivalent resulting from the operation of a nuclear facility is defined by the equation: (1)

$$M = \int H \; N(H)dH \tag{7.1}$$

where N(H)dH is the number of people receving a dose equivalent between H and H+dH, and the integration is carried out over the entire dose equivalent distribution and population exposed. M is usually expressed in the unit man rem.

As we have seen in sections 2 and 6, the dominant contribution to population dose equivalent resulting from high-energy accelerator operation is external radiation by neutrons.

7.2. Model for Calculation of Population Dose Equivalent for Accelerators.

An operating high-energy accelerator is a source of neutrons irradiating its surroundings. This exposure may be modified by the topography around the accelerator, or by conditions of accelerator operation, but is not influenced by meteorological conditions such as wind direction or rainfall. Population exposure is due only to the prompt radiation field produced by an accelerator during operation.

These facts suggest a simple model that may be used to calculate population dose. Imagine a high-energy accelerator located on a flat plane so that there is no shielding or shadowing due to hills, surrounded by a mixed urban population (Fig. 7.1) and the radiation field at large distances from a high-energy accelerator to a good approximation, isotropic in character and depending only on the intensity of and distance from the source. Equation (7.1) can then be transformed to:

$$M = \int_{t=0}^{1\,\text{year}} \int_{r_0}^{R} N(r,t)\, H(r,t)\, dr\, dt. \tag{7.2}$$

where N(r,t) dr dt is the number of people at a distance between r and r + dr from the accelerator at time between t and t + dt, H(r, t) is the corresponding dose equivalent rate, and r_0, R, are the limits of radial integration at the closest and furthest distances of approach under consideration to the accelerator.

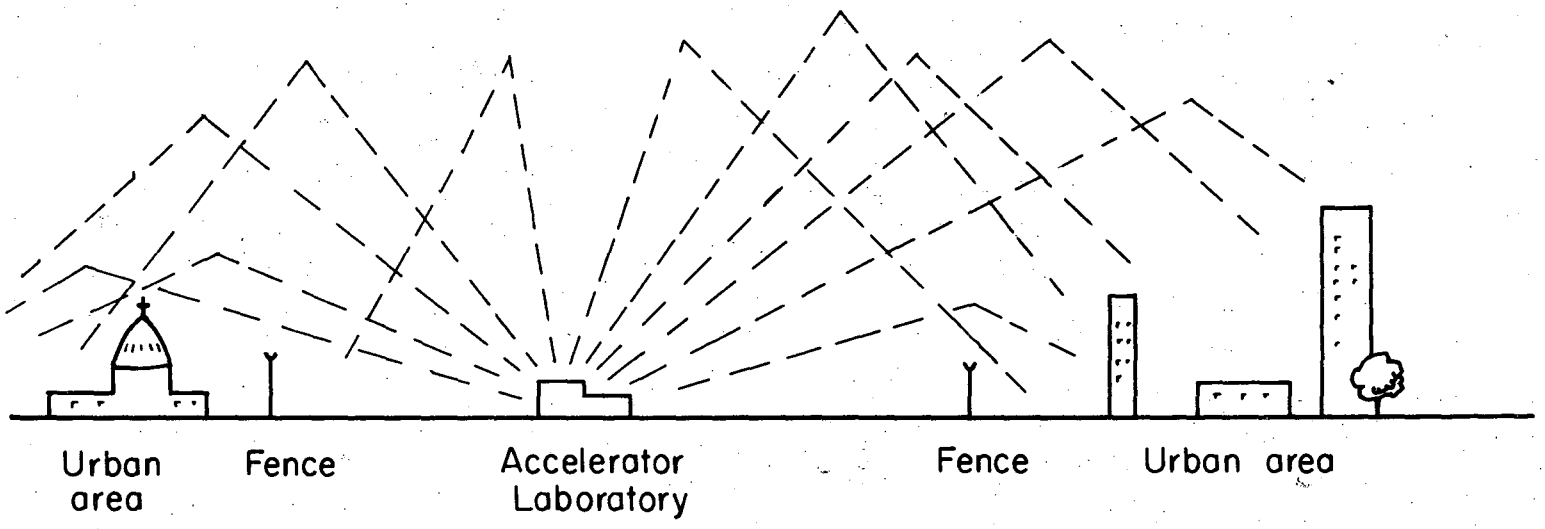

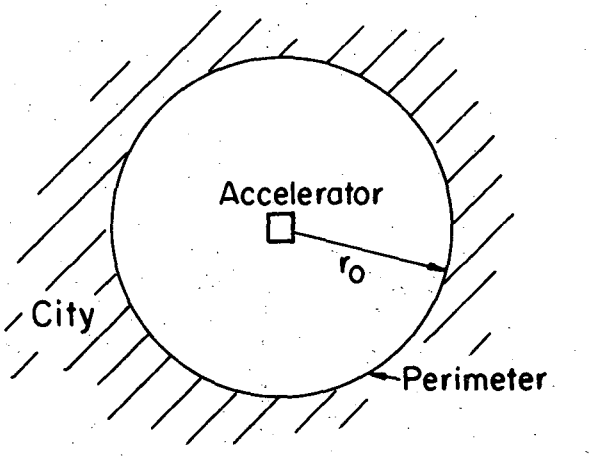

XBL748-3994

Fig. 7.1

In a homogeneous urban area it is plausible that the population density may be considered constant when averaged over long periods of time. This should not result in serious error in the estimate of population exposure provided the intensity of accelerator operation is uncorrelated with fluctuations in population (e.g., high intensity operation is not restricted to times of known low population). If this assumption is made, Eq.(7.2) may be simplified to:

$$M = \int_{r_0}^{R} H(r)\, N(r)\, dr \qquad (7.2a)$$

where $H(r)$ is the annual dose equivalent to a person at a distance from r to $r + dr$ from the accelerator and $N(r)$ is the number of people living in this range of distances.

As we have seen in section 6.1, the variation of dose equivalent as a function of distance from an accelerator is given by:

$$H(r) = \frac{aQ}{r^2}\, e^{-r/\lambda} \quad \text{for } r \geq 300 \text{ m} \qquad (7.4)$$

with the attenuation length in the range $225 \text{ m} \leq \lambda \leq 1000 \text{ m}$.

We define the fence post dose equivalent, H_0, by:

$$H_0 = \frac{aQ}{r_0^2}\, e^{-r_0/\lambda} \qquad (7.5)$$

and it follows that:

$$H(r) = r_0^2\, H_0\, e^{r_0/\lambda} \left(\frac{e^{-r/\lambda}}{r^2}\right) \qquad (7.6)$$

If we define an average population density, $\sigma(r)$, between distances r and $r + dr$ from the accelerator, we have

$$N(r)dr = 2\pi r \sigma(r) dr \qquad (7.7)$$

and substituting equations(7.6) and (7.7) into equation (7.3) we obtain:

$$M = 2\pi r_0^2\, H_0\, e^{r_0/\lambda} \int_{r_0}^{R} \frac{\sigma(r) e^{-r/\lambda}}{r}\, dr \qquad (7.8)$$

The integral of Eq. (7.8) may numerically be evaluated by assuming a uniform distribution of population within each ring around the accelerator.

M may then be approximated by:

$$M = 2\pi\, r_0^2 H_0\, e^{r_0/\lambda} \sum_{i=1}^{i=n} \sigma_i \int_{r_{i-1}}^{r_i} \frac{e^{-r/\lambda}}{r}\, dr, \qquad (7.9)$$

where σ_i is defined by:

$$\sigma_i = \frac{N_i}{\pi(r_i^2 - r_{i-1}^2)^2}. \qquad (7.10)$$

and N_i is the number of people living between r_{i-1} and r_i.

Population dose-equivalent, resulting from the operation of a nuclear installation, is a scalar quantity independent of distance from the installation and should therefore properly be calculated out to infinity. It has become conventional to assume that this has essentially been done if the calculation is carried to a distance of 80 km. from the installation. The validity of this assumption will depend upon the circumstances unique to each facility, but is usually justified.

In the numerical evaluation of equation (7.9), the number of annuli, n, is determined by the character of the convergence of the integral of equation (7.8).

7.3. Convergence of the Population Dose Equivalent Integral

Stephens et al[2] have explored the convergence of this integral with the simplifying assumption that the population density is uniform:

$$\sigma(r) = \sigma \qquad (7.11)$$

Under these conditions equation (7.8) simplifies to:

$$M = 2\pi\sigma H_0 r_0^2\, e^{r_0/\lambda} \int_{r_0}^{R} \frac{e^{-r/\lambda}}{r} \cdot dr \qquad (7.12)$$

$$= 2\pi\sigma H_0 r_0^2\, e^{r_0/\lambda}\, I(r_0, R) \qquad (7.12a)$$

The integral of equation (7.12) has the solution:

$$\int \frac{e^{-r/\lambda}}{r}\,dr = \ln r - r/\lambda + \frac{1}{2.2!}(r/\lambda)^2 - \frac{1}{3.3!}(r/\lambda)^3 + \ldots$$

but this is an inconvenient analytical solution, because the oscillating series converges only very slowly. The integral may, however, readily be evaluated by numerical means and Stephens et al[2] have reported numerical values for values of perimeter radius, r_0, between 300 m and 1000 m and attenuation length, λ, between 100 m and 1000 m.

In order to discuss the convergence of the integral

$$I(r_0, R) = \int_{r_0}^{R} \frac{e^{-r/\lambda}}{r}\,dr \qquad (7.13)$$

we define three parameters:

i. $M(\infty) = I(r_0, \infty)$ which is the population dose equivalent calculated out to an infinite distance from the accelerator.

ii. $M(80) = I(r_0, 80\text{ km})$ - the so-called 80 km population dose equivalent.

iii. $M(R) = I(r_0, R)$.

As we have already discussed $M(\infty)$ is the quantity that should properly be calculated in population dose equivalent estimates, while it is often conventional to quote M(80). In general:

$$M(\infty) \geq M(80).$$

The convergence of the integral $I_0(r_0, R)$ may conveniently be examined by plotting the parameter:

$$\frac{M(R)}{M(\infty)} \text{ as a function of r.}$$

Figure 7.2 shows this parameter, expressed as a percentage of $M(\infty)$, for values of λ between 100m and 1000m. Inspection of Fig. 7.2 shows that the integral converges quite rapidly and, under the conditions of the model, it is only necessary to extend integration

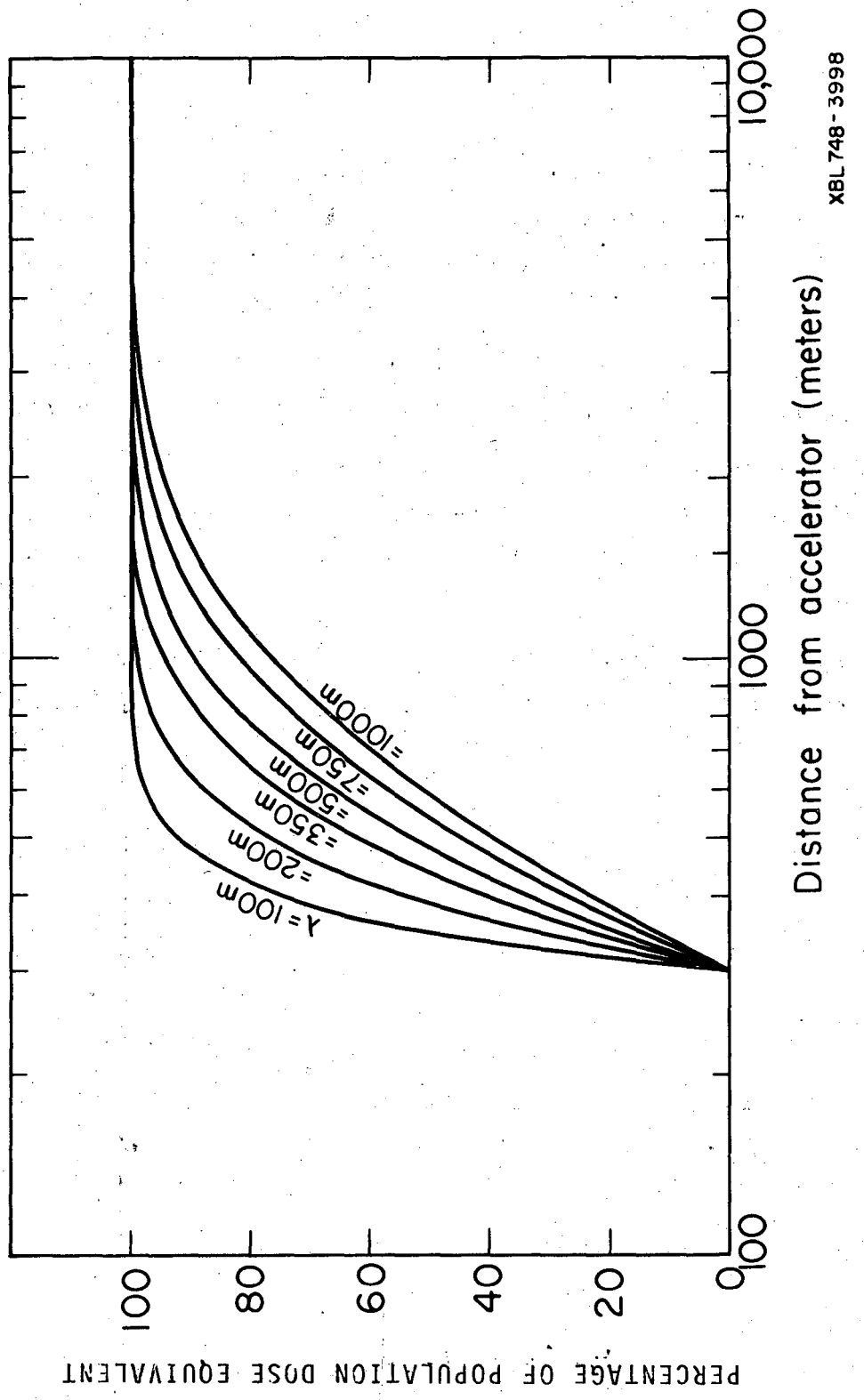
PERCENTAGE OF POPULATION DOSE EQUIVALENT
100
80
60
40
20
0
100
1000
10,000
Distance from accelerator (meters)
λ = 100m
=200m
=350m
=500m
=750m
=1000m
XBL 748-3998

Fig. 7.2

out to distances $\sim (r_0+3\lambda)$ from the accelerator to determine the population dose equivalent, i.e:

$$M(r_0+3\lambda) = M(\infty).$$

This knowledge could save extensive efforts in the evaluation of the "80 km population dose equivalent" often quoted in environmental monitoring reports.

7.4. Influence of the Parameters r_0 and λ on Population Dose Equivalent.

Stephens et al.[2] have investigated the influence of the perimeter radius, r_0, and the attenuation length, λ, on the magnitude of population dose equivalent, again when the population density around the facility may be assumed constant.

Figures 7.3 and 7.4 show calculated values of the parameter $M/2\pi\sigma H_0$ as a function of r_0 and λ. Inspection of these figures show that the population dose equivalent is approximately proportional to $\sim r_0^{4/3} \lambda^{2/3}$. The use of an empirical formula of the form:

$$M = k\sigma H_0 r_0^n \lambda^m \qquad (7.14)$$

may be convenient in interpolating tabulated values of M over a limited range (see Table 7.1). The values of k, m, and n vary somewhat, but over the physical range discussed here n takes values between 1.1 and 1.4, while m has values ranging from 0.60 to 0.80

7.5. Population Dose Equivalent at the Lawrence Berkeley Laboratory -- A Specific Example.

Stephens et al.[3] have reported calculations of population dose equivalent produced by the particle accelerators of the Lawrence Berkeley Laboratory.

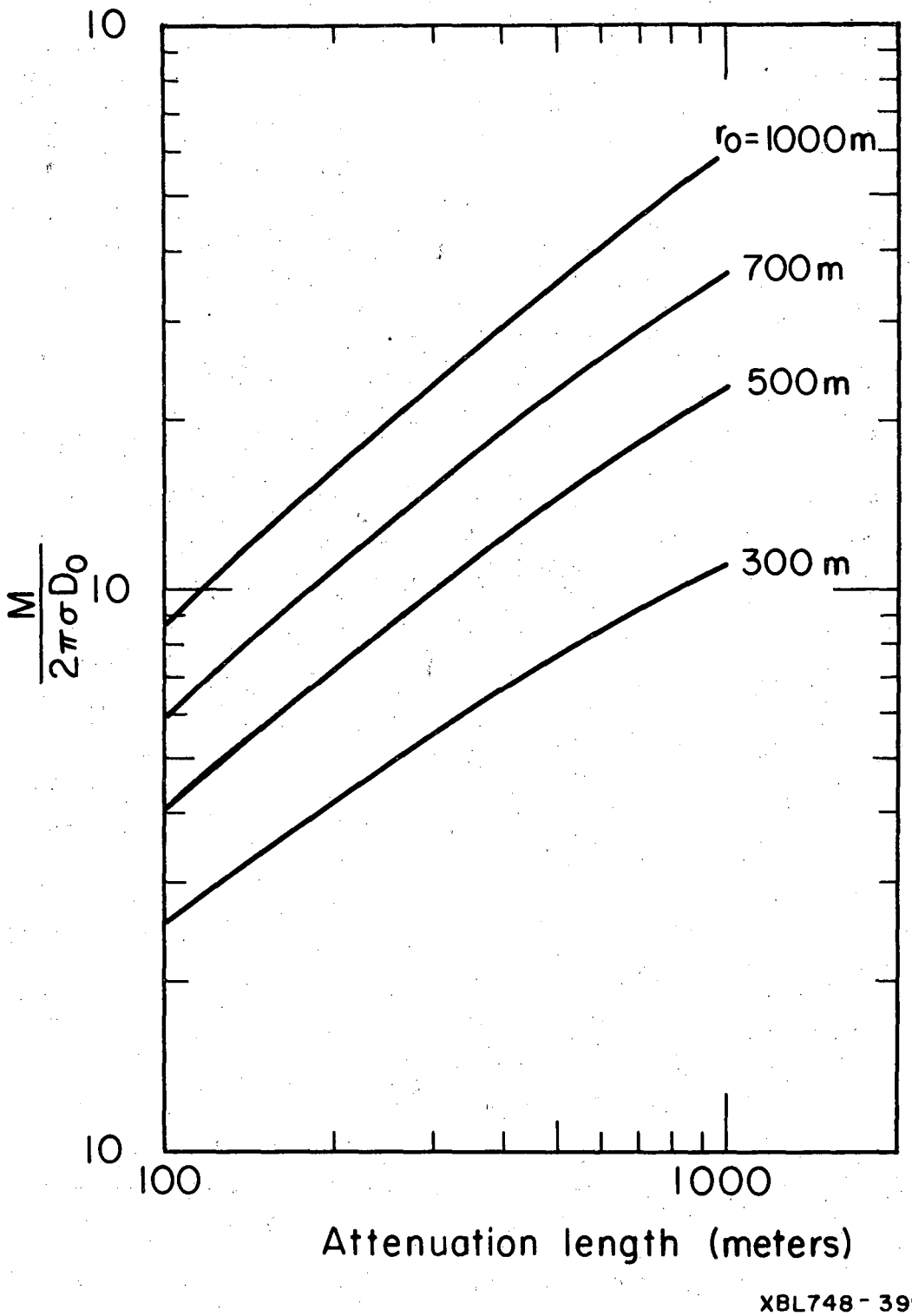

Fig. 7.3

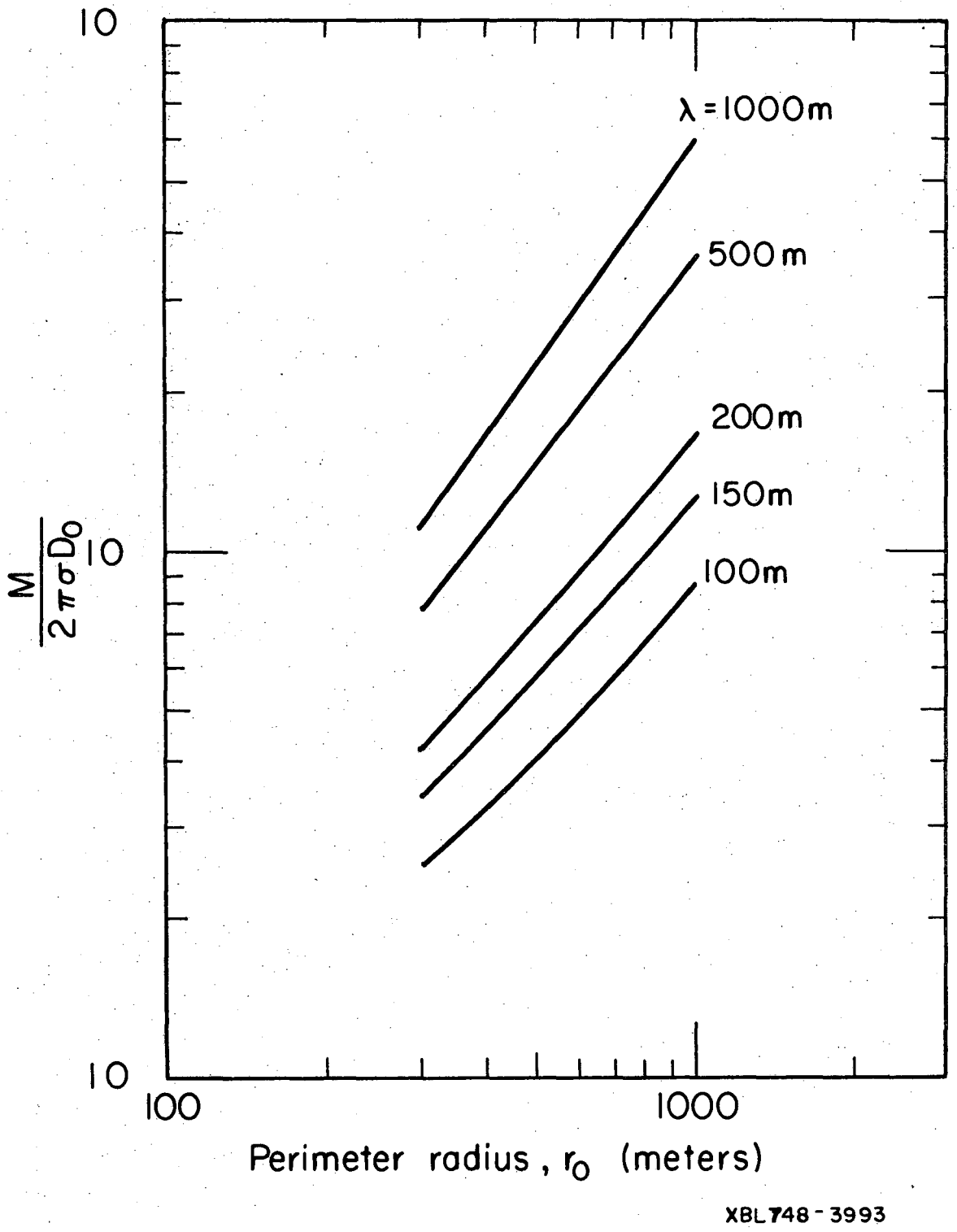
10
10
10
100
1000
λ = 1000m
500 m
200m
150m
100m
$\frac{M}{2\pi\sigma D_0}$
Perimeter radius , r_0 (meters)
XBL748-3993

Fig. 7.4

Table 7.1. Values of the parameter $\frac{M}{2\pi\sigma D_0}$ for different values of λ and r_0. (From Stephens et al.)

Perimeter radius r_0 (meters)	Attenuation length, λ (meters)						
	100	150	200	350	500	750	1000
300	2.51 E+4	3.40 E+4	4.19 E+4	6.10 E+4	7.60 E+4	9.58 E+4	1.11 E+4
500	4.01 E+4	5.76 E+4	7.34 E+4	1.14 E+5	1.47 E+5	1.91 E+5	2.28 E+5
700	5.86 E+4	8.52 E+4	1.09 E+4	1.74 E+5	2.27 E+5	3.03 E+5	3.65 E+5
1000	8.65 E+4	1.27 E+5	1.65 E+5	2.68 E+5	3.56 E+5	4.83 E+5	5.91 E+5

The Lawrence Berkeley Laboratory of the University of California is unusual among high-energy accelerator laboratories, in that it is contiguous with fairly densely populated areas. The Laboratory is situated on the western slope of hills running along the eastern side of the San Francisco Bay. The Berkeley Campus of the University of California is immediately adjacent on the west, while to the north and south, the Laboratory is surrounded by residential areas. To the east lie largely uninhabited watershed lands and Tilden Regional Park. (Section 6.)

The equivalent of 168,000 people live or work within about 5 kilometers from the Laboratory. The proximity of a large urban population to the Laboratory has led to the close surveillance of the environmental impact of the Laboratory's activities.[4] (See Section 6.).

The largest radiological environmental impact due to the Laboratory is due to the operation of four high-energy particle accelerators: the Bevatron, the SuperHILAC, and the 88-inch and 184-inch cylcotrons.

Stephens et al.[3] use a modified form of equation 7.9 to calculate population dose equivalent.

Equation (7.9) does not allow for the shielding provided to a large fraction of the populated area by the hills surrounding the Laboratory or by the buildings which people occupy. To do so, equation (7.9) may be written

$$M = \frac{2\pi\, r_0^{\,2}\, H_0\, e^{r_0/}}{S_1\, S_2} \sum_{i=1}^{i=n} \sigma_i \int_{r_i-1}^{r_i} \frac{e^{-r/\lambda}}{r}\, dr \qquad (7.15)$$

where S_1 and S_2 are shielding factors that take account of the shielding provided by hills and buildings respectively. Only approximate estimates were made of S_1 and S_2.

The principal sources of radiation produced by accelerator operation at the Laboratory are shielded from direct line of sight of much of the surrounding urban area by hills. Experimental data

obtained by McCaslin[5] suggests that radiation levels are depressed by a factor of almost two when hills intervene. From this preliminary data, a value $S_1 \approx 1.8$ is obtained.

The shielding factor for buildings, S_2, is estimated to be ≈ 1.2[3]. Thus the product $S_1 S_2$ has the value ≈ 2.2.

Stephens et al.[2] found that it was necessary to extend integration out to a distance of about 5 km from the Laboratory. (See Fig. 7.2.)

Figure 7.5 shows a map of the Laboratory and its immediate surrounding area. Fifteen annuli are shown drawn around the Laboratory in each of which the total number of residents were obtained from census data. In the calculation of M (equation 7.15) Stephens et al used the following numerical values:

n	= 15
r_0	= 366 meters (1200 ft)
$r_1 - r_0$	= 244 meters (800 ft)
$r_i - r_{i-1}$	= 304.8 meters (1000 ft) for $r \geq 2$
r_{15}	= 4877 meters (16,000 ft)
λ	= 850 meters
$S_1 S_2$	= 2.2.

Substituting these values into equation (7.15) we obtain:

$$M/H_0 = 5.875 \times 10^5 \sum_{i=1}^{15} \sigma_i \int_{r_i - 1}^{r_i} \frac{e^{-r/850}}{r}\, dr, \qquad (7.16)$$

with r in meters,

σ_i in persons/m^2.

Table 7.2 summarizes the numerical data for the evaluation of the integrands of equation (7.16).

The population dose equivalent due to LBL accelerator operation calculated using this model is then:

$$M/H_0 \approx 1023 \text{ man rem/fence-post rem.}$$

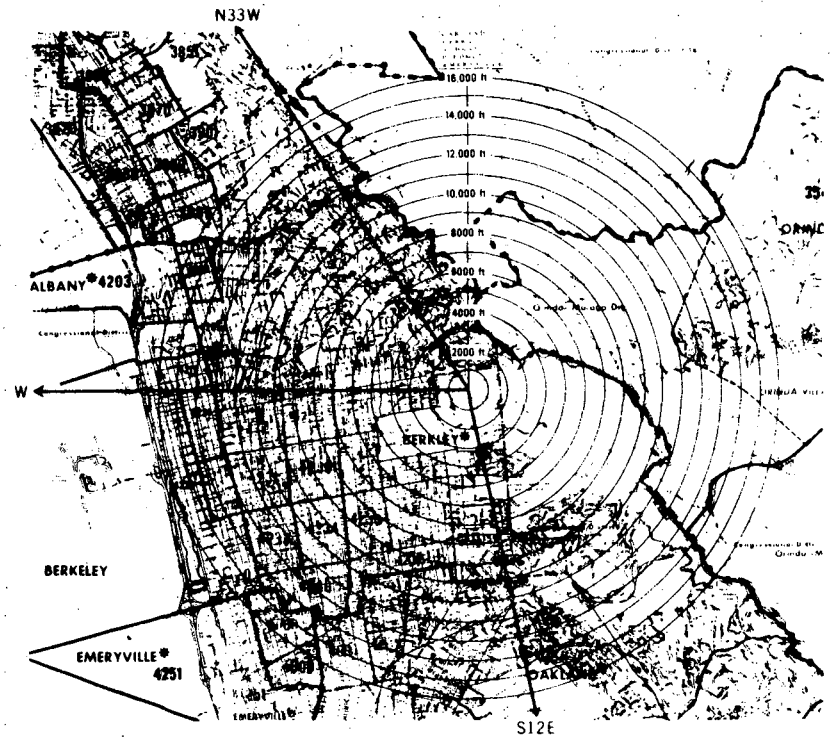
N33W
16,000 ft
14,000 ft
12,000 ft
10,000 ft
8000 ft
6000 ft
4000 ft
2000 ft
ALBANY 4203
W
BERKELEY
BERKELEY
EMERYVILLE
4251
S12E

Fig. 7.5

Table 7.2. Values of the integrands

At distance (meters) from	to	σ_i (persons/m^2)	I_i^*	M_i/H_0 Man rem/ fence-post rem
366 (1,200 ft)	610 (2,000 ft)	$\sigma_1 = 1.94\times10^{-3}$	2.938×10^{-1}	341.1
610 (2,000 ft)	914 (3,000 ft)	$\sigma_2 = 2.96\times10^{-3}$	1.690×10^{-1}	299.2
914 (3,000 ft)	1219 (4,000 ft)	$\sigma_3 = 3.19\times10^{-3}$	8.343×10^{-2}	159.2
1219 (4,000 ft)	1524 (5,000 ft)	$\sigma_4 = 2.97\times10^{-3}$	4.511×10^{-2}	80.2
1524 (5,000 ft)	1829 (6,000 ft)	$\sigma_5 = 2.98\times10^{-3}$	2.571×10^{-2}	45.8
1829 (6,000 ft)	2134 (7,000 ft)	$\sigma_6 = 2.18\times10^{-3}$	1.517×10^{-2}	19.8
2134 (7,000 ft)	2438 (8,000 ft)	$\sigma_7 = 2.94\times10^{-3}$	9.177×10^{-3}	16.1
2438 (8,000 ft)	2743 (9,000 ft)	$\sigma_8 = 2.66\times10^{-3}$	5.652×10^{-3}	9.0
2743 (9,000 ft)	3048 (10,000 ft)	$\sigma_9 = 2.14\times10^{-3}$	3.531×10^{-3}	4.5
3048 (10,000 ft)	3353 (11,000 ft)	$\sigma_{10} = 2.23\times10^{-3}$	2.231×10^{-3}	3.0
3353 (11,000 ft)	3656 (12,000 ft)	$\sigma_{11} = 2.17\times10^{-3}$	1.422×10^{-3}	1.8
3656 (12,000 ft)	3962 (13,000 ft)	$\sigma_{12} = 2.25\times10^{-3}$	9.141×10^{-4}	1.2
3962 (13,000 ft)	4267 (14,000 ft)	$\sigma_{13} = 2.25\times10^{-3}$	5.911×10^{-4}	0.8
4267 (14,000 ft)	4572 (15,000 ft)	$\sigma_{14} = 1.84\times10^{-3}$	3.844×10^{-4}	0.4
4572 (15,000 ft)	4877 (16,000 ft)	$\sigma_{15} = 1.56\times10^{-3}$	2.512×10^{-4}	0.2

$$^{*}I_i = \int_{r_{i-1}}^{r_i} \frac{e^{-r/850}}{r}\, dr$$

Stephens et al.[3] believe this estimate to be an upper limit because conservative values of population density and attenuation length are assumed.

It is of interest to note that the estimate of population dose equivalent for the Stanford Linear Accelerator which, like LBL, is located close to an urban population, is comparable in magnitude to that of LBL when calculated using similar assumptions.[6]

References
Section 7

1. International Commission on Radiological Protection, Publication 9, Para. 52, Pergamon Press, Oxford (1966).
2. Stephens, L.D., Thomas, R.H., and Thomas, S. B., Population Exposure from High-Energy Accelerators, Health Physics 29, 853 (1975).
3. Stephens, L.D., Thomas, R.H. and Thomas, S.B., A Model for Estimating Population Exposures Due to the Operation of High-Energy Accelerators at the Lawrence Berkeley Laboratory, Health Physics 30, 404 (1976).
4. Stephens, L. D. and Dakin, H. S., A High Reliability Environmental Radiation Monitoring System, Proc. of the VIth International Congress of the Societe Francaise de Radioprotection, Bordeaux, France, March 27-31, 1972, p. 753.
5. McCaslin, J.B., Health Physics Department, Lawrence Berkeley Laboratory, private communication (1974).
6. Swanson, W., Health Physics Department, Stanford Linear Accelerator Center, private communication, January 1976.

8. The Application of the "As Low as Practicable Concept" at Accelerators

8.1. Introduction

References

8. The Application of the "As Low as Practicable Concept" at Accelerators

At research accelerator laboratories the application of the "as low as practicable concept" is probably even more difficult than at other nuclear facilities. An accelerator research program demands great flexibility in mode of accelerator operation, beam intensity and radiation shielding. Because conditions continually change, cost-benefit studies of radiation protection practices are not often effective. In consequence, no general principles have as yet been developed, but specific examples may prove helpful.

Thomas[1] has described the application of the "ALAP" concept to high-energy accelerator shielding and found the cost of shielding to range between $40 to $50 per man rem.[1]

Reference

Section 8

1. Thomas, R. H., Implementing the Requirement to Reduce Radiation Exposure to ". . . As Low As Practicable" at the Lawrence Berkeley Laboratory, Health Physics 30, 271 (1976).

Bibliography

General

Freytag, E., Strahlenschutz an Hochenergie - beschleunigen (in German) G. Braun, Karlsruhe (1972).

Livingston, M.S. and J.P. Blewitt, Particle Accelerators, McGraw Hill New York (1962).

Patterson, H.W. and R.H. Thomas, "Accelerator Health Physics," Academic Press, New York (1973).

Rindi, A.R. and R.H. Thomas, The Radiation Environment of High-Energy Accelerators, Ann. Rev. Nucl. Sci. 23, 315 (1973).

Radiation Environment of High-Energy Accelerators and Dosimetry

Attix, F.H., W.C. Roesch and E. Tochilim (Eds.), Radiation Dosimetry 3 vols., Academic Press, New York (1966-69).

Kase, K. and W.R. Nelson, Concepts of Dosimetry, Stanford Linear Accelerator Center Internal Report, SLAC Report No. 153 (1972).

Thomas, R.H., Neutron Dosimetry at High-Energy Particle Accelerators, in Neutron Monitoring for Radiation Protection Purposes, vol. 1, p. 327, IAEA, Vienna (1973).

Shielding

Jaeger, R.G. (Editor-in-Chief), Engineering Compendium on Radiation Shielding. Vol. 1 (Shielding Fundamentals and Methods) (1968), and Vol. 3 (Shield Design Examples) (1970), Springer Verlag Inc, New York.

Bibliography, continued

Jaeger, J.T., Grundzeuge der Strahlenschutz Technik, Springer-Verlag, Berlin (1960).

Zaitser, L.N., M.M. Komochkov and B.S. Sychev, Fundamentals of Shielding for Accelerators (in Russian), Atomizdat, Moscow (1971).

Induced Radioactivity

Barbier, M., Induced Radioactivity, North Holland Publishing Co., Amsterdam (1969).

Environment

Rindi, A. and R.H. Thomas, "Skyshine - A Paper Tiger?", Particle Accelerators 7, 23 (1975).

Thomas, R.H. and A. Rindi, The Radiation Environment of High-Energy Accelerators, To be submitted to Critical Reviews in Environmental Control.

Acknowledgments

This "short course" draws together in one place material which has appeared in many articles published in the literature. No originality is therefore claimed, save perhaps in the manner of presentation, but the author is grateful to many of his past and present colleagues who have contributed to the work. To mention all of them would make too long a list but it would be churlish not to mention Mr. K.B. Shaw (N.R.P.B.) and Dr. G.R. Stevenson (CERN), both formerly of the Rutherford Laboratory, Mr. H.W. Patterson (LLL), formerly Group Leader of the Health Physics Group at Berkeley, and all the present members of the Health Physics Department at the Lawrence Berkeley Laboratory.

This work was done with support from the U.S. Energy Research and Development Administration.

FIGURE CAPTIONS

Fig. 1.1. The increase with time of the maximum energy achieved by different types of particle accelerators.

Fig. 1.2. The beam intensity as a function of particle energy of several high-energy accelerators (after Rosen).

Fig. 1.3. The annual increase in particle accelerators throughout the world (1930-1968) (after Rosen).

Fig. 2.1. Some typical high-energy neutron spectra (a) 1/E spectrum (for comparison). (b) Cosmic-ray spectrum. (c) Spectrum at concrete shielding bridge at CPS. (d) Spectrum on earth shield of CPS. (e) Spectrum outside Bevatron shielding. (f) Spectrum outside steel shielding of Nimrod external proton beam. (From Shaw, Stevenson and Thomas.)

Fig. 3.1. Quality factor as a function of stopping power in water (interpolated from ICRP recommendations).

Fig. 3.2. Particle flux density to dose equivalent rate conversion factors - a summary. (From Patterson and Thomas.)

Fig. 3.3. The neutron spectra derived from measurements of the recoil proton spectra in nuclear emulsions exposed at several locations around the Bevatron. In each diagram: (A) identifies the peak at 0.6 MeV due to the $^{14}N(n,p)^{14}C$ reaction of thermal neutrons; (B) identifies the 1.25 MeV peak due to α particles from the decay of the naturally radioactive constituents of the emulsion; the curve C shows the smooth recoil proton spectrum correlated for background, and the curve D shows the derived neutron spectrum. The notations B-25, B-27, etc. identify location of the emulsion exposure (after Lehman and Fekula, 1964).

Fig. 3.4. A graph relating the average number of grey prongs per star and different shapes of neutron spectra characterized by the logarithmic slope, γ, and the maximum energy of the spectra.

Fig. 3.5. Response functions for the four detectors used to determine neutron spectra at well-shielded locations.

Fig. 3.6. Response functions for additional detectors used to determine neutron spectra in high radiation levels.

Fig. 4.1. Schematic diagram of typical shielding geometry.

Fig. 4.2. Relative flux density distribution measurements along paths drawn at several angles to the point of incidence of the proton beam on a concrete shield. Measurements made with the $^{27}Al \rightarrow {}^{24}Na$ reaction. Incident proton energy 6 GeV. (Smith et al.)

Fig. 4.3. Typical example of the ratio of detector response as a function of distance from the point of incidence to the proton beam on the shield. The figure demonstrates the existence of an equilibrium spectrum. The curve labeled "axial profile" was obtained in the beam direction; that labeled "lateral profile" was obtained at a depth of four feet into the shield in a direction normal to the beam direction. Incident proton energy 6 GeV. (Smith et al.)

Fig. 4.4. Inelastic neutron cross sections as a function of energy in the range 0 to 1.4 GeV. (After Lindenbaum.)

Fig. 4.5. Comparison between calculated and measured values of attenuation lengths in concrete for neutrons. (After Patterson.)

Fig. 4.6. The angular relaxation parameter, b, as a function of reaction threshold energy. (Levine et al.)

Fig. 4.7. Comparison of measured and calculated flux density as a function of position in the earth shield of the CPS. The abscissa gives the distance along the beam line measured from an arbitrary point. The 25-GeV proton beam interacted with a beryllium target at T (12.5 m from the origin). The ordinate shows the neutron density measured with an Al detector. (Rindi and Thomas.)

Fig. 4.8. Neutron flux spectra at various depths in the earth's atmosphere produced by galactic protons near solar minimum. These calculations are compared with calculations of Lingenfelter and the measurements of Hess et al. (λ = geomagnetic latitude), (from Armstrong et al.).

Fig. 5.1. Relative contribution to photon dose rate due to six radionuclides at the surface of an iron cylinder (dia. 80 gm cm^{-2}) irradiated axially by 200 MeV and 3 GeV protons for an infinite time (from Armstrong and Barish).

Fig. 6.1. Photon and neutron dose equivalent rates measured at the boundary of the Stanford Linear Accelerator Center.

Fig. 6.2. **Measurements performed around different accelerators. On the abscissa is the distance from the accelerator in meters, on the ordinate is the product of the measured neutron flux density by the square of the distance. In these coordinates a $1/r^2$ variation shows up as a horizontal line. a) Measurements of fast neutron flux density performed with a long counter from a "source point" (the PS bridge) at the CERN 28-GeV Proton Synchrotron b) Measurements of fast neutron flux density performed with a moderated BF_3 counter at the Dubna 10-GeV Proton Synchrophasotron. c) Measurements of dose-equivalent rate performed with a 12-in. (30 cm) Bonner sphere system at the Brookhaven 30-GeV Proton AGS. d) Measurements of fast neutron flux density performed with a long counter at the CERN 600-MeV Proton Synchrocyclotron. e) Fast neutron flux density measurements performed with a BF_3 moderated counter at the 7.5-GeV electron synchrotron, DESY. f) Fast neutron flux density measurements performed with a long counter at the Rutherford Laboratory 50-MeV proton linear accelerator. The solid dots indicate the measurements taken for a p beam of 30 MeV,[9] and the open dots for a p beam of 50 MeV.** (Rindi and Thomas.)

Fig. 6.3. Model illustrating the mechanisms by which accelerator-produced radioactivity may appear in ground water.

Fig. 6.4. Specific activity of accelerator-produced radionuclides in ground water at accelerator site boundary.

Fig. 6.5. Map showing the location of the Lawrence Berkeley Laboratory.

Fig. 6.6. View looking east showing the location of the Lawrence Berkeley Laboratory in relation to the University of California and the city of Berkeley.

Fig. 6.7. View of the Lawrence Berkeley Laboratory showing the location of the environmental monitoring station.

Fig. 6.8. Environmental Monitoring Data - Olympus Gate Station.

Fig. 6.9. Environmental Monitoring Data - 88-Inch Cyclotron Station.

Fig. 6.10. Environmental Monitoring Data - Building 90 station.

Fig. 6.11. Environmental Monitoring Data - Panoramic Way Station.

Fig. 6.12. Comparison between the increasing intensity of the Bevatron (right hand scale) and the decreasing radiation levels of the Laboratory's site boundary and decreasing radiation worker collective exposure since 1959 (left hand scale. (Thomas.)

Fig. 7.1. Diagram showing model used to calculate population dose equivalent.

Fig. 7.2. The parameter $M(r)/M(\infty)$ as a function of r for r_o = 300 m with valves of λ between 100m and 1000m.

Fig. 7.3. The parameter $M/2\pi\sigma D_0$ as a function of attenuation length, λ.

Fig. 7.4. The parameter $M/2\pi\sigma H_0$ as a function of perimeter radius, r_0.

Fig. 7.5. Region around LBL. The concentric circles are drawn around the Bevatron at 1000-foot intervals.

This report was done with support from the United States Energy Research and Development Administration. Any conclusions or opinions expressed in this report represent solely those of the author(s) and not necessarily those of The Regents of the University of California, the Lawrence Berkeley Laboratory or the United States Energy Research and Development Administration.

TECHNICAL INFORMATION DIVISION
LAWRENCE BERKELEY LABORATORY
UNIVERSITY OF CALIFORNIA
BERKELEY, CALIFORNIA 94720